Journal of Robotics

Robotic Prosthetic Limbs

Lead Guest Editor: Ruwan Gopura
Guest Editors: Kazuo Kiguchi, George Mann, and Diego Torricelli

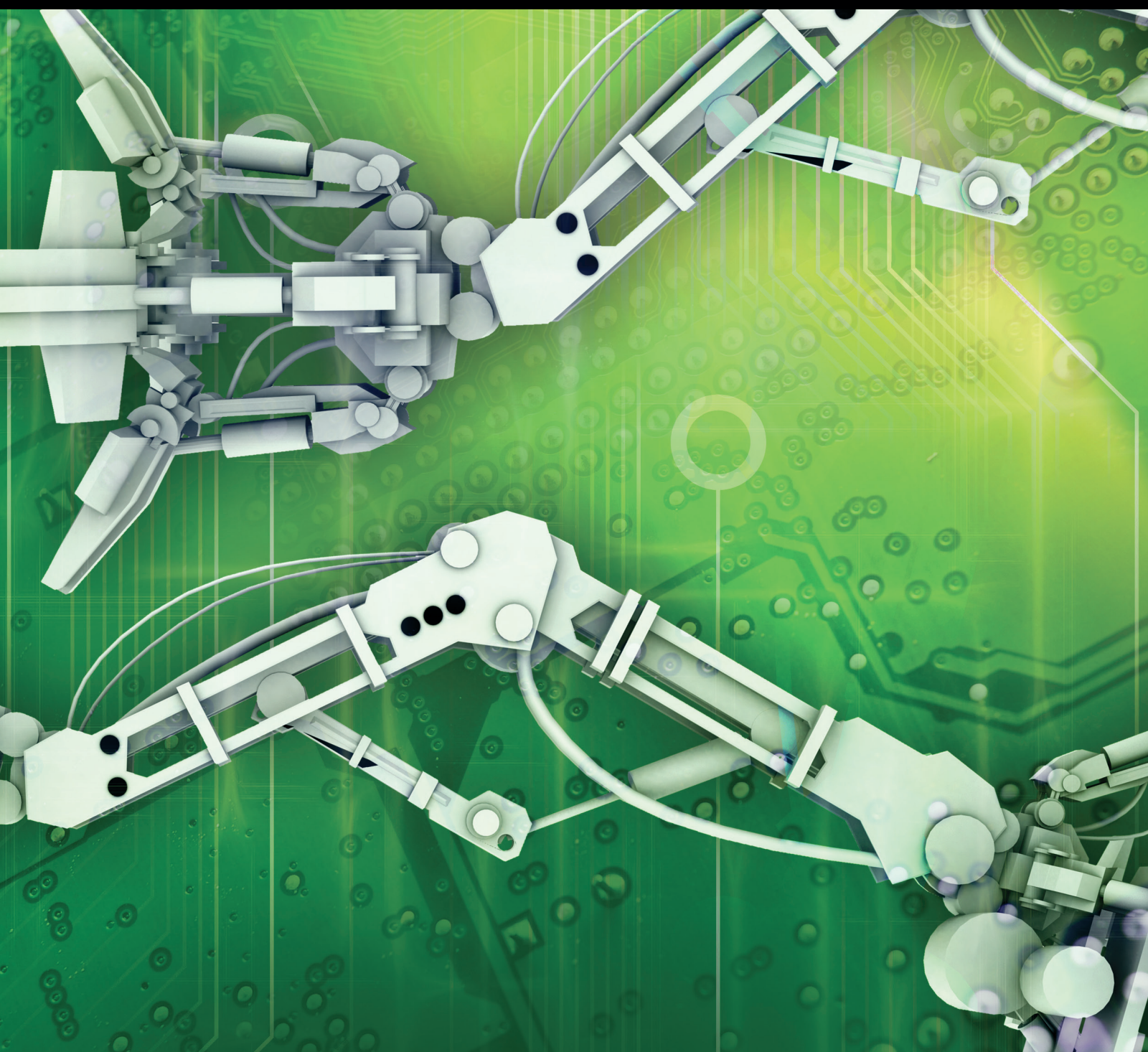

Robotic Prosthetic Limbs

Journal of Robotics

Robotic Prosthetic Limbs

Lead Guest Editor: Ruwan Gopura
Guest Editors: Kazuo Kiguchi, George Mann, and Diego Torricelli

Editorial Board

Contents

Robotic Prosthetic Limbs
Ruwan Gopura, Kazuo Kiguchi, George Mann, and Diego Torricelli
Volume 2018, Article ID 1085980, 2 pages

HyPro: A Multi-DoF Hybrid-Powered Transradial Robotic Prosthesis
C. L. Semasinghe, R. K. P. S. Ranaweera, J. L. B. Prasanna, H. M. Kandamby, D. G. K. Madusanka, and R. A. R. C. Gopura
Volume 2018, Article ID 8491073, 15 pages

Biomechanic and Energetic Effects of a Quasi-Passive Artificial Gastrocnemius on Transtibial Amputee Gait
Michael F. Eilenberg, Ken Endo, and Hugh Herr
Volume 2018, Article ID 6756027, 12 pages

Development and Evaluation of a Powered Artificial Gastrocnemius for Transtibial Amputee Gait
Michael F. Eilenberg, Jiun-Yih Kuan, and Hugh Herr
Volume 2018, Article ID 5951965, 15 pages

Adaptive Foot in Lower-Limb Prostheses
Thilina H. Weerakkody, Thilina Dulantha Lalitharatne, and R. A. R. C. Gopura
Volume 2017, Article ID 9618375, 15 pages

Networked Multimodal Sensor Control of Powered 2-DOF Wrist and Hand
Masaki Shibuya, Kengo Ohnishi, and Isamu Kajitani
Volume 2017, Article ID 7862178, 12 pages

Hindawi
Journal of Robotics
Volume 2018, Article ID 1085980, 2 pages
https://doi.org/10.1155/2018/1085980

Editorial

Robotic Prosthetic Limbs

Ruwan Gopura,[1] **Kazuo Kiguchi**,[2] **George Mann**,[3] **and Diego Torricelli**[4]

[1]*Department of Mechanical Engineering, University of Moratuwa, Moratuwa, Sri Lanka*
[2]*Department of Mechanical Engineering, Kyushu University, Fukuoka, Japan*
[3]*Faculty of Applied Science, Memorial University of Newfoundland, St. John's, NL, Canada*
[4]*Cajal Institute, Spanish National Research Council (CSIC), Madrid,, Spain*

Correspondence should be addressed to Ruwan Gopura; gopura@mech.mrt.ac.lk

Received 2 January 2018; Accepted 3 January 2018; Published 1 April 2018

In the present society, more than one million annual limb amputations are carried out globally due to accidents, war casualties, cardiovascular disease, tumors, or congenital anomalies. Robotic prosthetic limb is a well-established research area that integrates advanced mechatronics, intelligent sensing, and control for achieving higher order lost sensorimotor functions while maintaining the physical appearance of amputated limb. Robotic prosthetic limbs are expected to replace the missing limbs of an amputee restoring the lost functions and providing aesthetic appearance. The main aspects are enhanced social interaction, comfortable amputee's life, and productive amputee to the society. With the advancement of sensor technology, in the last few decades significant contributions have been made in this area. Much of the work is still in the research stage and more research and development work is anticipated in the coming years where the ultimate goal is to produce a device which can generate human-like motions.

This special issue is dedicated to establishing a multidisciplinary forum of discussion on the recent advances in robotic prosthetic limbs. Five articles have been selected to be published in this special issue. Two of them are on upper-limb prosthetic limbs and the other three are on lower-limb prostheses.

One of the articles is on upper-limb robotic prostheses. It proposes a multi-DoF hybrid powered transradial robotic prosthesis. Most hybrid prostheses use individual and decoupled joint control and use either electric or body-power actuation. Authors of this article have contributed to develop a robotic prosthesis named HyPro. It uses hybrid powering concept on restoration of grasp functions similar to a biological hand. HyPro is an underactuated robot with 15 degrees of freedom and can achieve five grasping patterns: power grasp, tip grasp, lateral grasp, hook grasp, and index point. The underactuated mechanism can achieve required hand preshaping for a given grasping pattern using electric-power in the pregrasp stage and body power is used in grasp stage to execute the final grasping action.

Another article is on transradial prosthetic limbs and it proposes a networked multimodel control method for a prosthesis having 2DOF wrist and 1DOF hand. The objective is to enhance the wrist controllability while processing information derived from the joint movement. Authors have applied a manipulative skill model of prehension and it is constrained by forearm properties, grasping object properties, and task. Experimental results confirm the fusion control is sufficient to control the wrist joint with respect to the work plane posture.

It is important to have adaptive capabilities in foot prosthesis to achieve the essential movements of lower-limb amputees as the natural foot enables to do. The authors one article have carried out a systematic review in order to understand the design concepts of adaptive foot prostheses using PRISMA method. Additionally, they have investigated requirements and design challenges of adaptive foot prostheses. Furthermore, adaptive foot prostheses have been classified and compared. Authors have foretold that future adaptive prostheses will consist of energy regenerative methods and will be more convenient for users.

Another article is on a transtibial robotic prosthetic limb. It presents a powered biarticular transtibial prosthesis, which is a combination of a commercial powered ankle-foot

prosthesis and a motorized robotic knee orthosis. The orthosis is controlled to emulate the human gastrocnemius based on neuromuscular models of matched nonamputees. Authors have evaluated the biarticular condition against the monoarticular condition under the condition that orthosis is behaving as a free-joint. The experimental results obtained from six participants with transtibial amputation do not completely support authors' hypothesis that metabolism decreases for all participants. However, some participants demonstrate large metabolic reductions with the biarticular condition. From the preliminary results it can be suggested that a powered artificial gastrocnemius may be capable of providing large metabolic reductions as compared to a monoarticular prosthesis.

Authors of one of the articles have developed and evaluated a prosthesis that actuates both knee and ankle joints. The prosthesis employs a quasi-passive clutched-spring knee orthosis, approximating the largely isometric behavior of the biological gastrocnemius. Two participants with unilateral transtibial amputation walk with the prosthesis on an instrumented treadmill while motion, force, electromyography, and metabolic data are collected and analyzed. The biarticular system is shown to reduce both affected-side knee and hip moment impulse and positive mechanical work in both participants during the late-stance knee flexion phase of walking, compared to the monoarticular condition. Based on the preliminary results authors have suggested that biarticular functionality may provide benefits beyond even those of the most advanced monoarticular prostheses.

Authors of all articles highlighted both the promise and the challenges faced by the field of robotic prosthetic limbs. Their articles further identified the critical need for additional prospective, in design and control of robotic prosthetic limbs. In summary, this special issue provides a snapshot on the current status of transradial and transtibial robotic prosthetic limbs.

Ruwan Gopura
Kazuo Kiguchi
George Mann
Diego Torricelli

Hindawi
Journal of Robotics
Volume 2018, Article ID 8491073, 15 pages
https://doi.org/10.1155/2018/8491073

Research Article

HyPro: A Multi-DoF Hybrid-Powered Transradial Robotic Prosthesis

C. L. Semasinghe, R. K. P. S. Ranaweera, J. L. B. Prasanna, H. M. Kandamby, D. G. K. Madusanka, and R. A. R. C. Gopura

Bionics Laboratory, Department of Mechanical Engineering, University of Moratuwa, Moratuwa, Sri Lanka

Correspondence should be addressed to C. L. Semasinghe; chathural.semasinghe@gmail.com

Received 20 May 2017; Revised 21 October 2017; Accepted 16 November 2017; Published 1 March 2018

Academic Editor: Yangmin Li

This paper proposes a multi-DoF hybrid-powered transradial robotic prosthesis, named HyPro. The HyPro consists of two prosthetic units: hand and wrist that can achieve five grasping patterns such as power grasp, tip grasp, lateral grasp, hook grasp, and index point. It is an underactuated device with 15 degrees of freedom. A hybrid powering concept is proposed and implemented on hand unit of HyPro where the key focus is on restoration of grasp functions of biological hand. A novel underactuated mechanism is introduced to achieve the required hand preshaping for a given grasping pattern using electric power in the pregrasp stage and body power is used in grasp stage to execute the final grasping action with the selected fingers. Unlike existing hybrid prostheses where each of the joints is separately controlled by either electric or body power, the proposed prosthesis is capable of delivering grasping power in combination. The wrist unit of HyPro is designed and developed to achieve flexion-extension and supination-pronation using electric power. Experiments were carried out to evaluate the functionality and performance of the proposed hybrid-powered robotic prosthesis. The results verified the potential of HyPro to perform intended grasping patterns effectively and efficiently.

1. Introduction

Transradial amputations refer to loss of both biological hand and wrist and are the most common form of upper extremity amputation according to statistics [1]. Traumatic accidents, vascular complications, and congenital deformity are notable causes leading to transradial amputation [1]. Transradial prosthesis is used as a wearable device by the transradial amputees. It consists of an artificial wrist and a terminal device which are either mechanically or electromechanically operated [2, 3]. Although there had been a marked improvement in functionality, performance, and appearance of subsequent generations of transradial prostheses, the robotic counterparts are still lacking in certain areas to restore or mimic the missing segments of the biological limb [3]. In particular, most transradial prostheses are designed to perform a few of the grasping tasks with limited degrees of freedom (DoF), in comparison to the biological wrist and hand that have 27 DoF [4].

In general, effectiveness of transradial prostheses has been determined based on power consumption, weight, mobility, appearance, and size of the device [5]. These also serve as benchmarks to compare and contrast different prosthetic developments. According to literature, three main categories of transradial prostheses can be identified based on method of powering: nonpowered, body-powered, and externally powered prostheses [3]. Nonpowered or cosmetic transradial prostheses are made considering anthropometry and appearance of hand and characteristically do not have any or limited functional capabilities [6]. At present, body-powered transradial prostheses are the most popular prostheses since they are lightweight, simple in operation, easily maintained, economical, and importantly capable of restoring certain functions of the biological hand [6]. Since they can only perform maximum two grasping actions from a single terminal device, different terminal devices are required to fulfill various activities of daily living (ADL) [7]. The externally powered transradial prostheses are mostly operated by means of electric and pneumatic actuators. These prostheses exhibit higher functional capabilities compared to other two categories. However, externally powered transradial prostheses are typically limited in operation due to

high power consumption, complexity in operation, reliability, bulkiness, and overweight of the device [7].

Elimination of these limitations may enable the researchers and developers to derive a suitable replacement for a missing limb segment. One approach in realizing this is to introduce a hybrid powering concept where the device is given the capability of functioning with both body and external power [8]. There are no considerable applications of this concept in context of prosthetic limbs, and yet hybrid-powered prostheses are in the introductory phase of its life cycle. In literature, handful number of researches are identified in relation to hybrid-powered prosthesis where most of them use different units in combination that operate independently by either electric or body power [9, 10].

Therefore, this paper proposes a novel hybrid powering concept with the key focus on grasp restoration by actuating prosthetic thumb and fingers using both electric and body power. In addition, a novel underactuated mechanism is proposed for the prosthetic hand unit to perform different grasping patterns. The notion of adaptive grasping is also considered for the development of prosthetic fingers. The mechanism uses electric power to achieve hand preshaping according to the intended grasping pattern and body power to execute the desired grasping action. Here, the robotic prosthesis is designed to carry out five grasping patterns, namely, power grasp, tip grasp, lateral grasp, hook grasp, and index point which are commonly used in ADL. As a result of introducing the hybrid powering concept in the form of a novel finger actuation mechanism, the prosthetic hand only requires two electric actuators to perform the selected grasping patterns. Here one electric motor is used to flex and extend the three-digit prosthetic fingers while the second electric motor is used to arrange thumb position. Therefore, the proposed prosthetic hand unit is essentially an underactuated device with 15 DoF. The shoulder retraction-protraction is used to deliver the required body power to complete the grasping action. The prosthetic wrist unit proposed in this paper is fully electric-powered unit that has only two DoF controlled by two servomotors. The fully assembled prosthesis is designed to be worn by a transradial amputee using a socket placed on the residual limb and a commonly available harness mechanism is used to transmit the body power.

The paper is organized as follows. Section 2 reviews the state-of-the-art transradial prostheses to identify their capabilities and shortcomings. Section 3 briefly discusses motion requirements for transradial amputee with anatomical and biomechanical factors. Section 4 presents the design of the proposed transradial prosthesis. The mechanism of the HyPro is described in Section 5 and the experiments are presented in Section 6. Section 7 discusses the experimental results. Section 8 concludes the paper.

2. Related Work

One of the key limiting factors of transradial robotic prosthesis is its weight. It can be found from the literature that there is a direct relationship between device weight and number of active DoF [8]. As an example, devices such as DEKA RC Gen3 arm [18], DLR/HIT II hand [19, 20], and MANUS hand [21] show higher weights than the devices like uGrip II [22], i-limb ultra [23], and Michelangelo [24] because of the availability of higher active DoF. Generally, this occurs due to the consequences of increasing number of actuators to achieve high active DoF. In response, the researchers have come with underactuated mechanism which couples the multiple movements to single actuator. However, such advancements have also failed to achieve significant weight reduction due to added weight of additional mechanical coupling and/or linkage systems [8]. Generally, the selection of required number of actuators depends on the desirable grasping patterns for which the robotic prosthesis is designed. It is important to have independently controlled actuators in developing a dexterous hand with individual finger movements. However, it is possible to achieve an array of grasping pattern actuation by using the coupling strategies such as differential clutching and linkage mechanism which minimizes the actuators required to operate the prosthesis.

Majority of prostheses are developed based on tendon-based and linkage-based mechanisms to achieve finger movements [8]. Ability to miniaturize the end effector is the key advantage of the tendon-based mechanisms used in the most transradial prosthetic devices. This advantage is mainly due to the ability of placing the actuators away from joints of fingers. In addition, the tendon-based mechanism helps in reducing bulkiness of the end effector while reducing the complexity of operation of prosthetic fingers [8]. However, this mechanism is known to have some drawbacks as well. The friction between tendon and tendon enclosures or sliding groves results in inefficiencies in power transmission. The durability of tendon is also a major concern. The four-bar linkage is the most common linkage-based mechanism found in the transradial prostheses. Such mechanisms generally showcase efficient power transmission while producing high grasping force and good grasp stability. However, prosthetic fingers or the end effectors are bulky when considering most prosthetic hands. In addition, the complexity of operation and higher weight are other factors associated with linkage-based mechanism. However, new linkage-based concepts have now been developed for underactuated mechanisms where some devices enable the passive finger control and enhance the object grasping capabilities. As an example, AR hand III is a novel anthropomorphic robot hand which has 15 joints driven only by three motors which is purely based on underactuated mechanism [25].

When powering of the robotic prostheses is considered, body-powered prostheses like HOSMER HOOK model 88X and OTTOBOCK hooks are light weight and simple to operate [24, 26]. However, they are limited to restoring a few grasping patterns mainly due to the usage of body power to operate. The electrically powered prostheses like i-limb ultra, Bebionic 3, and Michelangelo have more functional capabilities than body-powered device but have limitations arising due to bulkiness, weight, and complexity of operation [23, 24, 27]. The major drawback of those devices is their reliance on battery power. By combining favorable features found in each prosthetic limb into one prosthesis, most of the limitations can be mitigated.

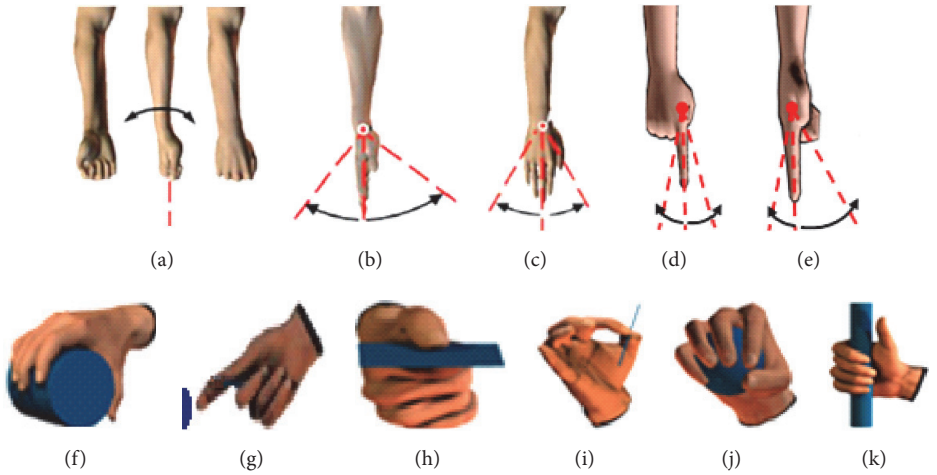

FIGURE 1: Motions of below elbow extremity (adapted from [14]) and common grasping patterns (adapted from [15]). (a) Forearm supination-pronation, (b) flexion-extension of hand, (c) radial-ulnar deviation of hand, (d) finger abduction-adduction, (e) finger flexion-extension, (f) power grasp, (g) index point, (h) lateral grasp, (i) tip grasp, (j) chuck or spherical grasp, and (k) Hook grasp.

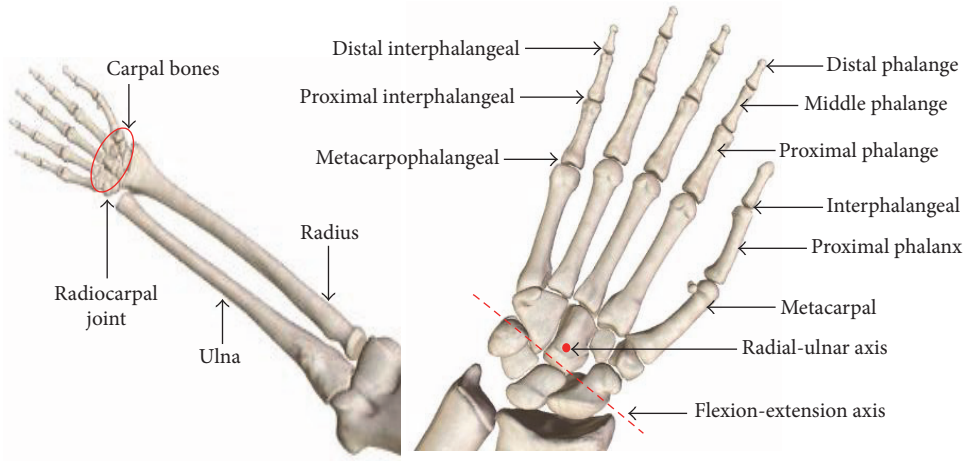

FIGURE 2: Anatomy of wrist and hand.

3. Motion Requirement of Transradial Amputee

A transradial prosthesis should ideally restore the motion requirement of the biological hand and wrist. In order to achieve this task, anatomy and biomechanics of the upper limb should be closely studied. The following section summarizes the salient aspects considered in developing the proposed hybrid-powered transradial prosthesis.

The below elbow upper limb consists of forearm, wrist, and hand. The radioulnar joint in the forearm facilitates wrist supination-pronation (see Figure 1). The wrist consists of two joints, namely, radiocarpal and midcarpal joints, which are located at the distal ends of the radial and ulna bones (see Figure 2). Radiocarpal joint allows flexion-extension and radial-ulnar deviation at the wrist [28]. The range of motion (RoM) for each DoF at wrist joint discussed above is summarized in Table 1.

Human hand consists of 27 bones, 29 joints, more than 30 muscles, and tendons to actuate the joints for the purpose of motion generation [29]. In order to handle various objects, joints of fingers are arranged in different configurations. All 3-digit fingers are comprised of metacarpophalangeal (MP), proximal interphalangeal (PIP), and distal interphalangeal (DIP) joints while thumb has only interphalangeal (IP) and metacarpophalangeal (MP) joints [12] as shown in Figure 2.

The joints in the five fingers provide 21 DoF for grasping objects that may vary in size, shape, and weight. The thumb has five DoF whereas other fingers only four. The flexion-extension of fingers are generated by three separate joints [12]. The abduction-adduction of fingers is only generated at the MCP joint. Table 2 lists RoM of each finger with respect to rest position as indicated in Figures 1(d) and 1(e).

The hand is capable of generating required articulation to support ADL. There are numerous finger arrangements, known as grasping patterns to perform several grasping

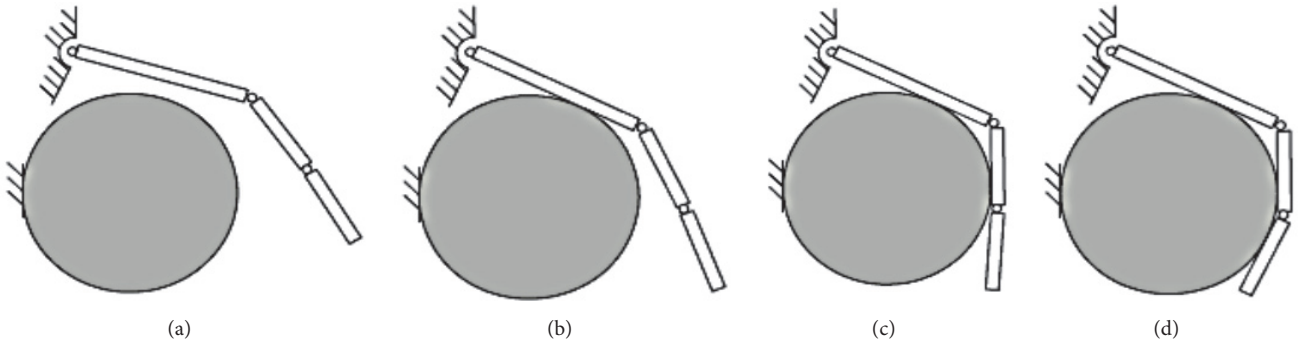

Figure 3: Sequence of steps followed to grasp a cylindrical object [16]: (a) approach of the finger, (b) contact of the first phalange, (c) contact of the second phalange, and (d) contact of the third phalange.

Table 1: Range of motions of wrist [11, 12].

Motion	Range
Flexion-extension	0°–75°/0°–(−70°)
Radial deviation-ulnar deviation	0°–20°/0°–(−35°)
Supination-pronation	0°–90°/0°–(−90°)

actions. The main function of the prosthesis is to mimic the most important grasping patterns used in day-to-day life [30]. During the grasp action, the fingers undergo two main stages which are pregrasp and grasp execution [31]. In the pregrasp stage, the fingers arrange for achieving the desired grasping pattern while reorienting the hand. The action of gripping the target will be performed during the grasp execution stage [31]. For example, when an average person wants to hold an iron, first the hand gets prepared for grasping during its pregrasp stage which is in the reach-to-grasp motion. Then grasp is executed by holding the iron by the desired grasp posture which is power grasp [31]. In the ADL, power grasp, index point, and lateral grasp are frequently used grasping patterns which are shown in Figures 1(f)–1(h) [30]. According to the literature, power grasp is the mostly employed grasping pattern with a frequency of 40% of ADL [30, 32]. Furthermore, frequencies of use of index finger extension, precision grasp, lateral grasp, and hook grasp are 13%, 12%, 7%, and 0.2%, respectively [15].

Finger adaptation is considered to be the most important feature when developing a prosthesis. Most of the prosthetic fingers are developed to generate human-like grasping action. During grasping of a cylindrical object, the phalanges of the prosthetic or biological finger follow the basic sequence of operations shown in Figure 3 [16, 33].

4. Design of HyPro

The HyPro consists of two major units, referred to as prosthetic wrist unit and prosthetic hand unit. Figure 4 illustrates the complete CAD model of the proposed hybrid powering transradial prosthesis without the socket.

The wrist unit is designed to operate using external power while the prosthetic hand uses a combination of both electric and body power. The hybrid actuation and underactuated

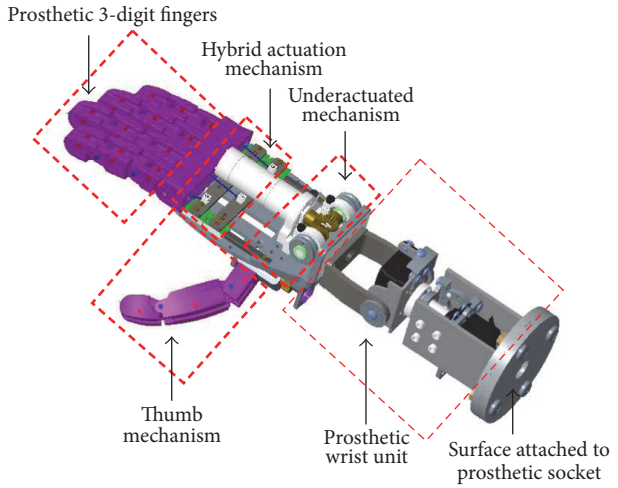

Figure 4: CAD model of HyPro.

mechanisms are located on the dorsal side of the prosthetic hand unit. The electric power is used for hand preshaping to perform the desired grasping pattern while body power is used to execute the grasp for picking objects. The grasping modes and respective powering methods used by HyPro are tabulated in Table 3.

The design details of HyPro are presented under five subsections: prosthetic wrist design, prosthetic 3-digit finger design, prosthetic thumb design, design of hybrid actuation mechanism, and design of underactuated finger flexion-extension mechanism.

4.1. Prosthetic Wrist Design. The proposed design for the prosthetic wrist includes two active DoF, namely, supination-pronation and flexion-extension. The main structure of the wrist can be simplified to a mechanism consisting of two motors which work as two separate units. As shown in Figure 5 supination-pronation unit and flexion-extension unit are actuated using two servomotors, servomotor 1 (HS-5685MH, Hitec servomotor) and servomotor 2 (HS-5585MH, Hitec servo motor), respectively. Each unit is designed to perform separate motions that can mimic the biological counterpart. The servomotor 1 is held by a servoblock attached to an aluminium structure which has been consolidated on

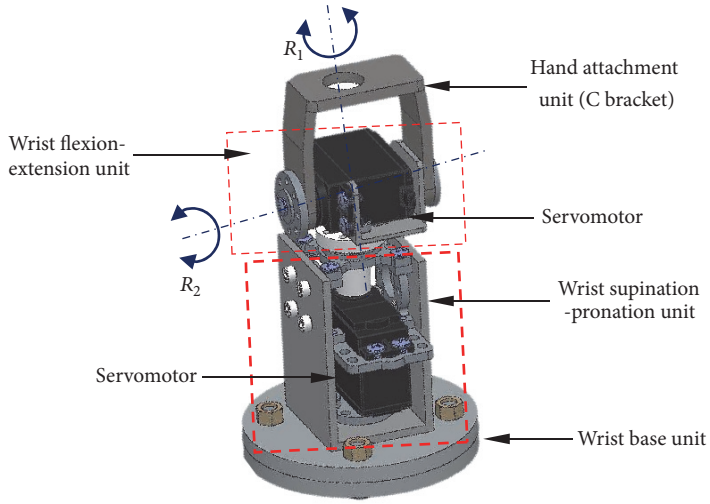

Figure 5: 2-DoF prosthetic wrist of HyPro.

Table 2: RoM of fingers [11, 13].

Motion/joint		Finger				
		Thumb	Index	Middle	Ring	Little
Flexion-extension	MCP	0°–70°	(−30°)–90°	(−20°)–90°	(−30°)–90°	(−30°)–90°
	PIP	-	0°–120°	0°–120°	0°–120°	0°–120°
	DIP	0°–90°	0°–80°	0°–80°	0°–80°	0°–80°
Abduction-adduction	MCP	(−50°)–40°	(−25°)–20°	(−25°)–20°	(−25°)–20°	(−25°)–20°
Opposition - reposition	CMC	(−9°)–31°	-	-	-	-

Table 3: Grasping and powering methods of HyPro.

Grasping mode	Powering method
Power grasp	Body power
Index push	Electric power
Tip grasp	Body and electric power
Hook grasp	Electric power
Lateral grasp	Body power

the wrist base unit. The servoblock contains an aluminium hub to transmit torque from the motor to prosthetic hand through the flexion-extension unit (see Figure 5). Flexion-extension unit is directly coupled with the hub of servoblock to transmit the torque of servomotor 1. The servomotor 2 is used to generate torque for wrist flexion-extension motion and the C-bracket is used to attach the prosthetic hand to the flexion-extension unit.

4.2. Prosthetic 3-Digit Finger Design. The fingers are designed considering 95th percentile anthropometric data of male population in the world [34]. The prosthetic finger closely matches the biological human finger from a functional point of view. The passive extension and adaptive grasping of phalanges have been achieved by employing elastic straps on the dorsal side of the prosthetic fingers. Different strap patterns were introduced between phalanges and the overall stiffness of the elastic straps was found to be 38.8 N/m from the physical experiments conducted on prosthetic finger samples. All the prosthetic fingers in HyPro are designed to work using a tendon-based mechanism where the finger gets flexed when the flexor tendon is pulled. Therefore, the prosthetic hand is voluntarily opened because of the extended fingers due to relaxation of elastic straps under zero force on the flexor tendons. Figure 6 shows the 3D model of the proposed prosthetic finger. Each of the segments of the prosthetic finger was fabricated from PLA material using 3D printing technology and 3 mm stainless steel pins were inserted to form the hinges. Finite element simulations were performed to assess the load bearing capacity of the prosthetic finger. Stress field plots indicate that regions nearby the hinges are most vulnerable for failure. However, each of the fingers is designed to bear 5 kg of force with a safety factor of 2.

4.3. Prosthetic Thumb Design. As in the case of 3-digit fingers, the prosthetic thumb is equipped with a tendon-based mechanism to flex the thumb. It is comprised of two phalanges similar to the biological thumb. In order to achieve passive extension and adaptive grasping abilities, two springs with different force constants were attached to each of the phalanges. The flexion-extension motion of the prosthetic thumb is achieved by pulling the flexor tendon using body

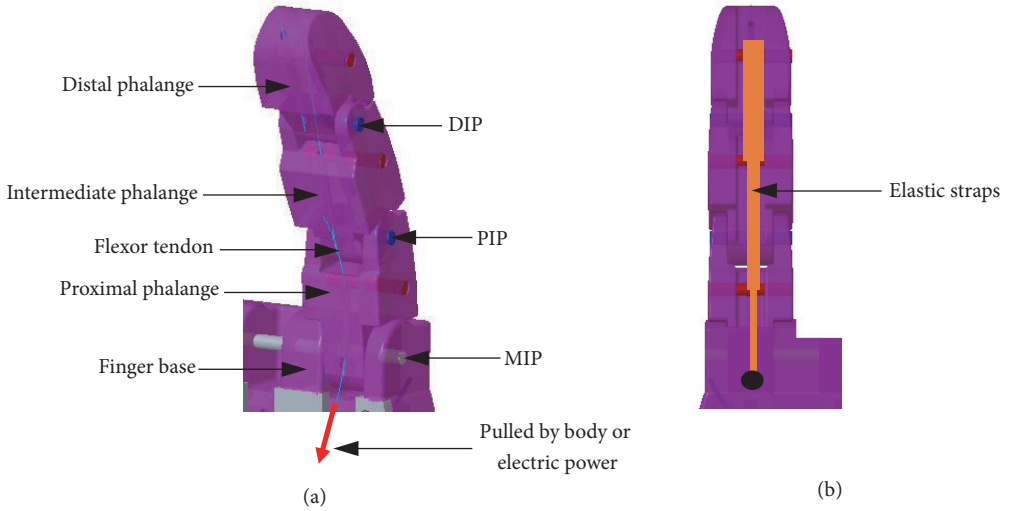

Figure 6: Model of prosthetic 3-digit finger: (a) 3-digit finger design with internal tendon flow path; (b) elastic straps arrangement of the finger model.

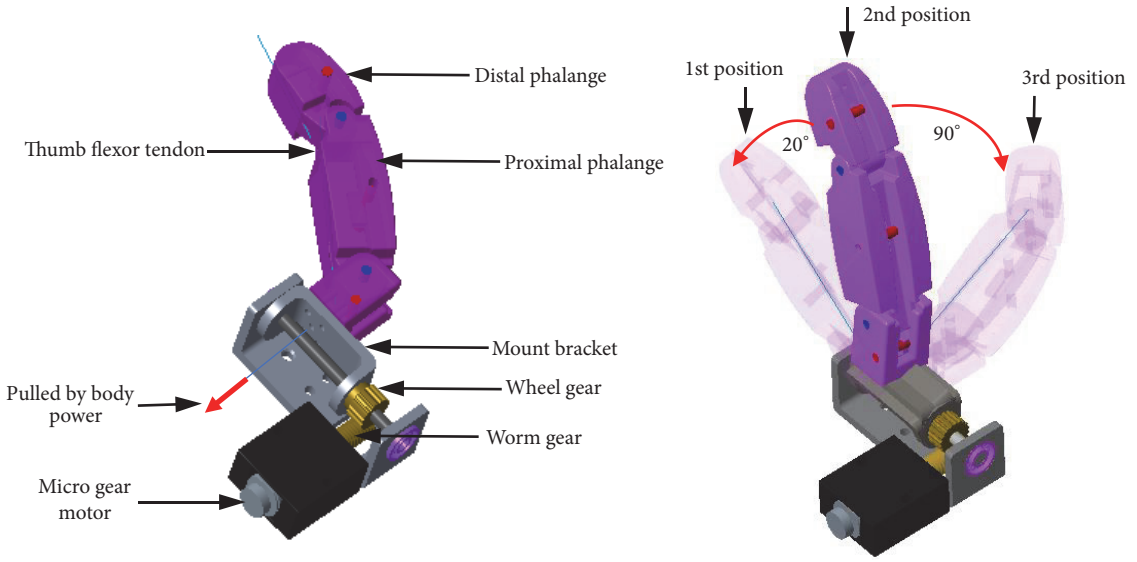

Figure 7: CAD model of prosthetic thumb.

power. In order to perform different grasping patterns, the thumb abduction-adduction movement is achieved using a micro gear motor (90 rpm micro gear motor with encoder). The worm and wheel gear drive provide a speed reduction of 1 : 10.

Figure 7 shows the 3D model of the proposed prosthetic thumb. HyPro is designed to perform only five key grasping patterns; hence, abduction-adduction movement is limited to three different positions to achieve desired grasping patterns. As shown in Figure 7, thumb shifts into 1st position for hand preshaping for power grasp. In order to preshape for tip grasping pattern the thumb moves to its 2nd position. For generating the index point posture, lateral grasping and hook grasping pattern thumb will be shifted to its 3rd position.

4.4. Design of Hybrid Actuation Mechanism. The prosthetic hand uses a tendon-based mechanism to actuate all the fingers by either body power or electric power. As per the design, the prosthetic middle, ring, and little fingers are flexed and extended simultaneously while the prosthetic index and thumb operate independently. In case of the prosthetic thumb, abduction-adduction has been implemented to achieve several grasping patterns. In electric-power actuation mode, the flexion-extension of all 3-digit fingers is performed using single DC brushed motor (38 rpm premium planetary gear motor with encoder). The motor rotation is used to flex only three or all four fingers as per the relevant control input. As shown in Figure 8, flexor tendon connected to each prosthetic finger is attached to the sliders, slider A and slider B. Here, slider A pulls the tendons from prosthetic middle,

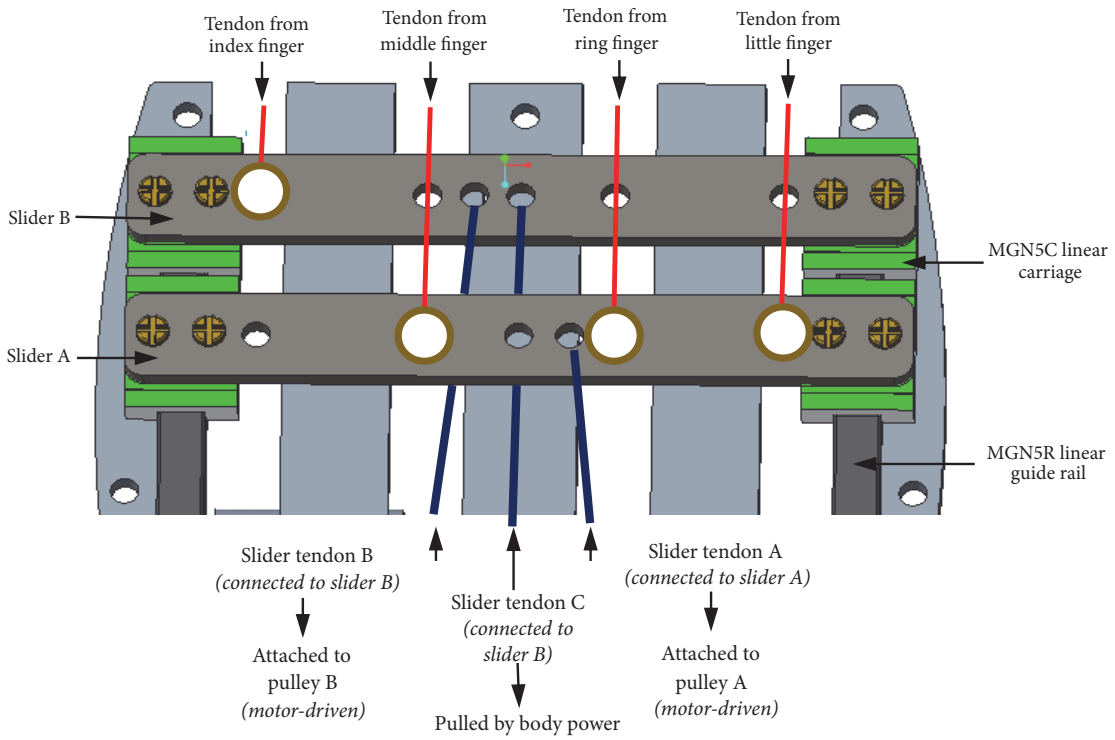

Figure 8: CAD model of the hybrid actuation mechanism.

ring, and little fingers while slider B pulls the tendon from prosthetic index finger.

Each slider is fixed on two carriage blocks (HIWIN MGN5C) where those carriage blocks linearly move on two linear guide rails (HIWIN MGN5R). Here both sliders can slide along the guide rail independently. Figure 8 illustrates the tendon connection to each of the sliders in HyPro. In order to flex prosthetic middle, ring and little fingers slider A has to be pulled by the slider tendon A. When the slider tendon B is pulled, the slider B moves linearly along the linear guide rails while pushing the slider A as well. Therefore, pulling the slider tendon B causes all four fingers to be flexed. Both slider tendon A and B are pulled using the same DC brushed motor which is electrically powered. The slider tendon C is designed to be pulled by body power which makes all four fingers flexed after pulling. Therefore, all four 3-digit fingers can be flexed by either pulling slider tendon B using DC brushed motor or pulling slider tendon C using body power. If the slider A is pulled by slider tendon A using DC brushed motor, the slider tendon C allows only index finger to flex or extend by pulling or releasing, respectively. When the effort on pulling slider tendons is released the fingers extend due to passive extension mechanism implemented on each finger. Here, the linear carriages and linear guide rails have been selected to satisfy the space requirement and to withstand the contact forces that occur on each slider due to unsymmetrical force distribution.

4.5. Underactuated Finger Flexion-Extension Mechanism. In HyPro, an underactuated mechanism is implemented to achieve finger flexion-extension with electric power. The proposed underactuated mechanism has resulted in reduction of weight and simplification of overall control of the prosthesis. This is mainly due to elimination of motors. However, the mechanism found inside HyPro is capable of performing five different grasping patterns using a single motor with the assistance of body power. When the DC motor gets actuated either slider tendon A or B winds on the pulleys causing the fingers to flex as planned. In order to pull one slider at a given instance, a simple mechanism has been implemented using couple of bearings. As shown in Figure 9(a), combinations of one-way and radial bearings are employed to achieve independent pulley rotation.

A one-way bearing allows a shaft inside to rotate freely only in one direction. If this one-way bearing is mounted inside a radial bearing as shown in Figure 9(b), the inner racer of the radial bearing will rotate when the shaft rotates in opposite direction due to the constrain of the shaft inside the one-way bearing. Figure 10 shows the working principal of the bilateral pulley-bearing assembly which explains the independent pulley movement capability using a single DC motor. Note that the tendon attachment pulley is mounted on the outer surface of one-way bearing and the pulley will only rotate when the one-way bearing is rotating inside the radial bearing.

When the motor shaft rotates in anticlockwise direction only, pulley A will rotate while pulling the slider A. It results in flexing prosthetic middle, ring, and little fingers. If the motor rotates in clockwise direction, only pulley B will rotate. The motion causes slider B to be pulled and slider tendon A tries to unwind from the pulley to release the strain energy stored in elastic straps. However, when slider B is pulled,

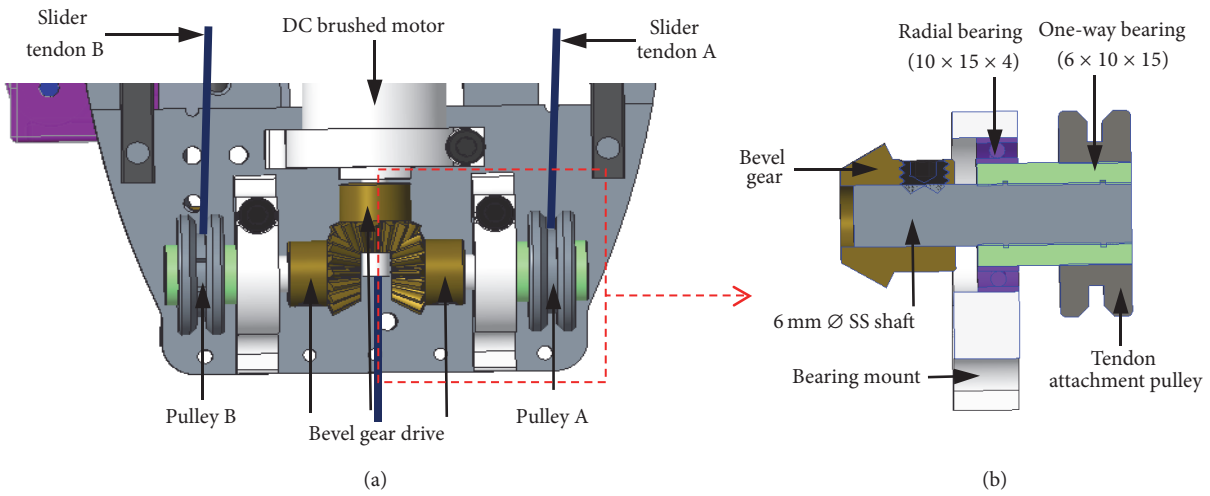

Figure 9: CAD model of the underactuated flexion-extension mechanism of finger.

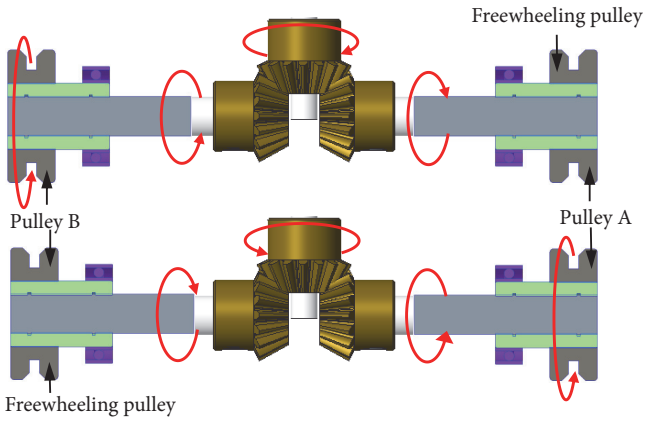

Figure 10: Bilateral pulley-bearing assembly of the underactuated mechanism.

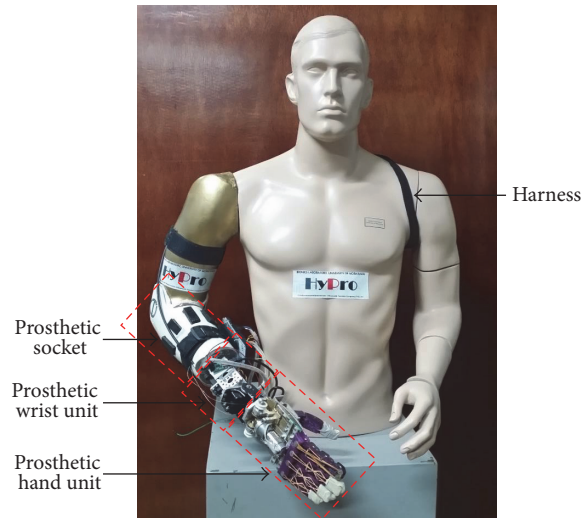

Figure 11: The HyPro.

slider A will also get pushed due to impending contact forces between the two sliders. As a consequence, all four fingers flex in the prosthetic hand. Then, when the shaft rotates in anticlockwise direction, the slider tendon B unwinds from the pulley while slider tendon A is winding on tendon attachment pulley.

4.6. Fabricated Model of HyPro. The fabricated model of the HyPro, including prosthetic hand unit, prosthetic wrist unit, prosthetic socket, and harness, is shown in Figure 11. Mass of the overall system including the battery pack (Li-Po 2200 mAh) is 1.8 kg in total. Fabricated model of HyPro hand has the 15 DoF as discussed in the design while having the two DoF in the HyPro wrist. Table 4 shows the achieved DoF in HyPro using body power from shoulder movement and electric power with two DC motors and two servomotors.

5. HyPro Hand Actuation Method

In order to grasp objects, five elements of the prosthesis are to be controlled. Those include slider tendon A, slider tendon B, thumb motor, slider tendon C, and thumb flexor tendon. Slider tendon A, slider B, and thumb motor are actuated by electric power while both slider tendon C and thumb flexor tendon are pulled simultaneously using body movement which is shoulder protraction-retraction. Each tendon has two states which are referred to as pulled and idle states. The thumb motor is used to attain three different work positions for achieving predefined grasping patterns. Table 5 describes the sequence of steps followed to achieve the required grasping pattern.

For example, to perform the lateral grasp, fingers are initially brought into hand preshaping by flexing the three-digit fingers fully and abducting the thumb to the 3rd position using electric power. Then the object is grasped by flexing the thumb using body power. Sequence of steps followed during lateral grasp is depicted in Figure 12. Similarly, actuation methods for other grasping patterns are obtained as per the sequences described in the Figure 13.

Table 4: Achieved DoF by HyPro.

Unit	Component	Joint	Movement	Actuation method	DoF
Hand unit	Thumb	Interphalangeal	Flexion-extension	Body power	1
		Metacarpophalangeal	Flexion-extension	Body power	1
			Abduction-adduction	Electric power	1
	Index finger Middle finger Ring finger Little finger	Distal interphalangeal	Flexion-extension	Body power or electric power	1 × 4
		Proximal interphalangeal	Flexion-extension	Body power or electric power	1 × 4
		Metacarpophalangeal	Flexion-extension	Body power or electric power	1 × 4
	Total number of DoF in HyPro hand unit				**15**
Wrist unit	Wrist joint	Radiocarpal	Flexion-extension	Electric power	1
			Supination-pronation	Electric power	1
	Total number of DoF in HyPro wrist unit				**2**

Table 5: Powering methods to actuate grasping patterns.

Control input signal	Mechanism				Output
	External power for hand preshaping			Body power for grasp execution	
	Slider tendon A	Slider tendon B	Thumb motor	Slider tendon C + thumb flexor tendon	
Power	Idle	Idle	1st position	Pulled	Power grasp
Tip	Pulled	Idle	2nd position	Pulled	Tip grasp
Index	Pulled	Idle	3rd position	Idle	Index point
Lateral	Idle	Pulled	3rd position	Pulled	Lateral grasp
Hook	Idle	Pulled	3rd position	Idle	Hook grasp

The electric power is only used to preshape the hand for achieving required grasping pattern with respect to the given control input signal. It is the same as changing terminal devices in conventional body-powered upper limb prostheses that enables grasping of different objects. Similarly, HyPro uses the same principle of grasp execution found in body-powered prostheses where shoulder retraction-protraction is used to execute the terminal device for grasping objects. Figure 14 illustrates how the body movement is used in achieving the grasping in the conventional body-powered prosthetic devices.

6. Experiments

Five different experiments were carried out in order to validate the design and performance of HyPro. These tests were performed to investigate the ability of the prosthesis to grasp and handle objects. In this section, experimental setups prepared for determining kinematics prosthetic fingers, adaptive behavior of prosthetic fingers, ability to perform grasping patterns, fingertip forces, and energy consumed during grasping patterns were systematically analyzed.

6.1. Experiment on Kinematics of Prosthetic Fingers. Prosthetic fingers are the key elements in any upper limb prosthesis. The fingers have to be properly designed to grasp an object with a selected grasping pattern. Therefore, the design of the prosthetic finger closely follows the biological finger to generate human-like motions. In order to validate the proposed design, a mathematical model of the prosthetic finger was prepared on a simulation platform, "Working Model 2D." Critical parameters for the model to be identified are length of digits in the prosthetic fingers and force constants of elastic straps. Model was used to evaluate the kinematics of the phalanges such as angular displacement of interphalangeal joints. In order to evaluate the actual prosthetic finger movement, an experiment was conducted using a movement analysis software package, "Kinovea." At first, markers were placed on each digit of prosthetic index finger (see Figure 15). Then, a high frame rate camera (120 fps @ 1080p) was used to record a video footage of flexion-extension of index finger. Finally, the marker movements were used to determine the interphalangeal angular displacements using Kinovea. Results are presented in detail in Section 7.

6.2. Experiment on Adaptive Behavior of Prosthetic Fingers. In order to identify the adaptive grasping behavior of a prosthetic finger, HyPro was used to grasp three cylindrical objects with different diameters. The cylinders were held firmly and the HyPro was given the input to grasp each object by gradual means. The sequence of snapshots extracted from a high frame rate video footage is included in Section 7 to showcase the adaptive grasping behavior of the proposed prosthetic fingers.

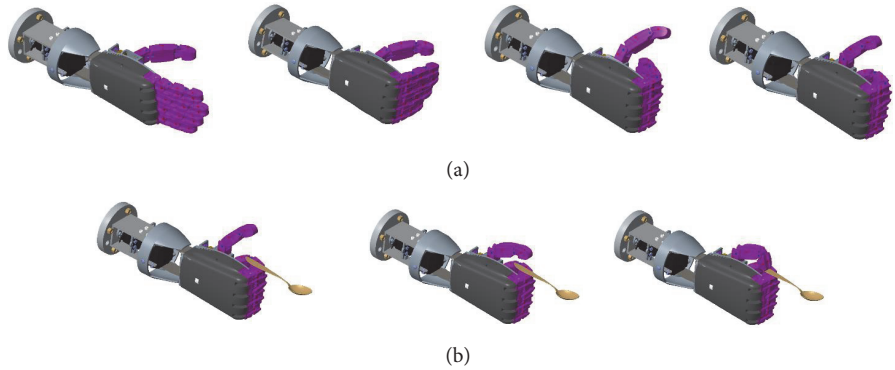

Figure 12: Holding a spoon using lateral grip: (a) hand preshaping by electric power; (b) grasp execution by body power.

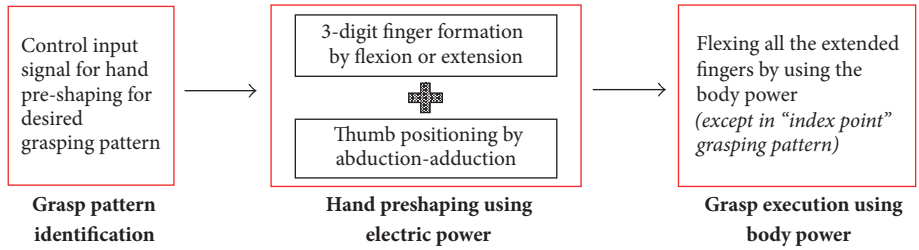

Figure 13: Sequence of achieving the desired grasping pattern.

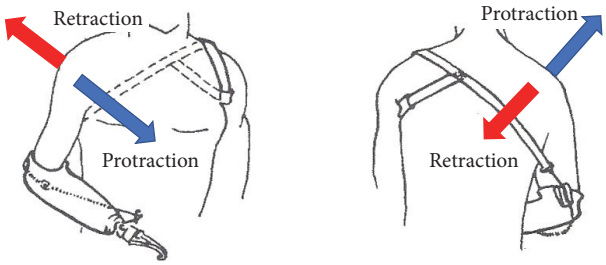

Figure 14: Shoulder motion to activate the prosthesis (adapted from [17]).

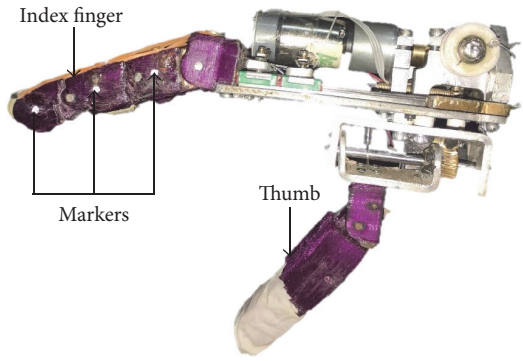

Figure 15: Marker placement on prosthetic index finger.

6.3. Experiment on Ability to Perform Grasping Patterns. The fabricated prosthesis hand was assigned with different tasks to evaluate the capability of achieving each of the five grasping patterns. In order to test the ability to perform power grasp, HyPro was given a water bottle to hold. Tip grasp, lateral grasp, and hook grasp were tested by making HyPro to hold a pen drive, a spoon, and a bag, respectively. The results of achieving those patterns are discussed in Section 7.

6.4. Experiment on Fingertip Forces. An experiment was conducted with prosthetic fingers to find the force exerted on objects during the grasping from the fingertip of prosthetic finger. During the experiment, the data on output forces was collected from all five fingers at the given instances of input forces given through the body-powered cable. The outcome of the results gathered has been briefly discussed in Section 7.

6.5. Experiment on Energy Consumed during Grasping Patterns. Energy consumption is a key measure to verify the effectiveness of HyPro over fully externally powered prostheses. The hybrid actuation mechanism is intended to increase battery life and reduce the effort exerted by body to actuate the prosthesis. In order to identify the energy requirement for hand preshaping during the pregrasp stage, an experiment setup was developed. It was subsequently used to determine the power requirement to perform all five grasping patterns. In order to measure the power consumption, current sensors were employed with a constant voltage input. A microcontroller (ATmega2560) was used to record data over a period of time.

The total energy consumption for each grasping pattern was then calculated using the current values measured for

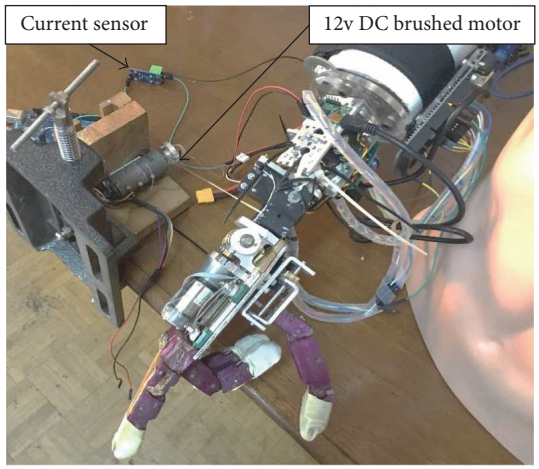

Figure 16: Experimental setup for obtaining current measure.

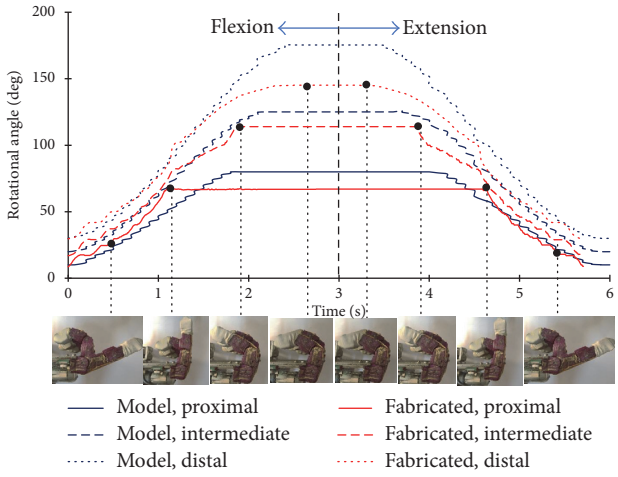

Figure 17: Kinematics of index finger.

a given duration. In order to find the power requirement to perform a desired grasping action, a separate 12v DC brushed motor was used to imitate the effort exerted by body power. The tendons supposed to be pulled by the body were attached to the motor shaft. The current measures were obtained using the microcontroller while performing desired grasping actions. The experimental setup for obtaining the current measures to determine energy consumption is shown in Figure 16.

7. Results and Discussion

In this section, the results obtained from the five different experiments described in the previous section are briefly discussed.

7.1. Kinematics of Prosthetic Finger. The graph in Figure 17 shows the results obtained for rotational angles for both simulated model and fabricated model of index finger for the given time instances with reference to finger base. It is noted that proximal digit model stops rotating after 1.7 s while intermediate digit rotates until 2.1 s during the flexion stage. The distal digit model rotates until 2.5 s during the flexion stage. Thus, it shows that the proximal digit stops rotating first, then intermediate digit, and finally the distal digit during the simulated model finger flexion. Although the time values obtained on fabricated finger model are leading compared to simulated model still it has shown the same sequence of digit rotations during the flexion stage.

During the extension stage in both simulated model and fabricated finger, the distal digit starts rotating first, then intermediate digit and finally the distal digit. When the finger comes to its rest position all digits stop rotation with reference to finger base. This validates that the prosthetic finger movement follows the human finger flexion-extension from both simulated model and fabricated model. The Figure 17 also shows the sequence of snapshots of fabricated prosthetic finger flexion-extension followed by the results shown in the graph.

7.2. Adaptive Grasping by HyPro Hand. The prosthetic fingers were given 3 tasks to review the adaptive grasping of fingers. As described in the experimental setup, 3 sequences of images (see Figure 18) were obtained to show the adaptive grasp movement in prosthetic fingers.

In all the tasks when the fingers are given an object to grasp first proximal digit gets contacted with object surface and stops rotating around metacarpi-phalangeal joint while other intermediate and distal digits are rotating to get contacted with the object. Then the intermediate digit gets contacted with object surface and stop rotating around proximal interphalangeal joint. Finally, the distal digit rotates until it gets contacted with the object. Therefore, all these movement patterns during the object grasping show the adaptive grasping of objects by the HyPro hand.

7.3. Grasping Patterns and Postures Achieved by HyPro. In order to identify the capability of HyPro hand in achieving the grasping patterns several tasks were given to observe the functionality. Figure 19 shows the set of activities achieved by HyPro for given tasks which are rest position, power grasp, index point, tip grasp lateral grasp, and hook grasp. All the tasks were achieved successfully by the HyPro.

It verified that the HyPro is capable of achieving all five grasping patterns. From the statistics, the considered set of grasping patterns has frequency of 72.2% out of all grasping patterns used in ADL [13, 30]. Hence, HyPro is capable of performing more than 70% of task found in ADL.

7.4. Force Exerted by Prosthetic Fingertip. From the results of the experiment, average fingertip force is plotted against input force given by pulling of the tendon (see Figure 20). It is found that at least 3.34 N force is needed for starting the flexion movement in prosthetic fingers and prosthetic finger exerts 0.1 N force on the object during the grasp with the increment of 1 N force of body power. In order to reduce the frictional losses, an efficient design of tendon flow paths is needed in future developments.

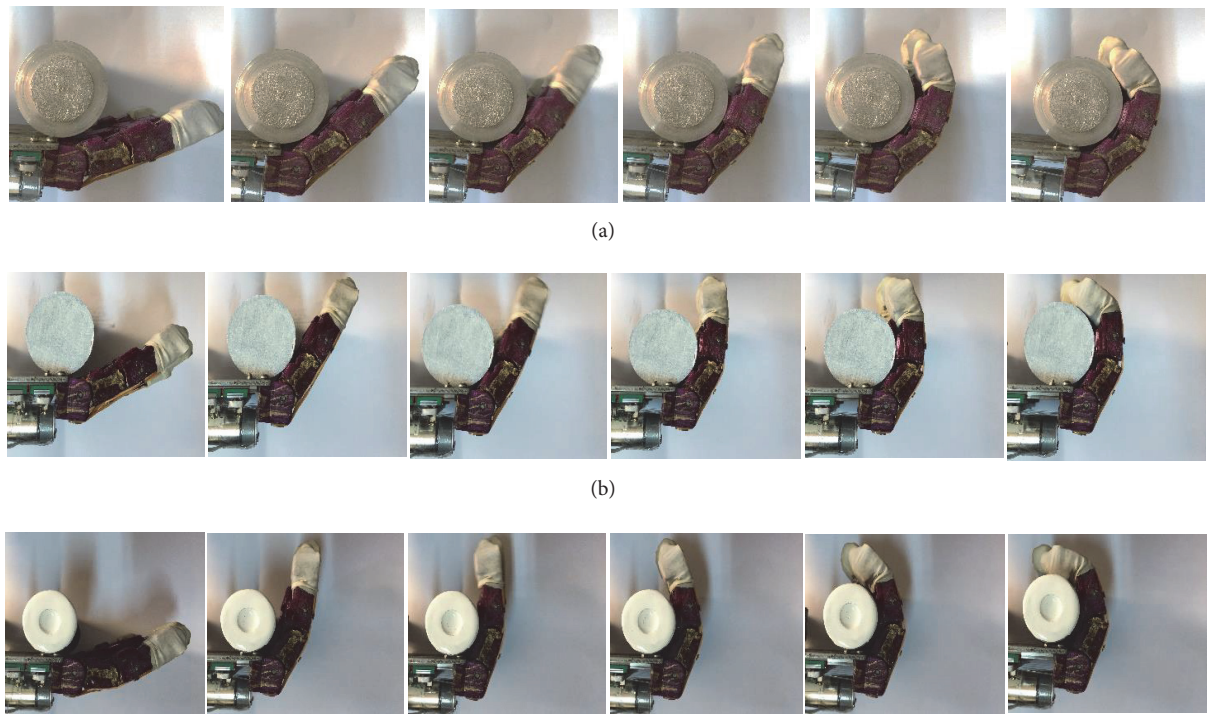

(a)

(b)

(c)

Figure 18: Adaptive grasping of objects: (a) grasping 52 mm diameter shaft; (b) grasping 45 mm diameter shaft; (c) grasping 32 mm diameter shaft.

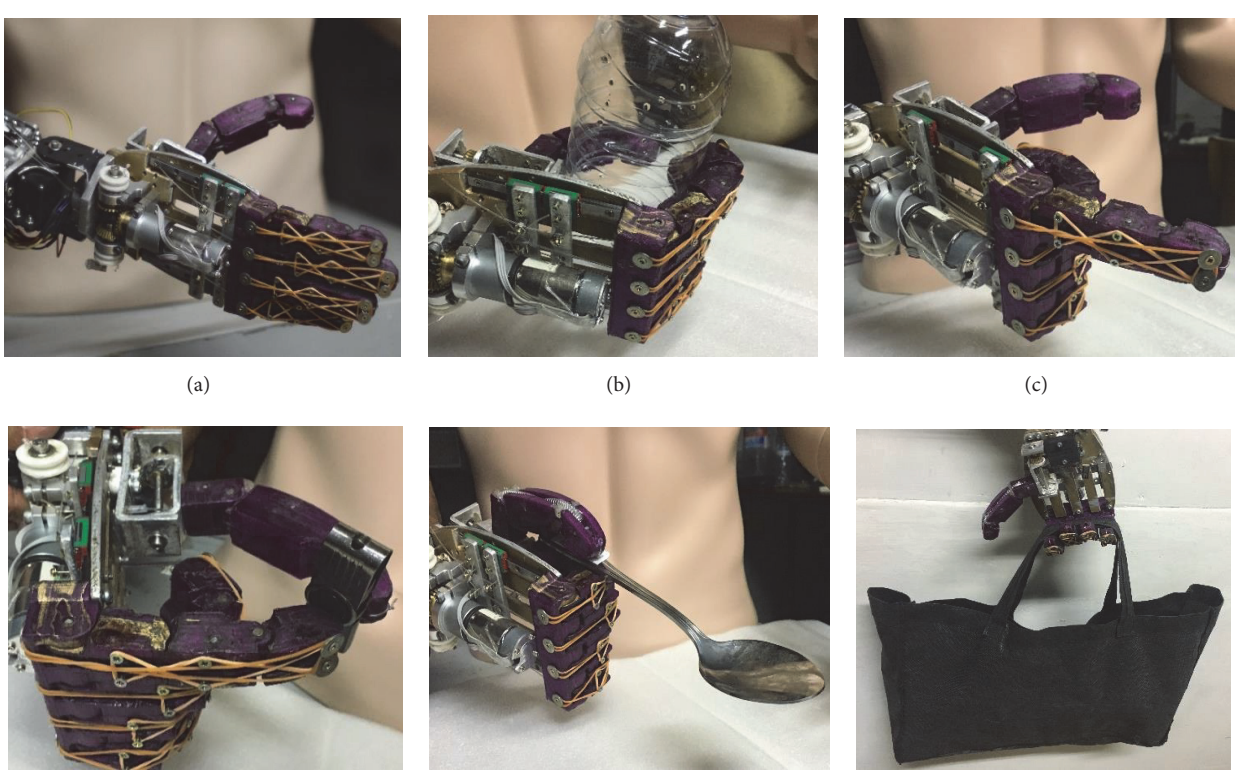

(a) (b) (c)

(d) (e) (f)

Figure 19: Grasping patterns achieved: (a) rest position; (b) power grip; (c) index point; (d) tip grip; (e) lateral grip; (f) hook grip.

Table 6: Power for executing the desired grasping patterns.

	% of total ADL	% of achievable patterns, f	Energy, body power, b_p (Ws)	Energy, electric power, e_p (Ws)	$f \times b_p$ (Ws)	$f \times e_p$ (Ws)
Power grasp	40%	55.4%	21.21	0	11.75	0.00
Index finger extension	13%	18.0%	0	18.79	0.00	3.38
Tip grasp	7%	9.7%	3.53	14.83	0.34	1.44
Lateral grasp	12%	16.6%	5.3	23.36	0.88	3.88
Hook grasp	0.2%	0.3%	0	13.19	0.00	0.04
Total energy consumption					12.97	8.74
% energy consumption					59.7%	40.3%

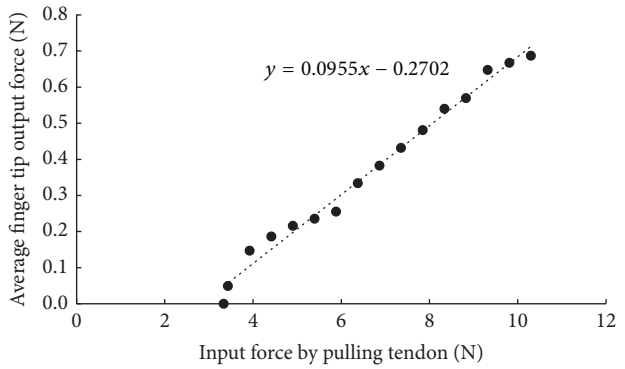

Figure 20: Relationship between average fingertip output force and input force.

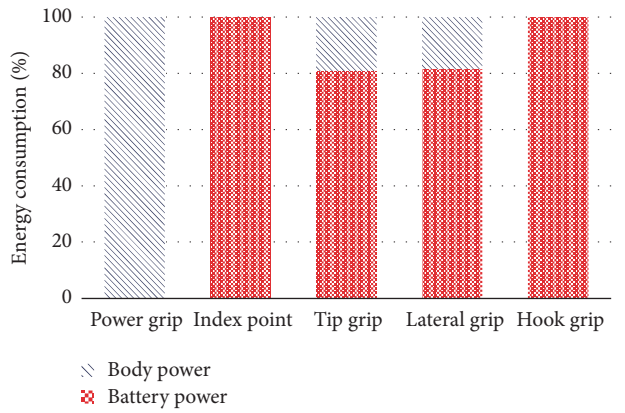

Figure 21: Energy distribution of each grasping pattern.

7.5. Energy Consumption and Power Saving. The energy required for hand preshaping and grasp execution is calculated using the electric current values obtained from the experiments explained in Section 6.4. Table 6 depicts the frequencies and the energy consumed using body power and electric power for each grasping patterns. If the hand is fully operated by the electric power, the total energy consumption of the battery would be the combination of both electric and body energy consumption. According to Table 6, HyPro has the ability of saving 59.7% of battery usage compared to being fully electrically powered. This considerable amount of battery power saving is mainly because of the power grasp being the most frequent pattern used in ADL. Hence, the hybrid powering concept enables minimizing the battery power consumption which leads to increase battery life. Moreover, the required power from the body movements of the wearer has decreased with the hybrid powering concept. This helps with more comfort and reduces fatigue in repetitive usage of the prosthesis.

Figure 21 shows the energy distribution between body power and battery power when performing each grasp. According to the battery power consumption for different grasps, the power grasp does not require the battery power. Externally powered prostheses are usable when only the power is available [8]. However, the HyPro is capable of performing power grasp even without the electric power. Therefore, it is one of the key advantages of the hybrid powering concept.

8. Conclusion

This paper proposed a hybrid-powered transradial robotic prosthesis, HyPro which can achieve five grasping patterns. The hand unit of HyPro is adopted with hybrid powering concept for grasp function restoration by using both body power and electric power. The proposed hand unit has 15 DoF and actuated only using two electric motors and body power. The wrist unit is capable of achieving two DoF: wrist flexion-extension and supination-pronation.

The complexity of controlling the motors is reduced since only two motors are used in this robotic prosthesis. Object grasping can be performed well since the amputee can control the force applied by prosthetic fingers by controlling his body movement from shoulder protraction-retraction. Compared to body-powered prostheses, HyPro has the ability to arrange prosthetic fingers for the desired grasping pattern using electric power. Hence, it does not require to change terminal devices in achieving different grasping patterns as in the conventional body-powered prosthesis. According to the results, the proposed hand unit is capable of saving 60% of the electric power. Moreover, the prosthetic fingers are capable of adapting to grasp objects like natural human fingers. Besides that, the hybrid design leads to other benefits such as reduction of complexity of controlling actuators and capability of using power grasp while electric power being absent. In particular, a bilateral amputee can use HyPro without the assistance of external party as it does not require

replacing terminal devices or performing switching action as with most commercially available prostheses.

Conflicts of Interest

The authors declare that they have no conflicts of interest.

References

[1] "ISHN.com - the magazine for safety & health professionals who direct safety & health programs in high-hazard workplaces," http://www.ishn.com/.

[2] D. S. V. Bandara, R. A. R. C. Gopura, K. T. M. U. Hemapala, and K. Kiguchi, "A multi-DoF anthropomorphic transradial prosthetic arm," in *IEEE RAS/EMBS International Conference on Biomedical Robotics and Biomechatronics*, pp. 1039–1044, São Paulo, Brazil, 2014.

[3] D. S. V. Bandara, R. A. R. C. Gopura, K. T. M. U. Hemapala, and K. Kiguchi, "Upper extremity prosthetics: current status, challenges and future directions," in *International Symposium on Artificial Life and Robotics*, pp. 875–880, Beppu, Oita, Japan, 2012.

[4] G. ElKoura and K. Singh, "Handrix: Animating the Human Hand," in *SIGGRAPH Symposium on Computer Animation*, pp. 110–119, University of Toronto, Canada, 2003.

[5] K. A. Raichle, M. A. Hanley, I. Molton et al., "Prosthesis use in persons with lower- and upper-limb amputation," *Journal of Rehabilitation Research and Development* , vol. 45, no. 7, pp. 961–972, 2008.

[6] F. Cordella, A. L. Ciancio, R. Sacchetti et al., "Literature review on needs of upper limb prosthesis users," *Frontiers in Neuroscience*, vol. 10, pp. 1–14, 2016.

[7] M. K. Hafshejani, M. Sattari Naeini, and A. Langari, "On the functional limitation in below elbow amputation men using Mechanical and Myoelectric prosthesis via TAPES questionnaire," *Life Science Journal*, vol. 9, no. 4, pp. 5579–5582, 2012.

[8] C. L. Semasinghe, J. L. B. Prasanna, H. M. Kandamby, R. K. P. S. Ranaweera, D. G. K. Madusanka, and R. A. R. C. Gopura, "Transradial prostheses: Current status and future directions," in *Manufacturing & Industrial Engineering Symposium*, pp. 1–7, Colombo, Sri Lanka, 2016.

[9] D. S. Childress and J. N. Billock, "An experiment with the control of a hybrid prosthetic system; electric elbow, body-powered hook," *Bulletin of Prosthetics Research*, vol. 10, no. 14, pp. 62–77, 1970.

[10] M. Stobbe, M. R. Dawson, and H. Jacqueline, "Development of a Hybrid Body Powered Transradial. Prosthesis with Myoelectric Switching," http://www.albertahealthservices.ca/grh/Page14577.aspx.

[11] J. C. Becker and N. V. Thakor, "A study of the range of motion of human fingers with application to anthropomorphic designs," *IEEE Transactions on Biomedical Engineering*, vol. 35, no. 2, pp. 110–117, 1988.

[12] S. Tanrikulu, S. Bekmez, A. Üzümcügil, and G. Leblebicioglu, "Anatomyand Biomechanics of the Wrist and Hand," *Sports Injuries*, pp. 1–9, 2014.

[13] M. J. Barakat, J. Field, and J. Taylor, "The range of movement of the thumb," *HAND*, vol. 8, no. 2, pp. 179–182, 2013.

[14] R. A. R. C. Gopura, D. S. V. Bandara, K. Kiguchi, and G. K. I. Mann, "Developments in hardware systems of active upper-limb exoskeleton robots: A review," *Robotics and Autonomous Systems*, vol. 75, pp. 203–220, 2016.

[15] T. Feix, J. Romero, H.-B. Schmiedmayer, A. M. Dollar, and D. Kragic, "The GRASP taxonomy of human grasp types," *IEEE Transactions on Human-Machine Systems*, vol. 46, no. 1, pp. 66–77, 2016.

[16] L. Wu, G. Carbone, and M. Ceccarelli, "Designing an under-actuated mechanism for a 1 active DOF finger operation," *Mechanism and Machine Theory*, vol. 44, no. 2, pp. 336–348, 2009.

[17] Upper Limb Prosthetics Information, http://www.upperlimb-prosthetics.info/index.php?p=1_9_Body-Powered.

[18] L. Resnik, S. L. Klinger, and K. Etter, "The DEKA Arm: Its features, functionality, and evolution during the veterans affairs study to optimize the DEKA Arm," *Prosthetics and Orthotics International*, vol. 38, no. 6, pp. 492–504, 2014.

[19] E. Kayaoglu, "DLR - Institute of Robotics and Mechatronics - Data sheet of DLR Hand II," http://www.dlr.de/rmc/rm/en/desktopdefault.aspx/tabid-3802/6102_read-8922/.

[20] H. Liu, K. Wu, P. Meusel et al., "Multisensory five-finger dexterous hand: The DLR/HIT hand II," in *Proceedings of the IEEE/RSJ International Conference on Intelligent Robots and Systems (IROS '08)*, pp. 3692–3697, September 2008.

[21] J. L. Pons, E. Rocon, R. Ceres et al., "The MANUS-HAND dextrous robotics upper limb prosthesis: mechanical and manipulation aspects," *Autonomous Robots*, vol. 16, no. 2, pp. 143–163, 2004.

[22] A. Polhemus, B. Doherty, K. Mackiw, R. Patel, and M. Paliwal, "uGrip II: A Novel Functional Hybrid Prosthetic Hand Design," in *Proceedings of the 39th Annual Northeast Bioengineering Conference, (NEBEC '13)*, pp. 303-304, USA, April 2013.

[23] Touchbionics.com, "i-limb ultra — Touch Bionics," http://www..touchbionics.com/products/active-prostheses/i-limb-ultra.

[24] Ottobock.co.uk, "Solution overview upper limb prosthetics - Ottobock UK," https://www.ottobock.co.uk/prosthetics/upper_limbs_prosthetics/product-systems/.

[25] D.-P. Yang, J.-D. Zhao, Y.-K. Gu et al., "An anthropomorphic robot hand developed based on underactuated mechanism and controlled by emg signals," *Journal of Bionic Engineering*, vol. 6, no. 3, pp. 255–263, 2009.

[26] Hosmer.com, "Hosmer Hooks," http://hosmer.com/products/hooks/index.html.

[27] Bebionic.com, "Life changing myoelectric hand packed with the latest technology - Bebionic," http://bebionic.com/the_hand.

[28] J. Hamill and K. M. Knutzen, *Biomechanical Basis of Human Movement*, Lippincott Williams & Wilkins, Pa, USA, 2006.

[29] D. S. V. Bandara, R. A. R. C. Gopura, G. Kajanthan, M. Brunthavan, and H. I. M. M. Abeynayake, "An under-actuated mechanism for a robotic finger," in *Proceedings of the 4th Annual IEEE International Conference on Cyber Technology in Automation, Control and Intelligent Systems, (IEEE-CYBER '14)*, pp. 407–412, China, June 2014.

[30] J. Z. Zheng, S. De La Rosa, and A. M. Dollar, "An investigation of grasp type and frequency in daily household and machine shop tasks," in *Proceedings of the 2011 IEEE International Conference on Robotics and Automation, (ICRA '11)*, pp. 4169–4175, China, May 2011.

[31] G. I. Bain, N. Polites, B. G. Higgs, R. J. Heptinstall, and A. M. McGrath, "The functional range of motion of the finger joints," *Journal of Hand Surgery (European Volume)*, vol. 40, no. 4, pp. 406–411, 2015.

[32] C. Pylatiuk, S. Schulz, and L. Döderlein, "Results of an internet survey of myoelectric prosthetic hand users," *Prosthetics and Orthotics International*, vol. 31, no. 4, pp. 362–370, 2007.

[33] P. Rea, "On the design of underactuated finger mechanisms for robotic hands," in *Advances in Mechatronics*, H. Martinez-Alfaro, Ed., 2011.

[34] Anthropometry and Biomechanics, "Msis.jsc.nasa.gov," https://msis.jsc.nasa.gov/sections/section03.htm.

Hindawi
Journal of Robotics
Volume 2018, Article ID 6756027, 12 pages
https://doi.org/10.1155/2018/6756027

Research Article

Biomechanic and Energetic Effects of a Quasi-Passive Artificial Gastrocnemius on Transtibial Amputee Gait

Michael F. Eilenberg, Ken Endo, and Hugh Herr

Biomechatronics Group, MIT Media Lab, Massachusetts Institute of Technology, Cambridge, MA 02139, USA

Correspondence should be addressed to Hugh Herr; hherr@media.mit.edu

Received 15 April 2017; Revised 16 August 2017; Accepted 25 September 2017; Published 1 March 2018

Academic Editor: Kazuo Kiguchi

State-of-the-art transtibial prostheses provide only ankle joint actuation and thus do not provide the biarticular function of the amputated gastrocnemius muscle. We develop a prosthesis that actuates both knee and ankle joints and then evaluate the incremental effects of this prosthesis as compared to ankle actuation alone. The prosthesis employs a quasi-passive clutched-spring knee orthosis, approximating the largely isometric behavior of the biological gastrocnemius, and utilizes a commercial powered ankle-foot prosthesis for ankle joint functionality. Two participants with unilateral transtibial amputation walk with this prosthesis on an instrumented treadmill, while motion, force, and metabolic data are collected. Data are analyzed to determine differences between the biarticular condition with the activation of the knee orthosis and the monoarticular condition with the orthosis behaving as a free-joint. As hypothesized, the biarticular system is shown to reduce both affected-side knee and hip moment impulse and positive mechanical work in both participants during the late stance knee flexion phase of walking, compared to the monoarticular condition. The metabolic cost of walking is also reduced for both participants. These very preliminary results suggest that biarticular functionality may provide benefits beyond even those of the most advanced monoarticular prostheses.

1. Introduction

The loss of a leg below the knee can have a formidable impact on one's quality of life [1–3]. The widespread, passive ankle-foot prostheses on the market today provide only a rudimentary approximation to the function of a human ankle joint [4, 5]. Instead of providing net mechanical work to the wearer during walking, these passive devices act at best in a spring-like manner; they can only provide as much mechanical energy return as is provided to them by the wearer, and they do not provide the articulation normally seen in the biological ankle-foot complex during walking. As evidence of this technological limitation, transtibial amputees display a variety of pathological features of their walking gaits. Specifically, transtibial amputees naturally select a 30–40% slower walking speed than those without amputation, and when walking at the same pace as a nonamputee, these amputees require 20–30% more metabolic power than their nonamputee counterparts [4, 6–8]. Further, these amputees exhibit increased levels of hip positive power during late stance phase. This increased hip power may be a compensatory response to lack of calf muscle function and could contribute to the aforementioned increase in metabolism while walking [4].

In the last several years, robotic advances in prosthetic technology have led to the introduction of powered ankle-foot prostheses (EmPower, BionX Medical Technologies, Inc., Bedford, MA), which, unlike the passive conventional devices, provide levels of mechanical work comparable to those provided by the human ankle-foot complex. As a result of this functional improvement, many of the aforementioned gait pathologies have been drastically reduced; amputees using the powered prostheses have preferred walking speed, metabolic cost at a given speed, and contralateral limb impacts that are not significantly different from those of nonamputees [9, 10]. These improvements are thought to stem from the propulsive net mechanical work provided by these devices to the wearer [9], as this propulsion helps to

redirect the center-of-mass, thereby reducing collisions of the contralateral limb [11–14]. This ankle propulsion may also assist swing-initiation of the affected-side limb [15–18].

These new prosthetic devices are, however, limited to emulating the function of the ankle-foot complex alone and consequently cannot restore the full function of the powerful gastrocnemius muscle. The gastrocnemius provides not only a plantar flexion moment at the ankle, but also a flexion moment at the knee. Without the knee-flexing function, compensatory mechanisms are required. Indeed, transtibial amputees exhibit higher hamstring muscle activity during level-ground walking than nonamputees [19], possibly as an attempt to stabilize or flex the knee in place of the nonfunctional gastrocnemius muscle. This higher muscle activity is still apparent when amputees walk with the powered ankle-foot prostheses, indicating that a monoarticular intervention at only the ankle-foot complex may not be sufficient to restore biological function. It is possible that this pathological muscle activity has detrimental effects on amputee gait. However, little work has been done to develop devices for restoring this missing gastrocnemius functionality.

Since those with transtibial amputation maintain their biological knee joints, a direct assistance of these joints requires the use of an exoskeletal device such as an orthosis that provides assistance in parallel to the existing joint. A variety of robotic orthoses have been developed to assist human knee joints for locomotion. Many of these devices utilize active components such as electric motors [20–22] or pneumatic actuators [23–26], but these elements tend to require a large power source or otherwise require off-board tethered actuation, limiting the scope of their applicability. Alternatively, some researchers have developed quasi-passive knee exoskeletons that do not provide net mechanical power to the wearer but instead require at most the minimal input power to operate the electronics and mechanical components [27–30]. In one such study, a spring-loaded, custom toothed clutch was designed for assisting extension moment during human running [29]. This device locked to support the knees of nonamputee participants during the stance phase and unlocked to be a free joint during the swing phase. Using this quasi-passive device, large knee moments of 190 Nm could be supported with an exoskeletal joint weighing only 710 grams. This, and other exoskeletons have been built to assist with knee extension in nonamputees, but no such devices to date have been built for knee flexion assistance, particularly for the gastrocnemius, in those with transtibial amputation.

In order to develop an assistive device for the gastrocnemius, it is important to first understand how this muscle functions. In vivo ultrasonography shows that the gastrocnemius muscle fascicle length is largely isometric during the early and mid-stance phases of level-ground walking [31], indicating that the passive tissues such as tendons are responsible for much of the power delivery from the gastrocnemius. Hence, the gastrocnemius may be approximated by a clutched spring, with the spring representing the compliant tendinous structures, and the clutch representing the isometrically acting muscle fibers. Indeed, a model of human gait by Endo and Herr with only spring-clutch structures at the knee joint was able to achieve human-like metabolic economy, while capturing the dominant kinetic features of human walking [32–34]. It is therefore possible that a physical clutch in series with a spring can provide much of the missing knee function of the gastrocnemius in transtibial amputees.

Researchers have begun to study the effects of a robotic device at the affected-side knee to provide the knee flexion moment of the missing gastrocnemius. In the first such study [35], a quasi-passive knee orthosis, dubbed an artificial gastrocnemius (AG) was built, based on the spring-clutch representation of the gastrocnemius in the aforementioned Endo-Herr model. The AG was physically realized as clutchable rotary spring at the orthosis knee joint. Two copies of this AG, worn along with a powered-ankle-foot prosthesis (PAFP), was tested on both legs of one bilateral transtibial amputee, with promising results: the amputee's metabolic energy expenditure was reduced with the AG-PAFP condition, compared to the amputee walking at the same speed with only conventional leaf-spring-type ankle-foot prostheses. However, since the PAFP was not tested independently of the AG, it is not clear what incremental effects the AG had over the PAFP alone. A need, therefore, exists to evaluate the incremental biomechanical and metabolic effects of the AG.

In this study, we design and evaluate a new version of the AG unit, based on the exoskeletal knee clutch design [29]. We evaluate the effects of this new AG-PAFP on the walking gait of transtibial amputees. We focus on the late stance knee flexion phase of walking, during which the knee flexes to prepare for the swing phase, so to detect improvements on the pathologies thought to be most likely affected by the lack of calf muscle function [4]. We expect that the energy stored in the spring of the AG early in the gait cycle will be returned during late stance knee flexion to replace positive muscle work. Specifically, we hypothesize that including a clutched-spring AG at the affected-side knee joint of transtibial amputees in conjunction with a PAFP will reduce both biological flexion moment impulse and positive mechanical work of the affected-side knee and hip joints during late stance knee flexion, as compared to the same conditions with only the PAFP. We further hypothesize that these changes will provide a corresponding reduction in metabolic cost of walking. We expect that this metabolic reduction will stem from reduced joints moments and net work in the affected knee and hip joints. We evaluate these hypotheses by analyzing the kinematics, kinetics, and metabolism of two transtibial amputees walking with the AG-PAFP combination on an instrumented treadmill. We compare these data between the two conditions where the AG is active versus acting as a free-joint.

2. Methods

Two devices were used for the intervention in this study. A powered ankle-foot prosthesis provided ankle function in the sagittal plane, and a quasi-passive artificial gastrocnemius (AG), that was a clutched-spring joint, was mounted on a knee orthosis on the affected-side knee. Together, these two devices represented a biarticular transtibial prosthesis that could actuate both joints independently.

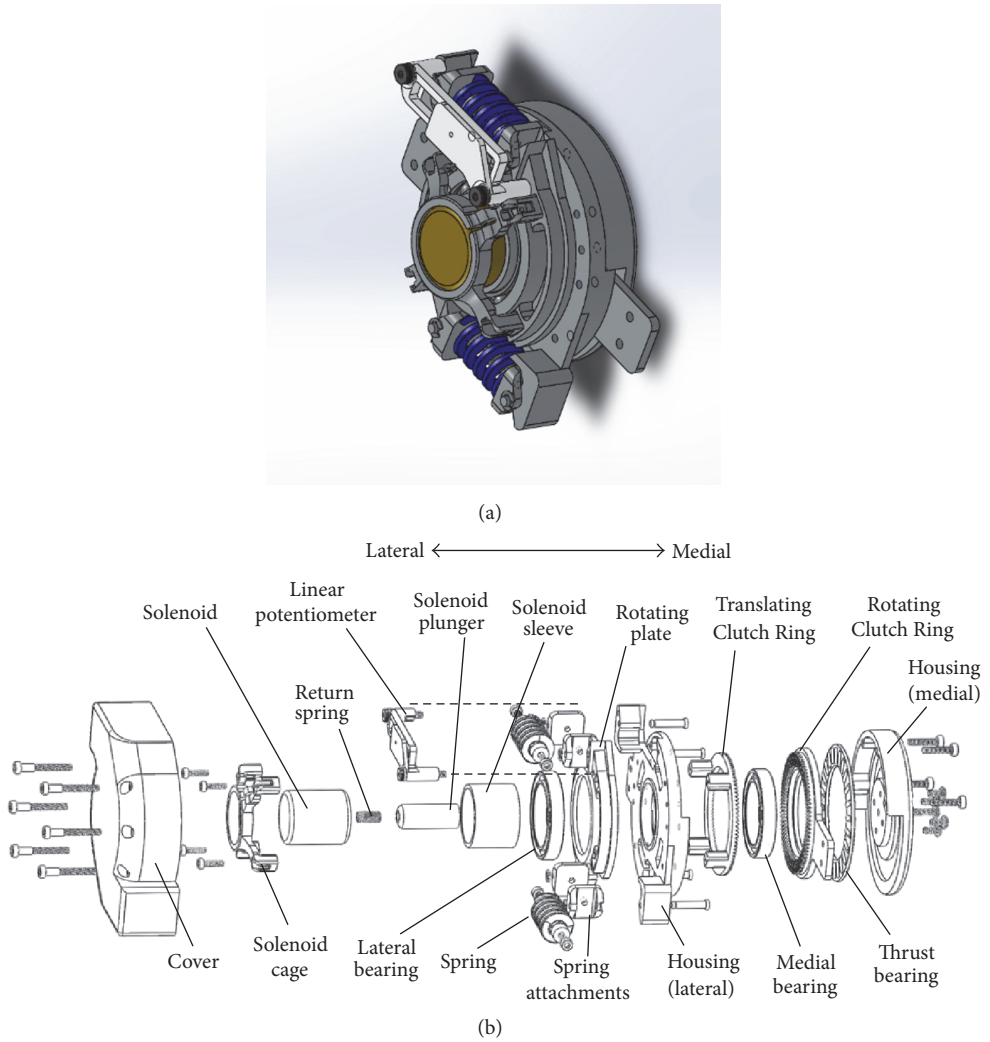

Figure 1: Joint mechanism of the quasi-passive artificial gastrocnemius. The exploded view of the joint design (b) is shown along with a rendering of the assembled joint without the cover (a). The *Housing* was attached to the proximal part of the orthosis, and the *Rotating Clutch Ring* attached to the distal part of the orthosis.

2.1. Powered Ankle-Foot Prosthesis. An EmPower powered ankle-foot prosthesis (BionX, Bedford, MA) was used as the prosthesis for all clinical trials. This prosthesis had the capability of providing positive net power at levels comparable to the human ankle-foot complex [9]. At the core of the prosthesis was a series elastic actuator, comprising a brushless DC motor, ball screw, and carbon fiber leaf spring. For dorsiflexion angles, a rigid hard-stop engaged, both to reduce the torque required by the motor in dorsiflexion and to act as a safety feature in the event of a power failure. The total mass of the prosthesis and battery was 1.8 kg.

The prosthesis controller employed a positive force feedback strategy that served to approximate the biological muscle dynamics and neural reflexes. A wireless communication link enabled real-time tuning of the control parameters.

2.2. Clutch-Spring Joint. The AG, shown in Figure 2, was a knee orthosis, comprising a pair of polycentric hinges that connected a thigh cuff to an 1/8″-thick aluminum bracket made of aluminum sheet stock (6061-T6). The bracket connected to the base of a participant's socket, between the prosthetic pylon attachment and the socket. The proximal side of the brace was strapped to the participant's thigh as a typical knee orthosis. A custom, dog-tooth rotary clutch spring with series compliance was attached lateral to the knee, in parallel with the hinges.

This clutch-spring joint was based on a previous design [29] but had the addition of series compliance and reversed the direction of the clutch teeth so that the teeth engaged to provide a knee flexion moment, rather than an extension moment to the wearer. In addition, our device lacked a planetary gear train that was present in the previous work. The machined clutch components were made of 6061-T6 aluminum alloy and included two rings of dog teeth, brought together by the action of a solenoid (LT8x9, Guardian Electric, Woodstock IL). As in Figure 1, the clutch controlled the relative rotation of the *Housing* to the *Rotating Clutch Ring*. A solenoid was built into the middle of the joint and translated

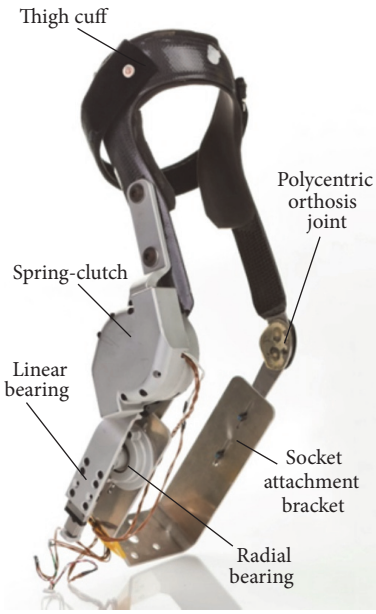

Figure 2: Quasi-passive artificial gastrocnemius (photo credit: Chris Conti Photography).

in the medial-lateral direction under action of its actuation power and a return spring. When the solenoid was energized, the *Translating Clutch Ring was engaged with the Rotating Clutch Ring*. The *Translating Clutch Ring* constrained the rotation of the *Rotating Plate* that, in turn, was connected to the *Housing* through two tangential linear compression springs. Thus, when the solenoid was energized, the *Housing* was coupled to the *Rotating Clutch Ring* through these springs. When the solenoid was inactive, the return spring separated the *Translating Clutch Ring* from the *Rotating Clutch Ring* and, hence, they were then free to rotate with respect to each other. The return spring stiffness was chosen experimentally so that when the clutch developed more than 0.5 Nm of torque, the tooth friction prevented the two rings from separating. This tooth-binding effect acted as a safety mechanism and was included as a part of the control algorithm, as described in Section 2.8. This aforementioned friction maintained the clutch in a clutched state until the torque level dropped back to the safe value of 0.5 Nm. As a result, the bulk of the stored spring energy could only be released gradually into the wearer's leg, rather than suddenly into the mechanism.

The *Housing* of the clutch was bolted to the thigh cuff of the knee orthosis. The *Rotating Clutch Ring* connected to a distal output link with a linear ball bearing and radial ball bearing, acting in series. These bearings accommodated for the kinematic difference between the polycentric hinges of the orthosis and the single-axis rotation of the clutch joint. Thus, only forces tending to flex or extend the joint could be transmitted through this set of bearings.

2.3. Sensing. The AG had onboard sensing for use in the control algorithm. Knee angle of the AG was measured using a 10 kOhm rotary potentiometer. Knee moment provided by the spring-clutch element to the wearer was estimated by measuring the deflection of one of the two identical tangential springs with an 8 kOhm linear potentiometer. The voltage output from the potentiometer was scaled with an experimentally determined gain to provide an estimate of torque applied by the AG to the wearer. This gain was found by applying various tangential forces to the distal end of the brace using a force gauge (gauge moment arm = 28 cm), while the clutch was engaged. With this force and the known moment arm of the gauge, the applied knee moment was computed and compared to voltage readings from the linear potentiometer to achieve a scaling factor for conversion from voltage to Nm/rad. The resulting measured spring-clutch knee torque reading is subsequently referred to as the AG knee moment. A similar calibration procedure was performed using the AG angle-sensing rotary potentiometer and an infrared camera system (model T40s, Vicon Motion Systems Ltc, Oxford, UK). In this calibration procedure, reflective markers were placed on the center of the joint and on the distal and proximal ends of the orthosis. Marker-based joint angle was computed by obtaining the relative angles of lines connecting the distal and proximal markers to the joint center marker. These angles were then compared to voltage readings from the angle-sensing potentiometer. Prosthesis-side ground contact was detected using a resistive pressure sole footswitch (model: FSW, B&L Engineering, Santa Ana, CA), inserted into the shoe between the prosthetic foot and the insole.

2.4. Failure Analysis. Unlike the titanium toothed rings in the exoskeletal clutch [29], the clutch in the present study was made from aluminum. Thus, it was necessary to reevaluate the load-bearing limits of the teeth. Finite element analysis (FEA) was performed using Solidworks (DS Solidworks Corp, Waltham, MA) to ensure this clutch could support the required knee moments. Tangential loads were simulated symmetrically on the tips of all teeth to simulate worst-case loading scenario.

2.5. Modeling and Spring Stiffness Selection. The selection of the spring constants for the tangential springs allowed for the control of rotary stiffness of the clutch-spring element. It was desirable for the stiffness of the clutch-spring joint to be such that the spring-clutch behavior of the artificial gastrocnemius would most closely reproduce the gastrocnemius muscle behavior of a healthy gastrocnemius. To this end, walking data from healthy nonamputees was fed as input to a modified version of the Endo-Herr sagittal-plane human leg model [32–34] during the development of the artificial gastrocnemius in [35].

2.6. Control. The quasi-passive artificial gastrocnemius produced no positive net mechanical work to the wearer but still required a control system to determine the appropriate times to engage and disengage the clutch. This controller took knee joint angle and stance information as input and engaged the clutch appropriately through each gait cycle. The clutch was controlled to engage at maximum stance knee flexion angle, enabling the spring to store energy during the subsequent

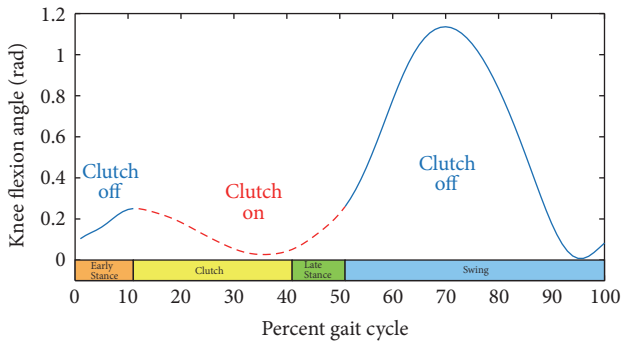

FIGURE 3: Example action of the clutch engagement. A typical knee flexion angle profile is shown for level-ground walking. The dashed red section indicates the region in the gait cycle when the clutch in the AG would be engaged. Colored bars show the sequence of intended finite-state-machine state transitions.

knee extension and flexion into swing phase, as shown in Figure 3.

2.7. Control Electronics. The computer platform for controlling the AG was a commercial single-board computer (model: Raspberry Pi Version B, Raspberry Pi Foundation, Cambridgeshire, UK). The computer was equipped with an 800 MHz ARM11 processor, 512 MB SDRAM, with Linux Debian. The system was powered by a 6-cell lithium polymer battery (nominal voltage of 22.2 V).

2.8. Control Algorithm. High-level control was implemented using a finite state machine, implemented in Python. The gait cycle was divided into four states, shown in Figure 4: (1) *Swing*; (2) *Early Stance*; (3) *Clutched*; and (4) *Late Stance*.

The *Swing* state was triggered from any other state when the affected-side foot left the ground, as detected by a drop in footswitch signal, FSW, to less than a fraction, foot_{SW} of the maximum possible signal. During *Swing*, the clutch was disabled, allowing the knee to swing freely.

The *Early Stance* state was triggered from the *Swing* state at foot contact of the affected-side with the ground, defined as FSW increasing to the stance threshold, foot_{ST}, provided that the time elapsed in the current state, t_{state}, was at least the minimum time required for the *Swing* state, t_{swing}. During the *Early Stance* state, the clutch was disabled, and the controller monitored the knee angle of the brace for maximum stance knee flexion, at which point the *Clutched* state would be engaged. A least squares algorithm, similar to the one used previously [29], continually predicted the time remaining before maximum knee flexion angle. This prediction provided time to initiate the engagement of the clutch, so that the clutch would be fully engaged as close as possible to the time of maximum knee flexion. In addition to this knee flexion detection algorithm, two safety features were in place to ensure that the motions detected were resulting from a walking gait. The *Clutched* state could only be enabled if the following two conditions were also met: (1) the knee was flexed a minimum angle of θ_{ES} from the angle at heel strike, θ_{HS}; (2) the maximum knee flexion angular velocity, $\dot{\theta}_{\text{max}}$, measured during the *Early Stance* state was at least $\dot{\theta}_{\text{ES}}$. The values θ_{ES} and $\dot{\theta}_{\text{ES}}$ were experimentally determined during early testing as the lowest values that successfully prevented false-triggering of the *Clutched* state outside of a steady, level-ground walking gait (Table 1).

The *Clutched* state served to activate the clutch near the maximum knee flexion during stance phase of walking. This state was activated when the following criteria were met: (1) the maximum stance flexion angle was predicted to occur within the time t_{delay} of the current time, (2) the knee angle was flexed more than a threshold, θ_{ES}, and (3) the maximum knee flexion angular velocity, $\dot{\theta}$, during the *Early Stance* state exceeded a threshold $\dot{\theta}_{\text{ES}}$. Conditions (2) and (3) were used to differentiate a walking gait with slow, nongait motions, the latter of which did not warrant activation of the clutch.

The *Late Stance* state served to turn off the clutch after it engaged. Once the clutch spring began to develop force, the clutch teeth would bind, preventing the clutch from disengaging until the spring force dropped sufficiently. Therefore, the clutch solenoid was deactivated by entering the *Late Stance* state when the time elapsed in the *Clutched* state, t_{state}, exceeded the clutch timeout threshold, t_{cl}.

In order to maximize spring energy storage and return, it was desirable to engage the clutch as near as possible to the moment of peak knee flexion in the *Early Stance* state. In fact, the clutch solenoid needed to be engaged slightly before the desired clutching time, as to account for the time required to close the gap between the two sets of clutch teeth. To achieve the necessary prediction of peak stance flexion, a look-ahead algorithm was used.

First, the knee angle during the *Late Stance* state was approximated as parabolic, given this assumption, the location of the vertex of the parabola may be found by performing a linear fit to the knee angular velocity data, via running sums, and solving for the zero-crossing. The algorithm used here was similar to one described by [29]. However, the earlier algorithm assumed a fixed time step that was not applicable with the system in this study, as the computer platform was not a truly real-time system. Hence, the algorithm proposed here did not presume a fixed time step.

The parameter $\boldsymbol{\beta} = [\beta_0 \;\; \beta_1]^T$ that minimizes the error in the least squares sense of linear model $\hat{y}(t) = \beta_0 + \beta_1 x(t)$ to time-series data $(x(t), y(t))$ is

$$\boldsymbol{\beta} = \left(\mathbf{X}^T\mathbf{X}\right)^{-1}\mathbf{X}^T\mathbf{y}, \tag{1}$$

where the matrix $\mathbf{X}$ has elements

$$X_{i,j} = \frac{\partial \hat{\mathbf{y}}}{\partial \beta_j} = \begin{cases} 1, & j = 0 \\ x_i, & j = 1 \end{cases} \tag{2}$$

and x_i is the ith element in the discretely sampled $x(t)$ vector. Expanding (1) yields

$$\boldsymbol{\beta} = \frac{\begin{bmatrix} \sum x_i^2 \sum y_i + \sum x_i \sum x_i y_i \\ \sum x_i \sum y_i + W \sum x_i y_i \end{bmatrix}}{W \sum x_i^2 - \left(\sum x_i\right)^2}, \tag{3}$$

Table 1: Parameter values for the AG controller.

Parameter	Description	Value
foot_{ST}	Footswitch threshold for entering the *Early Stance* state; fraction of the maximum possible value	0.2
foot_{SW}	Footswitch threshold for entering the *Swing* state	0.15
t_{swing}	Minimum time in the *Swing* state before it is possible to exit *Swing*	200 ms
θ_{ES}	Minimum knee flexion angle (rad) during the *Early Stance* state before the clutch can be engaged	0.087 rad
$\dot{\theta}_{\text{ES}}$	Minimum knee flexion angular velocity that must be observed during the *Early Stance* state before the clutch can be engaged	1.2 rad/s
t_{delay}	Delay time required between activation of the solenoid and the full engagement of the clutch	50 ms
t_{cl}	Maximum time to energize the solenoid	400 ms

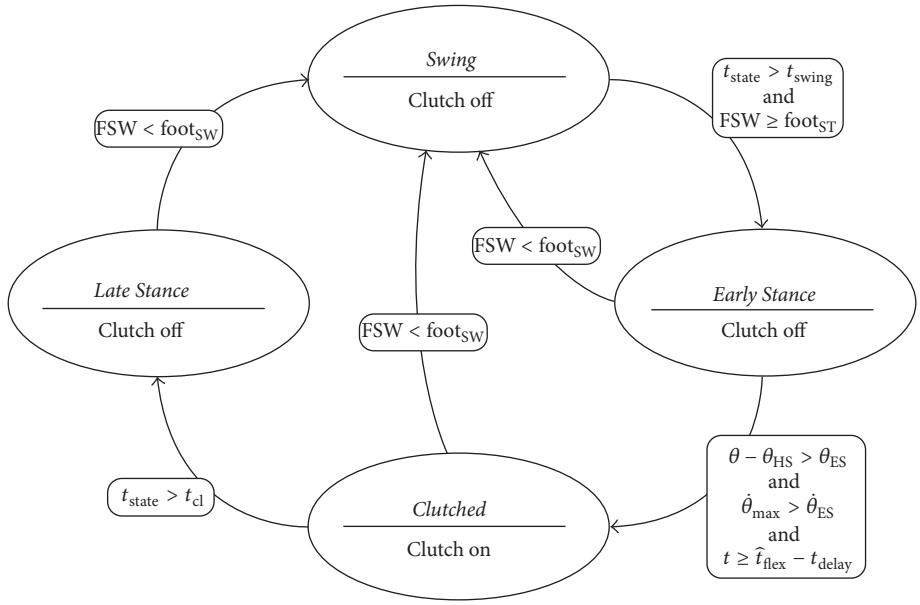

Figure 4: Finite state machine for the quasi-passive artificial gastrocnemius.

where all summations in (3) span i from 1 to W. For the task of estimating the angular velocity over time, the values of x_i were timestamps, and the values of y_i were knee angular velocity values. For the window of size W, the most recent W values of x and y were maintained in a queue. At each new timestep, the oldest values of x and y were popped from the queue, while the current x and y values were added to the queue, maintaining the 0th element as the first in the queue. This method allowed the sums to be updated each timestep without needing to store all values of the computed sums. Finally, the estimated time of the angular velocity zero-crossing was $\hat{t}_{\text{flex}} = -\beta_0/\beta_1$. It was found experimentally that the minimum error in clutching time between the initiation of the development of clutch torque and the peak knee flexion angle occurred when the clutch was engaged 50 ms prior to the predicted maximum knee angle. As a result, the time delay parameter, t_{delay}, was set to 50 ms.

2.9. Experimental Protocol. Two participants with below-knee amputation were involved in this study (Table 2). Both participants had right-side unilateral amputation and were of generally good health. The clinical evaluation was conducted at MIT (Cambridge, MA) and was approved by MIT's Committee on the Use of Humans as Experimental Subjects (COUHES). Each participant provided written, informed consent that was obtained before data collection was initiated.

Table 2: Amputee participant body parameters.

	Height (cm)	Weight (kg)
Subject 1	180	93
Subject 2	193	94

An infrared camera system (model T40s, Vicon Motion Systems Ltc, Oxford, UK) was used to track the three-dimensional motion, recorded at 100 Hz, of reflective markers, placed at 47 anatomical locations on the participants' bodies, based on the Helen Hayes marker model. Ground reactions forces and center of pressure locations were measured using a dual-belt instrumented treadmill (Bertec Corporation, Columbus, OH) with a sampling rate of 1 kHz. The net metabolic cost of walking during each condition was estimated using standard open-circuit gas exchange techniques (model: K4b2, COSMED, Rome, Italy).

At the beginning of each session, the participant was asked to don the powered prosthesis in place of their conventional prosthesis. The knee orthosis of the AG was then affixed to the prosthesis and donned by the participant.

For each participant, the prosthesis controller's power setting was adjusted using the commercial tuning app as the participant walked over a treadmill at 1.25 m/s so as to achieve net work from the prosthesis per step that was within one standard deviation of the mean for nonamputees walking at the same walking speed [36]. It was verified that the level of prosthesis net work remained within the desired range for both walking conditions for a given participant (0.045 to 0.16 J/kg) and that this level of net work stayed reasonably consistent across walking conditions for each participant.

A short time period of approximately 15 minutes was given to ensure that both the prosthesis and the artificial gastrocnemius orthosis were functioning properly. This acclimatization was evaluated by verifying that the clutch was engaging and disengaging at appropriate points in the gait cycle (as in Figure 3) and that the PAFP net mechanical work was reasonable as compared to biological values.

Both the powered prosthesis and artificial gastrocnemius were worn for all trials. The participants were asked to perform one standing trial to measure standing metabolism. Walking trials were performed on the treadmill at a speed of 1.25 m/s.

Two walking conditions were tested: (1) a baseline condition (*Baseline*) in which the AG acted as a free-joint at the knee with the spring-clutch disabled, and (2) an active condition (*Active*), in which the AG was controlled as a clutched spring at the knee with the described control algorithm. For both conditions, the powered ankle-foot prosthesis was active. The *Baseline* condition represented a monoarticular transtibial prosthesis, as the knee joint was a free-joint when the clutch was inactive. Yet the mass distribution of the device was identical to the *Active* condition. Thus, a direct comparison could be made to determine the incremental effects of the clutched-spring knee joint.

2.10. Data Processing. Fourth-order Butterworth filters were used to filter the marker position and ground reaction force data with 6 Hz and 25 Hz cutoff frequencies, respectively. The marker and force data were postprocessed through the SIMM (Musculographics Inc., Evanston, IL) inverse dynamics module to produce total joint moments and angles in three dimensions. However, only sagittal-plane dynamics were considered. Affected-side biological knee moment contribution was computed by subtracting the AG knee moment from the total knee moment estimated from the SIMM-based inverse dynamics.

Gait events were determined using vertical ground reaction force data from the embedded force plates. Approximate event timing was found by determining the times when the force increased beyond a 40 N threshold. Exact heel strike and toe-off times were found by progressing backward and forward in time, respectively, until the force value dropped to zero. Data were then cut to gait cycles based on heel strike times and resampled to 101 points. Gait cycles were discarded for the beginning and end of each trial, during the speed transients of the treadmill. Gait cycles in which the stride times were below 0.7 seconds or above 1.3 seconds or in which a foot crossed the midline of the treadmill were also discarded.

Table 3: Mechanical design parameters of the artificial gastrocnemius joint.

Parameter	Value
Maximum torque (Nm)	890
Torque sensor scale factor (Nm/V)	825
Number of teeth	90
Clutched-spring moment arm (mm)	32.1
Total orthosis mass (kg)	1.9

Joint powers were computed as the product of joint moments and joint velocities from SIMM-derived joint kinematics, where positive power was defined as that produced by the joint on the environment. Positive joint work during late stance knee flexion was computed as the positive contribution of the time-integral of joint power from maximum stance knee extension to toe-off. This region of the gait cycle was chosen for analysis because, as the knee flexes from the maximum extension angle, it provides an opportunity for the AG to provide positive power to the wearer. Joint flexion moment impulse was computed using the same integral for joint flexion moment. Net prosthesis work was computed by integrating the SIMM-derived joint torque over joint angle for the entire gait cycle.

Metabolic cost for each walking speed was computed by taking average oxygen and carbon dioxide data over a two-minute window at the end of each six-minute trial. The metabolic power was computed using the equation

$$P = K_{O_2}\dot{V}_{O_2} + K_{CO_2}\dot{V}_{CO_2}, \quad (4)$$

where P is the metabolic power in Watts, $\dot{V}_{O_2}$ is the volume flow rate of oxygen inhaled, $\dot{V}_{CO_2}$ is the volume flow rate of carbon dioxide exhaled, and K_{O_2} and K_{CO_2} are constants with values from literature [37], given as K_{O_2} = 16,580 W/L and K_{CO_2} = 4,510 W/L. The above equation is only valid for conditions when the metabolism is primarily aerobic. As a verification of this condition, the respiratory exchange ratio (RER), defined as $\dot{V}_{CO_2}/\dot{V}_{O_2}$, was monitored, and only metabolic results with RER values less than 1.1 were considered.

3. Results

3.1. Mechanical Design. The mechanical parameters of the design are summarized in Table 3. As in previous work [29], the teeth were manufactured using a contour milling process, and thus, the tooth spacing was limited by the 0.4 mm radius of the mills. Therefore, the tooth spacing was constrained to 4 degrees, or 90 teeth per revolution. The total mass of the orthosis, including battery and electronics, was 1.9 kg.

The aluminum teeth used in this design do not yield for applied knee flexion moments near to the expected values of 25 Nm [38] but start to yield at 35 times this expected load

Table 4: Net work per step by the powered ankle-foot prosthesis with the AG. The net work values were kept within the literature range of 0.045 to 0.16 J/kg.

	Baseline (J/kg)	Active (J/kg)
Subject 1	0.113 ± 0.028	0.130 ± 0.024
Subject 2	0.077 ± 0.016	0.082 ± 0.019

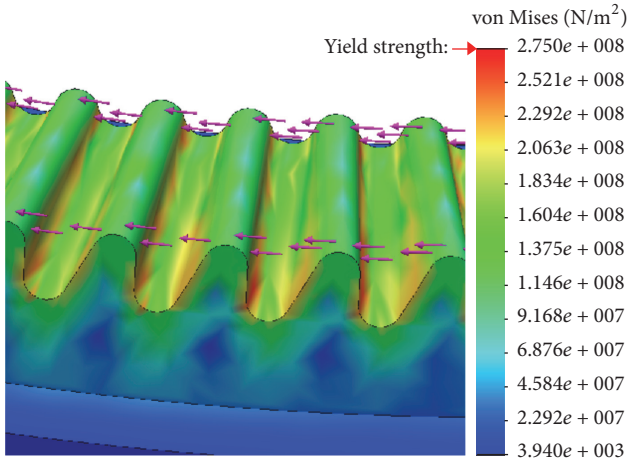

Figure 5: Results of finite element analysis with load evenly applied to all tooth tips tangentially. Results are shown for the yield condition, at which the applied torque to the clutch is 890 Nm.

(Table 3). The tooth stress at this failure load condition is shown in Figure 5.

3.2. Power Consumption. Given the solenoid specifications (22.2 V, 109 Ohms resistance), the power draw was 4.9 W. Assuming the maximum clutch-on time for each gait cycle of 0.4 ms and a typical cadence of 0.9 strides per second, the power consumption of the solenoid was 2.2 W. With the 1.1 W power draw of the Raspberry Pi, the average total power consumption of the device was 3.3 W during a typical walking gait.

3.3. Joint Spring Selection. The spring stiffness of the clutched-spring gastrocnemius element, derived from the modeling, was 92.9 Nm/rad [35]. To approximate this rotary stiffness about the knee joint, the two tangential linear compression springs were selected with spring constants of 51 N/mm. These springs acted on the joint with a moment arm of 32.1 mm, causing the equivalent joint rotary stiffness to be 105 Nm/rad.

3.4. Clinical Pilot Results

3.4.1. Acclimatization. In the time allotted for acclimatization, participants could walk with the AG and PAFP. Participants could walk comfortably with the AG, and the ankle prosthesis net work was appropriate for normal walking (see Table 4).

3.4.2. Ankle Prosthesis Net Work. As shown in Table 4, the net work produced by the powered ankle-foot prosthesis was within the desired range from literature [36].

3.4.3. Affected Knee Kinetics. Affected-side knee kinetics for both participants are shown in Figure 6 and summarized in Tables 5 and 6. Of particular note, the biological component of knee flexion moment impulse and the biological knee positive mechanical work during late stance knee flexion phase were both reduced by large percentage changes when subjects walked with the *Active* condition of the AG, compared to the *Baseline* condition.

3.4.4. Affected-Side Hip Kinetics. Hip flexion moment is shown in Figure 7, and hip flexion moment impulse values are summarized in Table 7. Hip net mechanical work values for both participants are shown in Table 8. As with the knee joint, both hip flexion moment impulse and positive mechanical work during late stance flexion were decreased slightly for both participants.

3.4.5. Metabolism. The net metabolic power (with the power required for standing subtracted out) is tabulated in Table 9. Both participants displayed small percentage reductions in metabolic cost when walking with the *Active* condition, as compared to the *Baseline* condition.

4. Discussion

Our novel design of a quasi-passive artificial gastrocnemius has been tested in our pilot study and found to be mechanically functional for the task of providing a flexion assist moment to the affected-side biological knee joint. The device exceeds the torque requirements while requiring only a small amount of electrical power. These properties make this a device a prime candidate for experiments for those with transtibial amputation, with the end goal of improving walking gaits for this population.

The preliminary findings from this study indicate that some measures of gait may be especially affected by the intervention. The pilot data support the hypothesis that this artificial gastrocnemius can reduce biological knee flexion moment and biological positive work of the affected-side knee, compared to a similarly weighted monoarticular prosthesis, during late stance knee flexion. Despite the short amount of time to get acclimated to the knee orthosis, the participants reduced their biological knee moment profiles, thereby allowing the AG to take over some of the kinetic loads. This behavior is consistent with other studies involving exoskeletal interventions at ankle [39] and hip joints [40]. The reduction of biological knee moment is beneficial from the standpoint of wearable device design, since it means that wearers of the AG were quickly able to replace biological function with that from the device.

Also as hypothesized, the affected-side hip flexion moment impulse and hip positive work of both participants were reduced during late stance knee flexion. These reductions are likely a result of the energy return of the spring, which served to help flex the hip. Although small, this effect

Table 5: Affected-side knee flexion moment impulse in late stance flexion with the AG compared between the two walking conditions with the quasi-passive artificial gastrocnemius: the Baseline condition, where the artificial gastrocnemius acted as a free-joint at the knee, and the Active condition, where the AG was appropriately engaged as per the controller. The values were computed over the late stance knee flexion phase of the gait cycle.

	Baseline moment impulse (Nm∗s/kg)	Active moment impulse (Nm∗s/kg)	Active Biological moment impulse (Nm∗s/kg)	Total % change from Baseline	Biological % change from Baseline
Subject 1	0.006 ± 0.004	0.009 ± 0.004	0.001 ± 0.002	+32	−78
Subject 2	0.055 ± 0.018	0.056 ± 0.013	0.039 ± 0.011	+2	−29

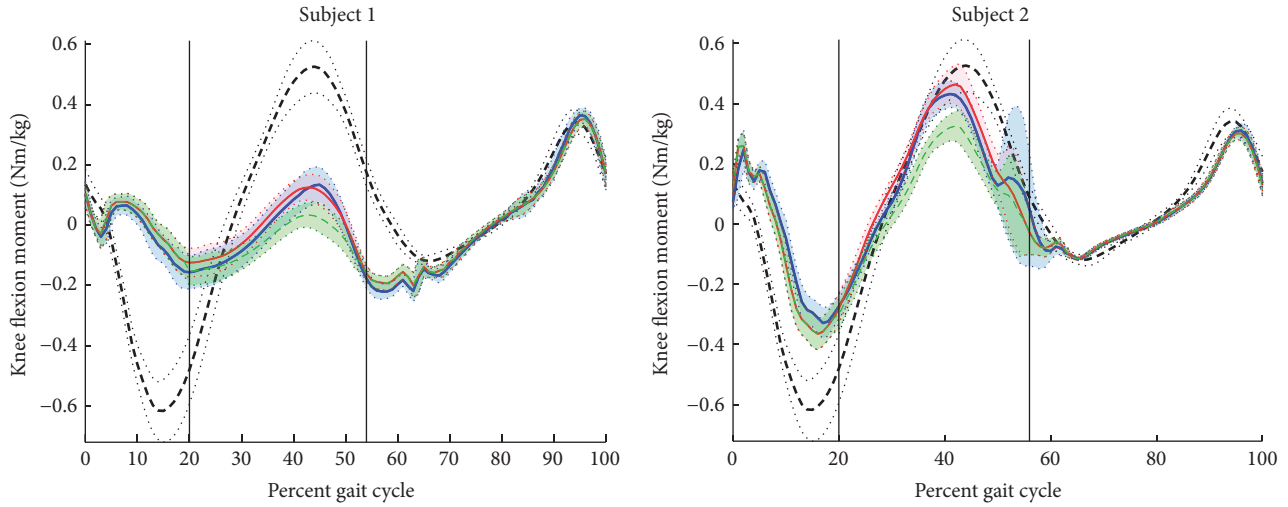

Figure 6: Affected-side knee flexion moment components with the AG shown for the *Baseline* condition where the clutch was disabled (thick solid blue line), the *Active* condition (thin solid red line), and the biological knee moment contribution during the *Active* condition (thin green dashed line). Shaded regions for these curves indicate ±1 standard deviation, bounded by light dotted lines. For reference, biological knee moment data are also shown for the nonamputee from which the clutch spring was tuned (thick black dashed line) ±1 standard deviation (black dotted lines). The vertical lines indicate the typical engagement and disengagement times for the clutch.

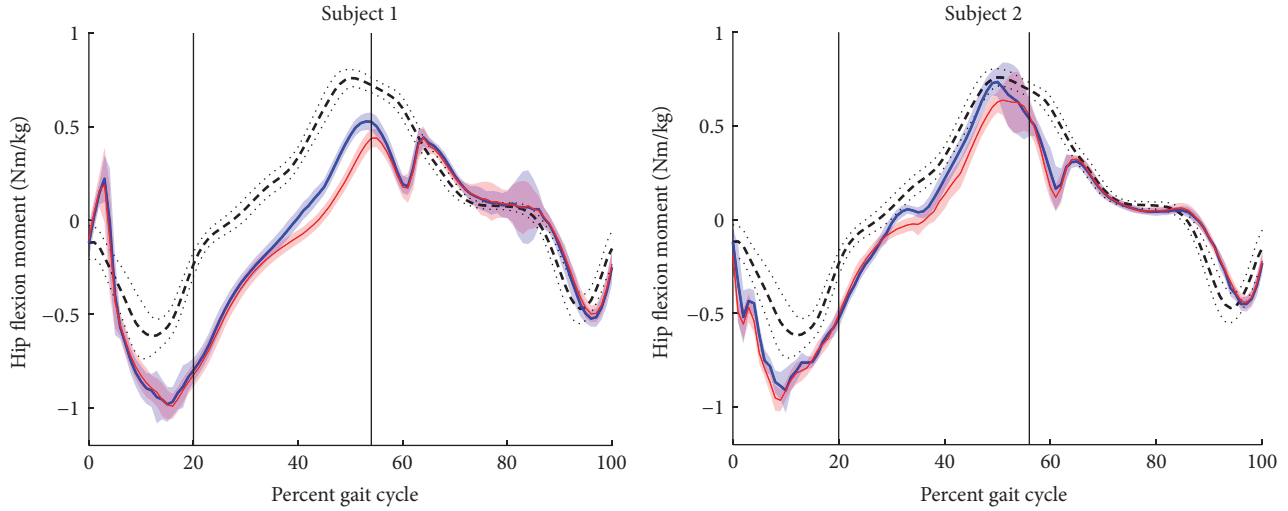

Figure 7: Affected-side hip flexion moment components with the AG shown for the *Baseline* condition where the clutch was disabled (thick solid blue line) and the *Active* condition (thin solid red line). Shaded regions for these curves indicate ±1 standard deviation. For reference, biological hip moment data are also shown for the nonamputee from which the clutch spring was tuned (thick black dashed line) ±1 standard deviation (black dotted lines). The vertical lines indicate the typical engagement and disengagement times for the clutch.

Table 6: Affected-side knee positive work in late stance flexion with the AG compared between the two walking conditions with the quasi-passive artificial gastrocnemius: the Baseline condition, where the artificial gastrocnemius acted as a free-joint at the knee, and the Active condition, where the AG was appropriately engaged as per the controller. The values were averaged over the late stance knee flexion phase of the gait cycle.

	Baseline total power (Nm∗s/kg)	Active total power (Nm∗s/kg)	Active biological power (Nm∗s/kg)	Total % change from Baseline	Biological % change from Baseline
Subject 1	0.006 ± 0.004	0.005 ± 0.003	0.002 ± 0.002	−6	−60
Subject 2	0.084 ± 0.064	0.062 ± 0.031	0.049 ± 0.030	−26	−41

Table 7: Hip flexion moment impulse in late stance flexion with the AG compared between the two walking conditions with the quasi-passive artificial gastrocnemius: the Baseline condition, where the artificial gastrocnemius acted as a free-joint at the knee, and the Active condition, where the AG was appropriately engaged as per the controller. The values were computed over the late stance knee flexion phase of the gait cycle.

	Baseline moment impulse (Nm∗s/kg)	Active moment impulse (Nm∗s/kg)	% change from Baseline
Subject 1	0.077 ± 0.006	0.057 ± 0.006	−26
Subject 2	0.134 ± 0.013	0.115 ± 0.012	−14

Table 8: Affected-side hip positive work in late stance flexion with the AG compared between the two walking conditions with the quasi-passive artificial gastrocnemius: the Baseline condition, where the artificial gastrocnemius acted as a free-joint at the knee, and the Active condition, where the AG was appropriately engaged as per the controller. The values were computed over the late stance knee flexion phase of the gait cycle.

	Baseline positive work (J/kg)	Active positive work (J/kg)	% change from Baseline
Subject 1	0.087 ± 0.011	0.063 ± 0.0090	−27
Subject 2	0.117 ± 0.016	0.095 ± 0.014	−19

Table 9: Metabolic power of the amputee participants with the AG.

	Subject 1	Subject 2
Baseline power (W/kg)	3.80 ± 0.19	3.04 ± 0.11
Active power (W/kg)	3.61 ± 0.19	2.94 ± 0.08
Percent change	−5%	−3%

may possibly compensate for the otherwise increased hip power exhibited by transtibial amputees [4].

Given the kinetic results, it is not surprising that slight metabolic improvements were demonstrated as well. Reductions in net positive biological mechanical work should correspond to reductions in concentric muscle work, since passive tissues, by definition, cannot generate net positive work. This reduction in muscle work, in turn, would be expected to reduce metabolic cost [41, 42].

5. Conclusions and Future Work

Despite the advances of today's monoarticular transtibial prostheses, their limitations still manifest in pathological gaits. This study builds on the hypothesis that dominant pathologies are caused by a lack of biarticular gastrocnemius function. Our approach of restoring this biarticular component via an artificial gastrocnemius has shown preliminary but promising results toward the improvement of transtibial prosthesis efficacy.

The quasi-passive nature of this novel artificial gastrocnemius means that the design could exclude heavy components like large batteries and motors. Yet still, this device has the capability to produce biological-levels of knee moments for assisting those with transtibial amputation. The low power draw also helps to make this device practical for daily use, as battery life would not likely be a problem over the course of a day.

The AG, despite lacking an ability to generate positive net mechanical work, did demonstrate an ability to reduce amputee metabolic cost of transport for the two amputees tested. This preliminary result suggests that biarticular devices may hold the potential to improve amputee quality of life beyond that with even the most advanced monoarticular devices. These metabolic benefits may stem from a combination of a reduction in knee and hip moments and powers in the affected-side leg.

However, given the lack of statistical power, more work is needed to verify this effect on more participants. In addition, the slight increase seen in the net mechanical work from the ankle-foot prosthesis during the ACTIVE conditions could

account for a nonnegligible portion of this small metabolic benefit. If, however, the metabolic improvement is confirmed for other amputees when ensuring no increase in positive work from the prosthetic ankle, it would show that metabolic improvements are possible for transtibial amputees without the need for the injection of net positive mechanical work.

It would be beneficial to perform additional experiments that more broadly explore this device. Each individual has their own gait idiosyncrasies, and a matching to other human gait solely based on height and weight has its limitations. Therefore, it is possible that, although the joint stiffness of the device was chosen via optimization, this stiffness value may not have corresponded to the optimal values for the given amputee participants. Additionally, inherent compliance in the brace itself may change the effective device stiffness from the designed specification. Future trials could more systematically vary the joint stiffness to find the metabolically optimal value and then compare it to that from simulation.

In addition, it may be desirable to reach beyond the quasi-passive model of the gastrocnemius muscle. Seeing that the biological gastrocnemius generates several joules of net work per step [43, 44], greater benefits could possibly be achieved by providing this net work to amputees. By definition, this net mechanical work cannot be produced with a quasi-passive device, and, therefore, a different mechanism would be needed to test this hypothesis. In the design of either quasi-passive or active transtibial leg prostheses, we feel biarticular gastrocnemius actuation is an important consideration.

Conflicts of Interest

The authors declare that there are no conflicts of interest regarding the publication of this article.

Acknowledgments

This work was supported by departmental funding in the MIT Media Lab.

References

[1] P. A. Struyf, C. M. van Heugten, M. W. Hitters, and R. J. Smeets, "The Prevalence of Osteoarthritis of the Intact Hip and Knee Among Traumatic Leg Amputees," *Archives of Physical Medicine and Rehabilitation*, vol. 90, no. 3, pp. 440–446, 2009.

[2] R. Gailey, K. Allen, J. Castles, J. Kucharik, and M. Roeder, "Review of secondary physical conditions associated with lower-limb amputation and long-term prosthesis use," *Journal of Rehabilitation Research and Development*, vol. 45, no. 1, pp. 15–29, 2008.

[3] D. M. Ehde, J. M. Czerniecki, D. G. Smith et al., "Chronic phantom sensations, phantom pain, residual limb pain, and other regional pain after lower limb amputation," *Archives of Physical Medicine and Rehabilitation*, vol. 81, no. 8, pp. 1039–1044, 2000.

[4] P.-F. Su, S. A. Gard, R. D. Lipschutz, and T. A. Kuiken, "Gait characteristics of persons with bilateral transtibial amputations," *Journal of Rehabilitation Research and Development* , vol. 44, no. 4, pp. 491–501, 2007.

[5] D. A. Winter and S. E. Sienko, "Biomechanics of below-knee amputee gait," *Journal of Biomechanics*, vol. 21, no. 5, pp. 361–367, 1988.

[6] N. H. Molen, "Energy/speed relation of below-knee amputees walking on a motor-driven treadmill," *Internationale Zeitschrift für Angewandte Physiologie Einschließlich Arbeitsphysiologie*, vol. 31, no. 3, pp. 173–185, 1973.

[7] R. L. Waters, J. Perry, D. Antonelli, and H. Hislop, "Energy cost of walking of amputees: the influence of level of amputation," *The Journal of Bone & Joint Surgery*, vol. 58, no. 1, pp. 42–46, 1976.

[8] J. Hu and R. G. Gordon, "Textured aluminum-doped zinc oxide thin films from atmospheric pressure chemical-vapor deposition," *Journal of Applied Physics*, vol. 71, no. 2, p. 880, 1992.

[9] H. M. Herr and A. M. Grabowski, "Bionic ankle-foot prosthesis normalizes walking gait for persons with leg amputation," *Proceedings of the Royal Society B Biological Science*, vol. 279, no. 1728, pp. 457–464, 2012.

[10] D. Hill and H. Herr, "Effects of a powered ankle-foot prosthesis on kinetic loading of the contralateral limb: a case series," in *Proceedings of the IEEE International Conference on Rehabilitation Robotics (ICORR '13)*, vol. 10, pp. 1–6, IEEE, Seattle, WA, USA, June 2013.

[11] C. H. Soo and J. M. Donelan, "Mechanics and energetics of step-to-step transitions isolated from human walking," *Journal of Experimental Biology*, vol. 213, no. Pt 24, pp. 4265–4271, 2010.

[12] A. D. Kuo, J. M. Donelan, and A. Ruina, "Energetic consequences of walking like an inverted pendulum: step-to-step transitions," *Exercise and Sport Sciences Reviews*, vol. 33, no. 2, pp. 88–97, 2005.

[13] J. M. Donelan, R. Kram, and A. D. Kuo, "Mechanical work for step-to-step transitions is a major determinant of the metabolic cost of human walking," *Journal of Experimental Biology*, vol. 205, no. 23, pp. 3717–3727, 2002.

[14] A. D. Kuo, "Energetics of actively powered locomotion using the simplest walking model," *Journal of Biomechanical Engineering*, vol. 124, no. 1, pp. 113–120, 2002.

[15] M. Meinders, A. Gitter, and J. M. Czerniecki, "The role of ankle plantar flexor muscle work during walking," *Journal of rehabilitation medicine*, vol. 30, no. 1, pp. 39–46, 1998.

[16] R. R. Neptune, S. A. Kautz, and F. E. Zajac, "Contributions of the individual ankle plantar flexors to support, forward progression and swing initiation during walking," *Journal of Biomechanics*, vol. 34, no. 11, pp. 1387–1398, 2001.

[17] A. L. Hof, J. Nauta, E. R. van der Knaap, M. A. A. Schallig, and D. P. Struwe, "Calf muscle work and segment energy changes in human treadmill walking," *Journal of Electromyography & Kinesiology*, vol. 2, no. 4, pp. 203–216, 1993.

[18] J. M. Caputo and S. H. Collins, "Prosthetic ankle push-off work reduces metabolic rate but not collision work in non-amputee walking," *Scientific Reports*, vol. 4, article no. 7213, 2014.

[19] M. R. Williams, A. Grabowski, H. Herr, and S. D'Andrea, *Electromyographic Effects of Using a Powered Ankle-Foot Prosthesis*, American Society of Biomechanics, 2012.

[20] J. F. Veneman, R. Kruidhof, E. E. G. Hekman, R. Ekkelenkamp, E. H. F. Van Asseldonk, and H. van der Kooij, "Design and Evaluation of the Gait Rehabilitation Robot LOPES," *IEEE Transactions on Neural Systems and Rehabilitation Engineering*, vol. 15, no. 3, 2007.

[21] J. E. Pratt, B. T. Krupp, C. J. Morse, and S. H. Collins, "The RoboKnee: an exoskeleton for enhancing strength and endurance during walking," in *Proceedings of the IEEE International Conference on Robotics and Automation (ICRA '04)*, vol. 3, pp. 2430–2435, IEEE, May 2004.

[22] P. P. Pott, S. I. Wolf, J. Block et al., "Knee-ankle-foot orthosis with powered knee for support in the elderly," *Proceedings of the Institution of Mechanical Engineers, Part H: Journal of Engineering in Medicine*, vol. 231, no. 8, pp. 715–727, 2017.

[23] D. P. Ferris, J. M. Czerniecki, and B. Hannaford, "An ankle-foot orthosis powered by artificial pneumatic muscles," *Journal of Applied Biomechanics*, vol. 21, no. 2, pp. 189–197, 2005.

[24] G. S. Sawicki and D. P. Ferris, "A pneumatically powered knee-ankle-foot orthosis (KAFO) with myoelectric activation and inhibition," *Journal of NeuroEngineering and Rehabilitation*, vol. 6, no. 1, p. 23, 2009.

[25] D. P. Ferris, K. E. Gordon, G. S. Sawicki, and A. Peethambaran, "An improved powered ankle-foot orthosis using proportional myoelectric control," *Gait & Posture*, vol. 23, no. 4, pp. 425–428, 2006.

[26] M. Wehner, B. Quinlivan, P. M. Aubin et al., "A lightweight soft exosuit for gait assistance," in *Proceedings of the IEEE International Conference on Robotics and Automation (ICRA '13)*, pp. 3362–3369, May 2013.

[27] M. B. Wiggin, G. S. Sawicki, and S. H. Collins, "An exoskeleton using controlled energy storage and release to aid ankle propulsion," in *Proceedings of the IEEE International Conference on Rehabilitation Robotics (ICORR '11)*, pp. 1–5, Zurich, Switzerland, June 2011.

[28] C. J. Walsh, K. Endo, and H. Herr, "A quasi-passive leg exoskeleton for load-carrying augmentation," *International Journal of Humanoid Robotics*, vol. 4, no. 3, pp. 487–506, 2007.

[29] G. Elliott, A. Marecki, and H. Herr, "Design of a clutch-spring knee exoskeleton for running," *Journal of Medical Devices, Transactions of the ASME*, vol. 8, no. 3, Article ID 031002, 11 pages, 2014.

[30] M. S. Cherry, D. J. Choi, K. J. Deng, S. Kota, and D. P. Ferris, "Design and Fabrication of an Elastic Knee Orthosis: Preliminary Results," in *Proceedings of the ASME 2006 International Design Engineering Technical Conferences and Computers and Information in Engineering Conference*, pp. 565–573, Philadelphia, PA, USA, 2006.

[31] M. Ishikawa, P. V. Komi, M. J. Grey, V. Lepola, and G.-P. Bruggemann, "Muscle-tendon interaction and elastic energy usage in human walking," *Journal of Applied Physiology*, vol. 99, no. 2, pp. 603–608, 2005.

[32] K. Endo and H. Herr, "A model of muscle-tendon function in human walking," in *Proceedings of the 2009 IEEE International Conference on Robotics and Automation, ICRA '09*, pp. 1909–1915, IEEE, Kobe, Japan, May 2009.

[33] K. Endo and H. Herr, "Human walking model predicts joint mechanics, electromyography and mechanical economy," in *Proceedings of the 2009 IEEE/RSJ International Conference on Intelligent Robots and Systems, IROS 2009*, pp. 4663–4668, St. Louis, MO, USA, October 2009.

[34] K. Endo, D. Paluska, and H. Herr, "A quasi-passive model of human leg function in level-ground walking," in *Proceedings of the 2006 IEEE/RSJ International Conference on Intelligent Robots and Systems, IROS 2006*, pp. 4935–4939, Beijing, China, October 2006.

[35] K. Endo, E. Swart, and H. Herr, "An artificial gastrocnemius for a transtibial prosthesis," in *Proceedings of the 31st Annual International Conference of the IEEE Engineering in Medicine and Biology Society: Engineering the Future of Biomedicine, EMBC 2009*, pp. 5034–5037, Minneapolis, MN, USA, September 2009.

[36] M. Palmer, *Sagittal Plane Characterization of Normal Human Ankle Function Across a Range of Walking Gait Speeds , Masters Thesis [Masters, thesis]*, MIT, 2002.

[37] J. M. Brockway, "Derivation of formulae used to calculate energy expenditure in man," *Hum Nutr Clin Nutr*, vol. 41, no. 6, pp. 463–471, 1987.

[38] A. S. McIntosh, K. T. Beatty, L. N. Dwan, and D. R. Vickers, "Gait dynamics on an inclined walkway," *Journal of Biomechanics*, vol. 39, no. 13, pp. 2491–2502, 2006.

[39] P.-C. Kao, C. L. Lewis, and D. P. Ferris, "Invariant ankle moment patterns when walking with and without a robotic ankle exoskeleton," *Journal of Biomechanics*, vol. 43, no. 2, pp. 203–209, 2010.

[40] C. L. Lewis and D. P. Ferris, "Erratum to "Invariant hip moment pattern while walking with a robotic hip exoskeleton" [J. Biomech. 44 (5) (2011) 789-793]," *Journal of Biomechanics*, vol. 47, no. 7, p. 1748, 2014.

[41] A. Hill, "The heat of shortening and the dynamic constants of muscle," *Proceedings of the Royal Society B*, vol. 126, pp. 136–195, 1938.

[42] A. Hill, "The efficiency of mechanical power development during muscular shortening and its relation to load," *Proceedings of the Royal Society B Biological Science*, vol. 159, no. 975, pp. 319–324, 1964.

[43] R. J. Zmitrewicz, R. R. Neptune, and K. Sasaki, "Mechanical energetic contributions from individual muscles and elastic prosthetic feet during symmetric unilateral transtibial amputee walking: A theoretical study," *Journal of Biomechanics*, vol. 40, no. 8, pp. 1824–1831, 2007.

[44] R. R. Neptune, K. Sasaki, and S. A. Kautz, "The effect of walking speed on muscle function and mechanical energetics," *Gait & Posture*, vol. 28, no. 1, pp. 135–143, 2008.

Hindawi
Journal of Robotics
Volume 2018, Article ID 5951965, 15 pages
https://doi.org/10.1155/2018/5951965

Research Article

Development and Evaluation of a Powered Artificial Gastrocnemius for Transtibial Amputee Gait

Michael F. Eilenberg, Jiun-Yih Kuan, and Hugh Herr

Biomechatronics Group, MIT Media Lab, Massachusetts Institute of Technology, Cambridge, MA, USA

Correspondence should be addressed to Hugh Herr; hherr@media.mit.edu

Received 15 April 2017; Revised 30 August 2017; Accepted 25 October 2017; Published 22 January 2018

Academic Editor: Kazuo Kiguchi

Existing robotic transtibial prostheses provide only ankle joint actuation and do not restore biarticular function of the gastrocnemius muscle. This paper presents the first powered biarticular transtibial prosthesis, which is a combination of a commercial powered ankle-foot prosthesis and a motorized robotic knee orthosis. The orthosis is controlled to emulate the human gastrocnemius based on neuromuscular models of matched nonamputees. Together with the ankle-foot prosthesis, the devices provide biarticular actuation. We evaluate differences between this biarticular condition and a monoarticular condition with the orthosis behaving as a free-joint. Six participants with transtibial amputation walk with the prosthesis on a treadmill while motion, force, and metabolic data are collected and analyzed for differences between conditions. The biarticular prosthesis reduces affected-side biological knee flexion moment impulse and hip positive work during late-stance knee flexion, compared to the monoarticular condition. The data do not support our hypothesis that metabolism decreases for all participants, but some participants demonstrate large metabolic reductions with the biarticular condition. These preliminary results suggest that a powered artificial gastrocnemius may be capable of providing large metabolic reductions compared to a monoarticular prosthesis, but further study is warranted to determine an appropriate controller for achieving more consistent metabolic benefits.

1. Introduction

For those living with transtibial (below-the-knee) amputation, prosthetic technology has yet to fully restore the functionality of the missing biological structures. As evidence of this technological limitation, transtibial amputees wearing conventional prostheses naturally select slower walking speeds than those with biological limbs, and, when walking at the same pace as nonamputees, they require more metabolic power than their nonamputee counterparts [1–4]. Further, transtibial amputees exhibit kinetic pathologies, particularly during the late-stance knee flexion phase of gait, where the knee flexes to prepare for the swing phase. Transtibial amputees walking with conventional prostheses increase their affected-side hip positive and negative power during this phase, compared to nonamputees, possibly in response to the lack of power from the calf muscles [4].

Unlike conventional prostheses, new robotic powered ankle-foot prostheses (PAFP) can output net mechanical work similar to that of the human ankle-foot complex. Consequently, amputees using powered prostheses have preferred walking speed, metabolic cost at a given speed, and contralateral limb impacts that are not significantly different from those of nonamputees [5, 6].

These robotic prostheses, however, still act only at the ankle joint and hence can only provide monoarticular ankle function. In contrast, the gastrocnemius calf muscle both plantar flexes the ankle and flexes the knee. Hence, amputees walking with monoarticular prostheses must compensate for this lack of function by increasing activation of the remaining knee flexors in the hamstring group [7–9]. This increase in activation is still seen with robotic ankle-foot prostheses [7]. Therefore, it is likely that biarticular interventions are required to provide a more complete restoration of the missing musculature.

Only few studies have been done to evaluate how a biarticular robotic device could improve metrics of gait for transtibial amputees beyond monoarticular devices. In the first such study, researchers approximated the gastrocnemius muscle as isometric during walking and built a

clutched-spring joint into a knee orthosis, called an artificial gastrocnemius (AG), to replicate the modeled function of an isometric muscle in series with a compliant tendon [10]. This AG-PAFP combination was shown to reduce metabolic cost of a bilateral transtibial amputee, as compared to a conventional passive transtibial prosthesis.

However, this previous study was limited in that it did not evaluate the individual contributions of the PAFP and AG on metabolism. Hence, it is not known whether the metabolic effects stemmed from the actions of the PAFP, AG, or both devices. Researchers have since attempted to isolate the incremental influence of the AG on metabolism and kinetic measures by comparing an AG-PAFP combination to a PAFP-only condition with identical mass distribution. This study provided preliminary evidence that the inclusion of the AG may, in fact, improve metabolism and influence several kinetic measures, compared to the PAFP-only condition [11].

Still, these two aforementioned studies only considered isometric behavior of the biological gastrocnemius muscle. In contrast, the human gastrocnemius muscle is responsible for 3–5 Joules of positive net mechanical work per step [12, 13]. This positive net work is impossible to reproduce with a quasi-passive device, yet its presence may be critical to the advancement of active transtibial prostheses of greater efficacy.

For the present study, we develop a novel AG that can provide positive net mechanical work. We develop a controller, based on a neuromuscular model, for said device that emulates the functionality of the missing gastrocnemius. We also develop a torque controller to enforce this functionality. We anticipate that the applied moments and positive net work from the AG will replace affected-side biological knee positive work and flexion moments. Further, we expect that the AG's improvement of calf muscle function will reduce the late-stance pathologies typically seen in the affected-side hip [4]. Therefore, we hypothesize that the use of this AG, in conjunction with a PAFP, will reduce both biological flexion moment impulse and positive mechanical work of the affected-side knee and hip joints during late-stance knee flexion, as compared to the same conditions with only the PAFP. We further hypothesize that these changes will provide a corresponding reduction in metabolic cost of walking via the reduction in metabolically expensive positive muscle work.

2. Powered Biarticular Transtibial Prosthesis Design

It has been shown that adding mass to the lower extremities can have a detrimental effect on walking metabolism [14]. Hence, the goal in this project was to provide interventions to a participant walking on a treadmill by remote actuation, so to minimize mass affixed to the wearer. To this end, we developed a cable-driven tethered exoskeleton system, comprising a motor drive module, a cable transmission linkage, a robotic knee joint, and a custom knee orthosis. We first describe the mechatronic design of these four elements and then describe the torque control of the system in the next section.

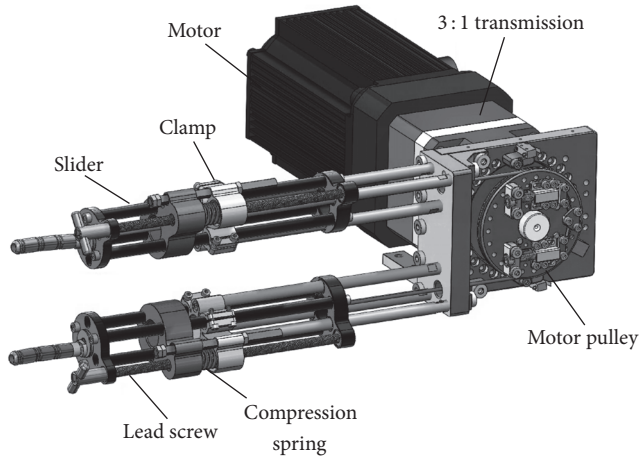

Figure 1: Motor drive module: actuation source. The tensioner attached to the motor drive unit and provided the ability to preload the cables to a desired tension without adding series compliance to the system.

2.1. Motor Drive Module. The core of the motor module was a powerful offboard actuation source and real-time sensing and control system. The actuation source included a 3 kW AC servo motor (SGMSV-30A3A61, YASKAWA), a 3 : 1 gear reducer (042PLX0030-LB-04027, CGI INC), and a custom cable tensioner. The sensing and control system, designed for real-time control and system safety, included a host personal computer, an EtherCAT® master controller (SPiiPlusNTM, ACS Motion Control), local servo controllers (V200AE1A002000200, Yaskawa), and an EtherCAT® slave I/O system (750-534 EtherCAT Coupler, WAGO). This system had multiple analog and digital inputs that were used for gathering feedback signals in real-time from the device for the purposes of data collection and feedback control. A 90 mm diameter pulley was mounted to the transmission output shaft to actuate the drive cable.

A spring-based tensioner system was used to preload the cable. This tensioner was a bracket with an internal slider, driven by a lead screw (Figure 1). This joint enabled the bracket to expand to take up cable slack. A spring was placed in series between the sliding element of the bracket and the stationary element, serving as an indicator of cable preload. As the lead screw was manually rotated, the bracket expanded and provided tension on the cable. The reaction force from the cable conduit was transmitted through the bracket and loaded the spring. Therefore, by measuring the spring deflection during the cable preloading, the cable tension could be approximated. Once the cable was pretensioned, screws were tightened to lock the slider to make the tensioner a rigid structure. Therefore, the tensioning springs did not introduce series compliance to the system during operation of the cable drive.

2.2. Cable Linkage. The cable linkage consisted of an inner cable, flexible conduits, rigid tubing, and a pulley system. A 3 mm diameter 7 × 19 braided steel inner cable was used to transmit power from the motor to the knee joint pulley

(a) (b) (c)

Figure 2: Conduit linkage as it interfaces with the artificial gastrocnemius and participant. The complete biarticular prosthesis system is shown (a) along with close-up views of the conduit linkage pulley system (b) and components of the flexible conduit sections (c).

in a similar way as a Bowden cable drive. However, instead of a flexible conduit throughout the entire tether, sections of rigid tubing and a pulley system were used (Figure 2). The tubing was made of 0/90 carbon fiber, with 22.2 mm outer diameter and 19.1 mm inner diameter. This system had a distinct advantage over a traditional, flexible Bowden cable drive: the losses due to friction between the cable and conduit were near-zero through the tubing sections, as the cable did not contact the sides of the conduit.

Short, flexible conduit sections were used to link the straight rigid tubing together in order to provide articulation. Typical Bowden cable conduits have the tendency to straighten when tension is applied to the cable. Rather than using such a conduit, short, interlocking aluminum conduit elements were designed (Figure 2(c)). These elements were designed in case the length of the inner bore of the conduit did not change upon bending. Each element had a male and female end, that, when mated, produced a ball-and-socket joint, through which the cable could pass. These elements were strung together in series to produce flexible conduit sections of the desired lengths. Polytetrafluoroethylene (PTFE) liners (3 mm inner diameter, 6 mm outer diameter) provided low-friction interface within these sections of conduit elements.

The conduit linkage was arranged behind and above the treadmill, so to provide minimal interference to a wearer of the knee joint (Figure 2(a)). The conduit linkage allowed two degrees of freedom in the sagittal plane, via the vertical and horizontal hinging of the conduit sections. Some limited motion in the coronal and transverse planes was also possible with this system. The remaining flexibility needed near the waist of a human subject was provided by a section of several conduit elements linked in series, forming a flexible section of conduit.

The added mass from this conduit system was expected to provide some downward force to the wearer during walking. This force was estimated by using a force gauge to hold up the AG with the conduit linkage at the location where a typical participant's knee would be during walking.

2.3. Robotic Knee Joint. The actuated robotic knee consisted of a pulley, driven by the tether cable, which sat lateral to the wearer's affected-side biological knee joint (Figure 3). This pulley was free to rotate on ball bearings in the sagittal plane about the knee center with respect to the joint housing. The pulley itself was connected to the output link through a torsional spring (stiffness = 1200 Nm/rad), which acted as a series compliance between the cable drive and the output link.

A rotary potentiometer (8 kOhm), mounted between the joint housing and the output link, was used to measure joint angle. This potentiometer was mounted on the lateral side of the joint, with the potentiometer shaft going through the center of the joint and attaching to the output link on the medial side (Figure 3). Torque sensing was accomplished via the use of a full-bridge strain gauge (SGT-2/350-FB13, Omega Engineering, Inc.), mounted on the output link so that bending of the link in the sagittal plane would be detected by the strain gauge. The strain gauge was connected to a custom preamplifier that included a common-mode input filter to reject electromagnetic interference and a second-order low-pass filter with a cutoff frequency of 585 Hz.

The designed robotic joint had physical parameters within the desired values (see Table 1). Although the robotic joint itself had a mass of only 0.6 kg, the orthosis for attaching it to the body required the addition of 0.8 kg and 1.3 kg, respectively, for the amputee and nonamputee subjects. In addition, the suspended cable linkage provided approximately a 0.6 kgf downwards force at the knee. Regarding cable pretension, it was found that 30–50 N of cable pretension kept cable friction low without introducing bandwidth-limiting cable slack.

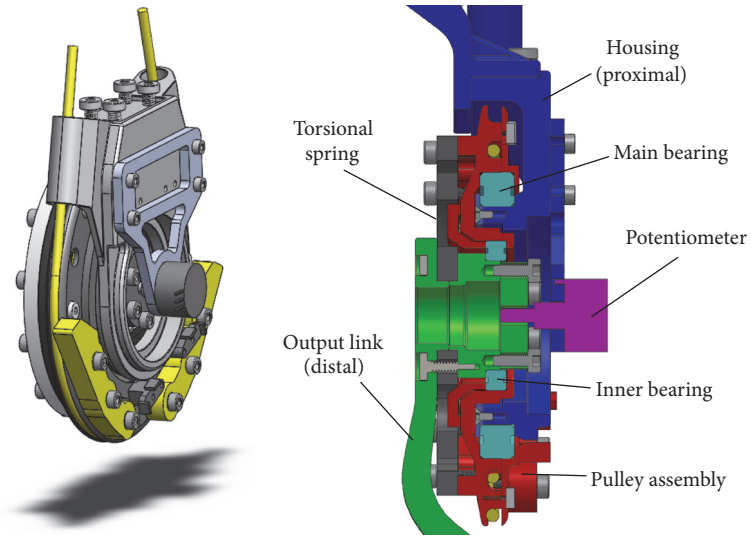

Figure 3: Powered artificial gastrocnemius joint. The assembled joint is shown without proximal and distal attachments (a). A color-coded coronal plane section view of the same mechanism is also shown (b), where parts that connect as a rigid body are shaded with the same color. The housing (blue) attaches to the proximal mount that is affixed to the thigh cuff. The pulley (red) rotates with respect to the housing via the main bearing (teal). The output link (green) is affixed to the distal mount that connects to the socket. This link rotates with respect to the pulley via the inner bearing, with the torsional spring connecting the output link to the pulley. The potentiometer measures the relative rotation of the housing and the output link. Hard stops (not shown) are mounted to the pulley assembly and engage with the housing at the limits of joint rotation.

Table 1: Design parameters of the powered artificial gastrocnemius.

Parameter	Desired value	Achieved value
Joint range of motion (radians)	1.3	2.1
Size	(Minimal)	50 mm radius, 53 mm wide
Weight (kg)	(Minimal)	1.4–1.9
Center-of-rotation range (mm)	20	20
Maximum output torque (Nm)	60	90
Torque sensing resolution (Nm)	0.01	0.01

2.4. Custom Knee Orthosis and Robotic Ankle-Foot Prosthesis. A custom knee orthosis was built for each amputee participant to use the AG (Figure 4). Each amputee participant was brought to a certified prosthetist to get a cast made of their residual limb while their normal prosthetic socket was being worn. The prosthetist then created carbon fiber orthoses that were form-fitted for each individual. Consequently, an orthosis could be strapped to the affected-side leg while the prosthetic socket was being worn. The orthoses each comprised a carbon fiber thigh cuff and a carbon fiber shank cuff that fitted over the existing prosthetic socket. These cuffs were joined by a pair of polycentric knee orthosis hinges.

A set of bearings was designed to transmit only tangential and sagittal plane forces from the output link of the robotic joint to the shank cuff of the custom orthosis (Figure 4(c)). This bearing set consisted of (1) a linear bearing to allow for distal-proximal freedom between the robotic joint and orthosis, (2) a ball joint to provide 3-axis rotational freedom, and (3) A linear brass sleeve bearing on a 6 mm steel shaft to allow medial-lateral freedom.

The orthosis was designed to accommodate a robotic ankle-foot prosthesis (PAFP) (EmPower, BionX Medical Technologies, Inc., Bedford, MA) attached to a given amputee's socket with a standard prosthetic pylon (Figure 4). This prosthesis was a commercial product capable of large amounts of positive net work during walking.

3. System Dynamics and Torque Control Design

Despite the large offboard power source, the AG still required system dynamics analyses and control strategies to compensate for parasitic effects like cable friction and other dynamics between the motor and output joint. The goal was to make the system behave as though these dynamics did not exist, so that, from a high-level control standpoint, the AG could be considered close to an ideal torque source. In this section, we describe the characterization of the AG system dynamics. We also describe the development of a low-level torque controller

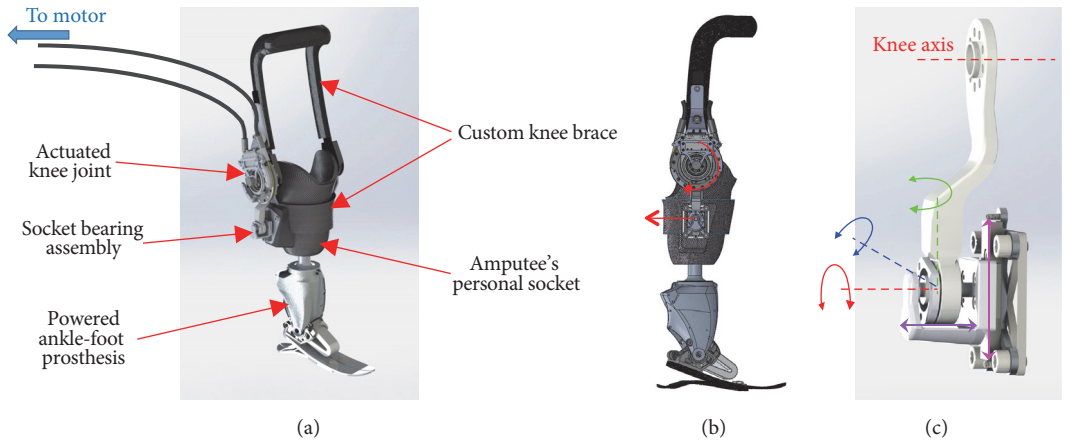

FIGURE 4: Knee orthosis and socket attachment. Rendering of the powered AG knee orthosis is shown with the robotic knee joint and powered ankle-foot prosthesis (a). A side-view of the same is shown, with arrows indicating the intended applied torque from the knee actuator and the resulting tangential force on the socket from the actuator (b). Also shown is the bearing assembly with resulting degrees of freedom (c) that is mounted on the socket attachment of the orthosis. This assembly transmits the tangential force from the actuator while allowing for motion from the polycentric knee joints as well as misalignment in the orthosis.

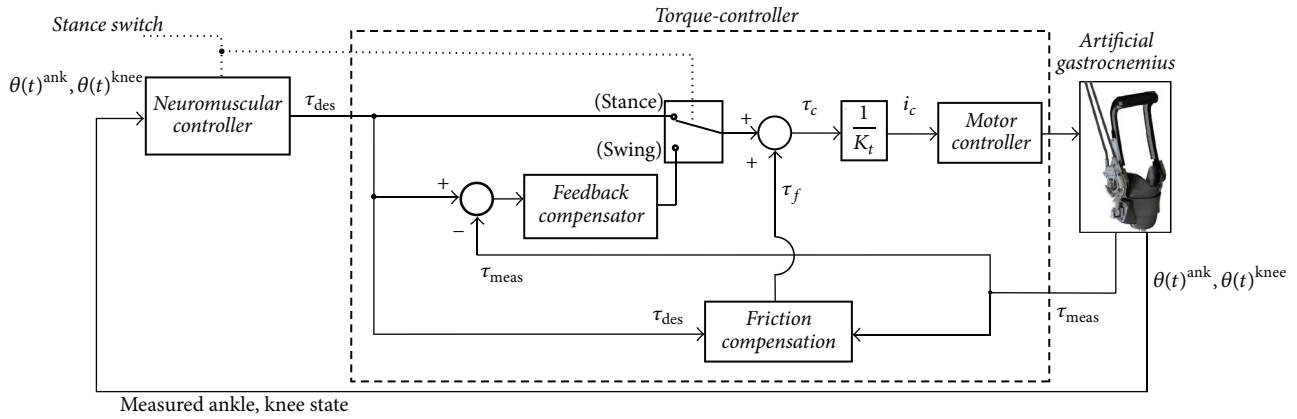

FIGURE 5: Torque control schematic. The control system for the AG is composed of an inner torque-controller loop that enforces desired torque at the joint and an outer loop involving a neuromuscular model as a controller that receives joint kinematics as input. The controller switches between open-loop control (stance) and closed-loop torque control (swing) as appropriate given the gait cycle phase. Motor torque control is performed at the lowest level by controlling motor current, scaled by the torque constant, K_t.

in terms of torque bandwidth and also performance during walking.

3.1. Open-Loop System Characterization. System identification tests for the AG were performed using a knee orthosis built for nonamputee participants. The orthosis was worn by a healthy adult male participant so to include the full dynamics of the human-machine system. The participant stood still, keeping his knee bent slightly, but resisting motion from the device. A swept-sine torque signal of varying amplitudes from 2 to 10 Nm was commanded to the motor, with frequencies ranging from 0.1 to 200 rad/s in increments of 10 rad/s. Additional data were collected with the flexible conduit section in the cable conduit linkage bent approximately 15 degrees, so as to capture the range of friction in this section. The magnitude of the command signal was adjusted for each frequency to maximize torque while preventing excessive discomfort to the wearer. Joint moment data were collected from the AG strain gauge. When attached to the human leg as in the system identification experiments, the robotic joint had a −3 dB open-loop torque bandwidth of 100 rad/s.

3.2. Artificial Gastrocnemius Torque Control Scheme. The AG was a torque-controlled system. A high-level neuromuscular controller (NMC) took as input affected-side ankle angle $\theta(t)^{ank}$ and knee angle $\theta(t)^{knee}$ as functions of time and produced a desired knee joint torque, τ_{des}. A low-level torque controller enforced this desired torque at the physical joint. For the purposes of this torque control, the gait cycle was divided into two phases: stance and swing (Figure 5). Stance phase began at heel-contact and ended at ToeOff. Swing phase began at ToeOff and ended at subsequent heel-contact. A footswitch (model: FSW, B&L Engineering, Santa Ana, CA), worn as an insole in the shoe on the leg wearing the knee orthosis, was used to detect stance and swing phases.

Table 2: Amputee matching to nonamputee participants.

Amputee number	Nonamputee match	Amputee height (cm)	Matched height (cm)	Amputee weight (kg)	Matched weight (kg)
S1	NA2	180	180	92	90
S2	NA1	175	175	74	73
S3	NA3	193	188	89	95
S4	NA3	188	188	98	95
S5	NA4	175	180	110	103
S6	NA4	180	180	104	103

3.2.1. Stance Phase Torque Control. An open-loop control methodology was used for the stance phase of the gait cycle, wherein the control input was τ_{des}, and the output was motor torque, τ_c (Figure 5). A feed-forward friction compensation term, τ_f with iterative learning, was used to reduce the torque errors between the desired torque, τ_{des} and the measured torque, τ_{meas}, resulting from friction in the cable drive. This friction compensation was implemented as a torque profile as a function of time within a gait cycle. A running counter was used to estimate the elapsed fraction of the current gait cycle by comparing the time spent in the current gait cycle to the total time of the previous gait cycle: gc = *counter*/*lastsamples* where gc is the estimated elapsed fraction of the current gait cycle, *counter* is the number of control cycles elapsed in the current gait cycle, and *lastsamples* is the total number of control cycles of the previous gait cycle.

The function was updated at each gait step by smoothly incorporating the observed torque error in two steps:

$$\tau_{\text{learn}}(\text{gc}, n+1) = \tau_{\text{err}}(\text{gc}, n) \cdot \alpha + \tau_f(\text{gc}, n) \cdot (1-\alpha), \quad (1)$$

$$\tau_f(\text{gc}, n+1) = \tau_{\text{learn}}(\text{gc}, n), \quad (2)$$

where gc is the elapsed fraction of the gait cycle, n is the gait cycle number, and α is the learning rate. Once a new learned profile τ_{learn} was computed for an entire gait cycle (1), it was subsequently used in the feed-forward term τ_f on the subsequent gait cycle (2). Thus, the error recorded during a gait cycle would be incorporated in the controller two gait cycles later. A value of α of 0.5 was found to provide a reasonable learning rate, for which the learned friction compensation profile was updated such that a new learned behavior was fully incorporated in approximately 10 seconds. Similar iterative learning methods have been successful in wearable robotics in the presence of cable frictional losses [15].

3.2.2. Swing Phase Torque Control. To reduce resistance during swing phase, a feedback torque controller was used along with the iterative friction compensation. This controller took the form

$$\tau_{\text{comm}} = K_i \int (\tau_{\text{des}} - \tau_{\text{meas}})\, dt, \quad (3)$$

where τ_{comm} is the motor torque command from the feedback controller. Standard loop-shaping techniques were performed in MATLAB using the open-loop data to determine this control law and the parameter K_i. In order to provide a fast response during state changes, this torque controller was run throughout the gait cycle, but its output was applied to the robotic joint only during the swing phase.

3.2.3. Closed-Loop System Characterization. System characterization tests were performed for the swing phase feedback torque controller (without the friction compensation), with a swept-sine desired joint torque as input and measured strain gauge joint torque as output, in a similar manner as the open-loop system characterization tests. The closed-loop bandwidth (−3 dB) and the phase margin were estimated from the data using a fast Fourier transforms of both inputs and outputs. When applying the swing phase closed-loop torque controller, the closed-loop system bandwidth was 14 Hz (87 rad/s), with a gain margin of 1.6 and a phase margin of 69 degrees.

3.3. Torque Control Performance during Walking. In addition to the transparency requirement, it was necessary to ensure that the nonzero desired torque values could be tracked by the AG within a reasonable range. The root mean squared (RMS) stance phase torque error, between the desired torque from the NMC and the measured joint torque from the AG strain gauge, was 1.45 ± 0.72 Nm (6 percent of the average maximum torque of 23 Nm) on average across the amputee participants listed in Table 2. A representative plot of this performance is shown in Figure 6.

3.4. Torque Control Metabolic Validation. Clinical metabolic tests were performed to test the transparency of the robotic knee joint; it was required that the described torque control techniques could provide sufficiently low resistance to wearers as not to adversely affect their metabolism. Success was defined as a nonsignificant difference in metabolism between two conditions during treadmill walking: (1) torque-controlled AG knee orthosis worn on one leg with zero torque commanded and (2) AG knee orthosis worn, acting as a free-swinging joint (with the cable drive disconnected). For the purposes of this metabolic validation trials with nonamputees, a custom-built, carbon fiber orthosis, molded by a prosthetist, was used to mount the robotic joint on the leg of nonamputee participants.

Six healthy participants (age = 27 ± 5.7 years, body mass = 71 ± 10 kg, and height = 181 ± 4 cm) were asked to walk on a treadmill while metabolic data were collected. The clinical evaluation was conducted at MIT (Cambridge, MA) and was approved by MIT's Committee on the Use of Humans

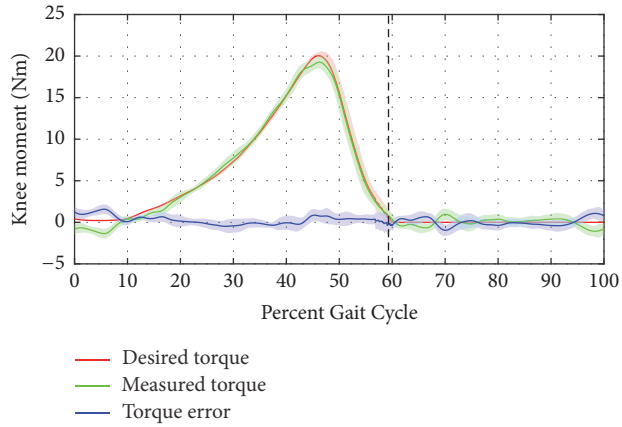

FIGURE 6: Representative closed-loop system response during walking trials. Data were collected with an amputee participant. The torque error (blue) represents the difference in joint moment between the desired AG device torque (red) and the measured strain-gauge device torque (green). The vertical dashed line indicates ToeOff.

as Experimental Subjects (COUHES). Each participant provided written, informed consent which was obtained before data collection was initiated. Each participant was asked to walk at a typical walking speed of 1.25 m/s under three conditions, in random order: (1) walking normally without the AG, (2) wearing the orthosis with the cable drive disconnected, and (3) wearing the orthosis with torque controller set to zero torque. For all conditions, participants wore a portable oxygen consumption mask attached to a standard open-circuit gas analysis system (model K4B^2, COSMED, Rome, Italy). This system estimated metabolic energy consumption based on measurements of oxygen inspired and expired carbon dioxide.

Metabolic cost for each walking speed was computed by taking average oxygen and carbon dioxide data over a two-minute window at the end of each six-minute trial. The metabolic power was computed using the equation

$$P = K_{O_2}\dot{V}_{O_2} + K_{CO_2}\dot{V}_{CO_2}, \quad (4)$$

where P is the metabolic power in Watts, $\dot{V}_{O_2}$ is the volume flow rate of oxygen inhaled, $\dot{V}_{CO_2}$ is the volume flow rate of carbon dioxide exhaled, and K_{O_2} and K_{CO_2} are constants with values from literature [16], given as K_{O_2} = 16,580 W/L and K_{CO_2} = 4,510 W/L. It was confirmed that the average ratio of $\dot{V}_{CO_2}/\dot{V}_{O_2}$ was less than 1.1 for all trials.

The metabolic consumption of the participants walking with the zero-torque control condition (3.40 ± 0.40 W/kg) was not significantly different from that of the disconnected condition (3.55 ± 0.45 W/kg), $p = 0.18$, although significantly lower metabolism was found for the normal-walking condition without the AG (2.60 ± 0.44 W/kg), $p < 0.001$, as compared to the zero-torque condition.

The results of these system dynamics and metabolic tests show two important performance characteristics. First, the AG can accurately provide high levels of torque to the wearer; the average observed RMS error of 1.45 Nm is well within biological variation; in comparison, the average step-to-step standard deviation in peak knee flexion moment during mid-stance phase for the nonamputee participants is 4.8 Nm. Second, the AG can behave sufficiently close to a free-hinging joint so that the metabolism of the wearer reflects the use of the latter. These two performance characteristics allow the AG to be treated as a near-ideal torque source at both low and high knee moment values. Hence, a higher-level control strategy, such as a neuromuscular controller, may be used without needing to reconsider the system dynamics of the hardware.

4. Neuromuscular Controller

A neuromuscular controller (NMC) was used to provide torque commands to the AG so to emulate the behavior of the biological gastrocnemius, similar to earlier work in robotic prosthesis control [17, 18]. The NMC was based on a musculoskeletal model of a human gastrocnemius. This model took joint kinematics and neural stimulation signals as input and produced joint moments as output. For control purposes, a simulated spinal reflex produced the neural stimulation signals by feeding back the internal state of the musculoskeletal model. Together, the musculoskeletal model and neural reflex took only joint kinematics as input and produced joint moments as output and formed the NMC for controlling the AG.

4.1. Musculoskeletal Model. Nonamputee kinematic, kinetic, and muscle activation data (Appendices A and B) were used to inform the parameter selection of a musculoskeletal model of the human legs. This model comprised a hill-type muscle model for nine effective muscles and attachment geometry of the human leg as described in [19], including optimizer settings and parameter bounds.

The free parameters of the musculoskeletal model were chosen via optimization. The goal was to have the output moments from the optimization closely resemble those from the biological data while keeping simulated metabolic cost close to the measured values. The optimization scheme in [19] was used. For each amputee participant, a corresponding nonamputee was chosen whose height and weight most closely matched that of the given amputee (Table 2). The parameter values of the musculoskeletal model were then optimized based on the walking data at the preferred walking speed for the given nonamputee participant. This preferred speed was that which had the lowest metabolic energy cost per unit distance. This method produced a model that was individually tuned for each amputee.

Several variations of these cost functions have been utilized for determining the parameters of similar models [19, 20]. In the current work, two methods of evaluating the optimizations were utilized (Appendix C). For both methods, the cost included both kinetic and metabolic similarities of the model to the recorded human walking data. The metabolic cost was represented as cost of transport (COT), which was the metabolic energy cost per unit distance traveled. Upper and lower bounds for the model parameters were

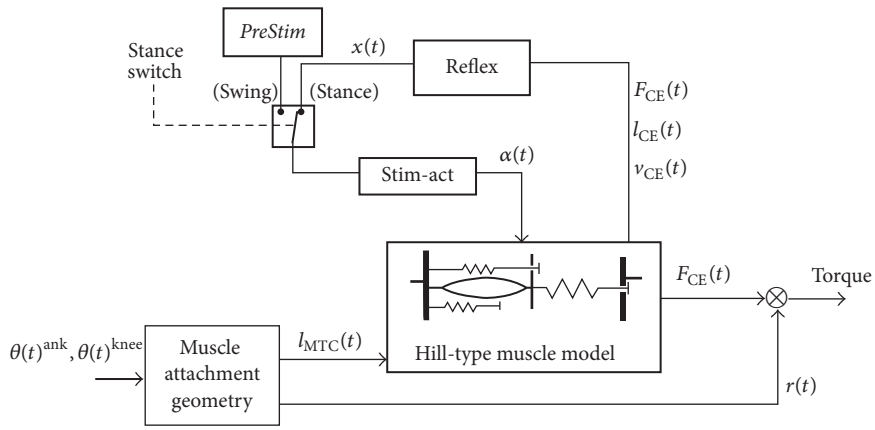

Figure 7: Neuromuscular controller including spinal reflex loop. The input to the neuromuscular controller was the kinematics of the ankle and knee joints $\theta(t)^{\text{ank}}$ and $\theta(t)^{\text{knee}}$. The internal reflex loop fed back muscle force, length, and velocity, and produced an internal activation signal to drive the simulated hill-type muscle model. Lookup tables were used to convert from joint kinematics to muscle-tendon length $l_{\text{MTC}}(t)$ and moment arm $r(t)$.

taken from [19]. Optimization settings were also identical to those from [19], except that the present study limited the number of generations to 50, as convergence was observed. See Appendix D for details on the optimization results.

4.2. Spinal Reflex Model. For the purposes of device control, the muscle model required a neural driving signal $x(t)$ to produce the activation $\alpha(t)$. Force, $F_{\text{CE}}(t)$, length, $l_{\text{CE}}(t)$, and velocity, $v_{\text{CE}}(t)$, feedback was used to model the spinal reflex of the gastrocnemius muscle, in the form described in [18] (Figure 7), with a lower bound of the reflex set to PreStim = 0.001. The stimulation-activation dynamics described in [21, 22] were used to obtain $\alpha(t)$ from the spinal reflex signal, $x(t)$, in the same manner as [19]. Additional details can be found in Appendix E.

The reflex gains and threshold values were optimized for the gastrocnemius muscle by simulating the effects of the reflex loop with the musculoskeletal model in the same manner as a previous study in ankle-foot prosthesis control [18]. These parameters were optimized to minimize the mean squared error between the reflex-based activation signals and the muscle EMG patterns from EMG data, given kinematic data. The optimization was performed using a genetic algorithm followed by a gradient descent method. For each data set corresponding to a nonamputee participant, the gastrocnemius morphological parameters of the musculoskeletal model were taken from the results of the corresponding morphological optimization.

4.3. Neuromuscular Controller Implementation. For the purpose of prosthesis control, the musculoskeletal model took as input walking state information and produced desired torque commands to the robotic joint during the stance phase. The ankle joint angle was read from an electrogoniometer (Delsys, Boston, MA) which measured the affected-side ankle angle, and the affected-side knee joint angle was read from the AG onboard joint angle sensor. The NMC was disabled during the swing phase by setting the neural stimulation to zero using the stance phase switch and ignoring any residual commanded torque. The muscle-tendon length and moment arm geometry were encoded in lookup tables to allow real-time computation of these values from joint kinematics. For additional tuning, the force gain of the reflex controller was made adjustable in real-time. This gain was chosen for adjustment since the controller's output power in simulation, based on nonamputee data, was found to be the most sensitive to changes in this parameter. The NMC was implemented in MATLAB Simulink and compiled to a C executable that communicated at 1 kHz to the master controller that, in turn, controlled the motor.

For each amputee participant, a corresponding model was used, which was based on a height-weight matched nonamputee participant's walking data (Table 2). The COT values for all nonamputee participants across walking speed are shown in Table 3. The participants all had minimal COT at either 1.25 or 1.5 m/s.

With this neuromuscular controller, the AG emulated the behavior of a biological gastrocnemius muscle by taking only the sensor-based ankle and knee joint kinematics as input. Thus, the AG was a self-contained unit that acted as an externally worn gastrocnemius muscle with neural and musculoskeletal dynamics encoded in its control.

5. Clinical Trials

In the final clinical trials, six participants with transtibial amputation walked on an instrumental treadmill while wearing a PAFP-AG combination while biomechanical and metabolic data were collected (Figure 2(a)).

5.1. Experimental Setup. The walking speed for a given amputee was set as the preferred speed determined from the matched nonamputee walking data (Table 3). This speed was set for all walking conditions. The clinical evaluation was conducted at MIT (Cambridge, MA) and was approved by MIT's Committee on the Use of Humans as Experimental Subjects (COUHES). Each participant provided written, informed consent before data collection was initiated.

Table 3: Metabolic cost of transport for nonamputee participants.

Participant	0.75 m/s	1.0 m/s	1.25 m/s	1.5 m/s	1.75 m/s	2.0 m/s	Optimal speed (m/s)
NA1	0.419	0.364	0.326	0.339	0.362	0.380	1.25
NA2	0.462	0.386	0.371	0.375	0.404	0.467	1.25
NA3	0.481	0.389	0.347	0.341	0.368	0.400	1.5
NA4	0.395	0.339	0.305	0.315	0.348	0.408	1.25

Each amputee was first asked to don only the PAFP, and the electrogoniometer was installed on the PAFP for subsequent use with the AG. The participant was then instructed to walk on the treadmill while the prosthesis power was adjusted using the commercial tuning app so to achieve average prosthesis power within two standard deviations from the average biological ankle power at the given walking speed [23]. Prosthesis tuning was subsequently adjusted slightly during subsequent trials as needed in an attempt to maintain prosthesis power within these limits.

Next the amputee donned the AG orthosis along with the PAFP. A short time period was given to ensure that both devices were functioning properly. Then the amputee was asked to walk on an instrumented treadmill at the given walking speed with the same data collection methods used for developing the NMC, including the instrumented treadmill, and reflective markers. Each trial consisted of 90 seconds of data collection.

In addition to using the optimized parameters of the NMC, additional conditions were tested wherein the force feedback reflex gain of the NMC was adjusted manually. This adjustment allowed some level of controller tuning based on the actual participant feedback. While a participant walked on the treadmill with the AG and PAFP, this gain was incrementally increased from its optimized, Default value (the *Default* gain setting) until either further increases in gain were said to be undesirable by the participant or the average power from the device was no longer increasing with higher controller gain (the *Max* gain setting). The gain was then decreased until the average power coming from the device was in the range of the biological gastrocnemius, of 3–5 Joules (the *BioGain* setting) [12, 13]. If the *Default* setting provided less than or equal to 3–5 Joules of net mechanical work per step, an additional gain was set to mid-way between the *Default* gain and the *Max* gain. This additional gain setting was called *Half*.

Once the aforementioned conditions were recorded with the motion capture system, metabolic data were collected using the same gas analysis system as the other data collection sessions (see Section 3.4). The participants were first asked to perform one standing trial to measure standing metabolism. Next, the walking conditions described above were repeated, in random order. Each metabolic trial lasted 6 minutes.

5.2. Data Processing. The same data processing methods as in the NMC development (see Appendix B) were used to obtain gait events, sagittal plane joint moments and angles, and metabolic cost from the recorded data, except that a point-mass of 2 kg was added at the affected-side knee joint of the SIMM model to represent the dynamical effects of the robotic joint and conduit mass. Also affected-side biological knee moment contribution was computed by subtracting the measured AG knee moment from the total knee moment estimated from the inverse dynamics.

The walking metabolism was compared for each amputee participant across trials, where each trial involved a different value for the force feedback reflex gain of the NMC. The optimal gain was found as the one that resulted in the lowest metabolic power for a given amputee. The walking condition (called the OPT condition) corresponding to this optimal gain was then compared to the walking condition where the AG was controlled to behave as a free-joint (called the ZERO condition).

Joint powers were computed as the product of joint velocity from joint kinematics and joint moments derived from the motion capture data, where positive power was defined as that produced by the joint on the environment. Where available, mechanical power from the powered prosthesis was taken from PAFP telemetry data, computed using the prosthesis onboard torque and angle sensors. For two subjects (S2 and S3), these data were not available, so PAFP mechanical power was computed in the same manner as the other joints, using SIMM-derived ankle angular velocities and moments from the motion capture data. AG applied mechanical power was computed from motion capture-based knee joint angular velocity and internal AG torque from strain gauge data.

Positive and negative joint work contributions were defined as the time integral of the positive and negative components of joint power, respectively, integrated over the late stance knee flexion phase (from mid-stance maximum knee extension to ToeOff), and divided by the time in that phase. Flexion and extension moment impulse values were computed in the same way, but using joint moments instead of powers.

Theoretical reductions in metabolic power were computed by assuming the average mechanical power provided by the combined AG knee actuator and ankle prosthesis in the OPT condition, as compared to the ZERO condition (with zero net work assumed for the AG knee in the ZERO condition), could perfectly replace muscle fiber mechanical power. With the efficiency of skeletal muscle assumed to be 25% [24], the reduction in muscle metabolic power was computed as 4 times the observed mechanical power provided by the AG knee actuator and ankle-foot prosthesis in the OPT condition. The resulting change in metabolic power was then compared to the measured metabolic power from the ZERO condition to determine theoretical percent reduction.

Statistics were run on metabolic powers and also bilateral ankle, knee, and hip joint features (flexion and extension

Table 4: Walking conditions for minimal metabolic power (OPT condition). For all but the last row, numbers represent the settings and results during the OPT condition. In the last row, positive values indicate that the given robotic joint produced greater net work in the OPT condition than in the ZERO condition.

Participant	S1	S2	S3	S4	S5	S6
Condition name	Bio	Max	Default	Default	Default	Half
Force gain scaling	0.1	8	1	1	1	1.5
Force gain (1/N)	$3.69e-5$	$4.99e-3$	$3.99e-4$	$6.19e-4$	$5.11e-4$	$7.66e-4$
AG mean power (W/kg)	0.054	0.118	0.028	0.027	0.105	0.031
Change in AG mean power from ZERO (W/kg)	−0.001	+0.020	+0.056	+0.077	+0.011	+0.009

Table 5: Metabolic cost of transport using the artificial gastrocnemius. Values given represent the net metabolic power, above that of basal metabolic rate. Positive values for percent change indicate that the participant required less metabolic power with the neuromuscular controller, compared to the control condition of zero-torque at the knee. Theoretical metabolic reduction, based on the change in knee orthosis and ankle-foot prosthesis applied average power from the ZERO condition to the OPT condition, and assuming 25% muscle efficiency, is also shown for comparison.

	S1	S2	S3	S4	S5	S6
ZERO Condition Net Metabolic Power (W/kg)	2.95	3.51	3.60	5.06	3.34	3.52
OPT Condition Net Metabolic Power (W/kg)	3.13	3.08	3.87	4.95	2.97	3.38
Percent change in metabolic power from ZERO condition to OPT condition	5.8	−12.1	7.4	−2.3	−11.1	−4.0
Theoretical percent change in metabolic power	−7.2	−15.7	−9.3	−8.3	−14.1	−4.6

moment impulses and positive and negative joint work contributions) by performing a two-sided, paired t-test between these features during the OPT condition and ZERO condition. Statistically significant differences were defined as those with p values less than or equal to 0.05.

5.3. Clinical Results

5.3.1. AG Overall Device Performance. In the final amputee trials with the AG-PAFP combination, the metabolically optimal (OPT) conditions were found for each participant, based on the adjusted parameter of the force-reflex gain. The gain settings and average output power from the AG joints are summarized in Table 4.

5.3.2. Metabolic Power. Walking metabolism is shown in Table 5 for the walking conditions in which the metabolic cost was found to be lowest, compared to the theoretically calculated values using device average power. Large percentage reductions in metabolism were found in two of the six participants. Two participants showed small metabolic reductions, and the two remaining participants had metabolism values higher with the AG intervention, compared to the zero-torque condition. Within the participants with a metabolic reduction in the OPT condition, these metabolic reductions were well correlated with the theoretical values based on device mechanical power ($r = 0.9$), as shown in Table 5. However, Subject 1 and Subject 3 displayed increases in metabolism in the OPT condition, as compared to the ZERO condition, which was not predicted with the theoretical calculations. Overall, the metabolic power between the ZERO and OPT conditions was not found to be statistically significant ($p = 0.43$).

5.3.3. Joint Kinetics. Comparing the ZERO and OPT conditions, statistically significant differences were found in the biological knee flexion moment impulse and biological hip positive work of the affected leg during the late-stance knee flexion phase of gait. The knee flexion moment impulse was reduced by an average of 0.0223 Nm∗s/kg ($p = 0.03$), from the ZERO condition (0.0413 ± 0.0262 Nm∗s/kg) to the OPT condition (0.0190 ± 0.0252 Nm∗s/kg). Figure 8 illustrates the AG and biological knee moment contributions over the gait cycle. The affected-side hip showed a decrease in positive

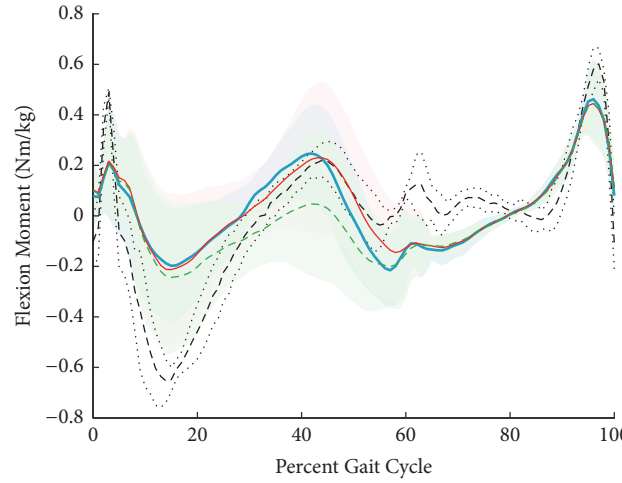

Figure 8: Components of affected-side knee moment of amputee participants with the powered AG, averaged across participants. The net value, which is the sum of biological knee and AG values, is shown for two walking conditions: the ZERO condition (thick solid blue line) and the OPT condition (thin solid red line). The contribution from the biological knee joint is also shown for the OPT condition (dashed thin green line). Nonamputee data, averaged across participants, are shown for reference, with the mean (dashed black line) ± one standard deviation (dotted black lines).

work of 0.0739 J/kg ($p = 0.004$) from the ZERO condition (0.2621 ± 0.0848 J/kg) to the OPT condition (0.1882 ± 0.0734 J/kg). All other tested kinetic features did not indicate significant differences between conditions.

5.4. Discussion. Although a statistically significant metabolic reduction across participants was not found in this study, the large percentage reductions in metabolism for some participants, as in Table 5, indicate that it is likely that a metabolic advantage may be achieved with a powered artificial gastrocnemius, provided appropriate conditions are satisfied. It is yet unclear what exact conditions must be met to provide metabolic reductions for all participants. However, within the participants with a metabolic reduction in the OPT condition, these reductions were fairly well correlated with the theoretical values based on device mechanical power ($r = 0.9$), as shown in Table 5. Therefore, it is possible that higher levels of mechanical power from the AG would increase the chance of producing a statistically significant metabolic reduction across participants.

The kinetic changes, as also illustrated in Figure 8, support the hypothesis that the AG causes a reduction in affected biological knee flexion moment impulse and hip positive net work, but not knee positive work or hip moment impulse. Considering the short trial times, this result indicates that participants were capable of rapid kinetic responses to the interventions, on the order of several minutes or less. The knee moment impulse reduction may stem from an attempt by the participants to prevent the total knee moment from changing in the presence of the external disturbance. This result is consistent with other studies, as humans have been observed to maintain invariant joint moments at both the ankle [25] and hip joints [26] when an external torque from an exoskeleton is applied. This finding has a potential consequence: if the applied joint moment from the AG exceeded the affected knee moment from the ZERO condition, the participant might attempt to maintain total joint kinetics by providing an active extension moment with their quadriceps, so to prevent the total knee flexion moment from increasing. This behavior may put an upper-limit on the flexion torque that can be provided by the AG without incurring a cost from the quadriceps in the form of active knee extension efforts.

5.4.1. Potential Mechanisms for Metabolic Reductions. First, it is possible that this reduction in knee moment itself may play a role in the metabolic reduction in some of the participants, as the production of muscle force exacts a metabolic cost [27]. However, the generation of isometric muscle force alone is comparatively less costly compared to the generation of mechanical work. Therefore, other factors are likely at play.

The similarity of the observed metabolic reductions to the theoretical values (Table 5) suggests that much of the power provided by the AG goes to replacing muscle fiber positive work, as modeled in the theoretical cost values. The reduction in affected-side hip positive work with AG assistance indicates that energy may be transferred from the AG up to the hip from the knee. These hip work reductions seen in late-stance knee flexion coincide with the initiation of hip flexion during preswing, indicating that the AG probably helps to initiate leg swing. This result is consistent with what is known about the normal function of the human gastrocnemius muscle during walking [28, 29].

6. Conclusions and Future Work

To create the first fully powered artificial gastrocnemius for transtibial amputees, we develop a versatile knee orthosis that is capable of kinetic behavior comparable to the biological gastrocnemius. The control strategies provide low errors between desired and measured joint torque across a wide dynamic range. Good torque tracking of zero-torque commands allow for metabolic transparency, while the torque tracking at higher torque levels enables the system to replicate desired behavior. This large dynamic range is attributed to the tethered system that enabled large power capability without the commensurate cost of added actuator mass. Others have made use of this type of platform for this reason [30, 31]. Unlike other researchers, however, our use of a cable linkage mitigates transmission losses in the cable drive compared to a pure Bowden cable transmission, since only part of the cable is in contact with the conduit surfaces. This system is well suited for simulating a gastrocnemius muscle at the knee for amputee participants.

The clinical study presented here represents an effort to improve upon earlier biarticular transtibial prostheses by using an active element for the affected knee joint. Such an active device can provide positive net work, unlike previous quasi-passive counterparts [10, 11]. If this net robotic work replaces positive muscle work, we expect to see large reductions in metabolism with the biarticular conditions, as compared to the monoarticular conditions. Indeed, with the application of sufficient positive work, the results suggest that it may be possible to provide metabolic and kinetic assistance to transtibial amputee walking gaits beyond that provided by a powered ankle-foot prosthesis alone. This study also provides suggestive evidence that metabolic improvements may stem from not only reductions in muscle activity at the assisted joint, but other joints as well, such as the hip. This finding is consistent with other work in lower-extremity exoskeletons [32].

However, this study also highlights the difficulty of reducing metabolic demand in humans, even in the presence of an existing pathology. Even the smallest unwanted perturbations can severely hinder an intervention that would otherwise cause a successful metabolic improvement. Thus, in the development of assistive wearable devices, it is of utmost importance to consider the biomechanical consequences of applying torques and powers to the human body. Future work could utilize a torque control strategy to more systematically vary output power levels of the AG to determine if higher net positive work could further improve metabolic cost of the wearer, as researchers have performed with an ankle exoskeleton [33]. An additional next step would be to use a modified NMC to command both the knee and ankle joints of the powered artificial gastrocnemius with one, unified model. Indeed, such a control strategy would provide better synchronization between the knee and ankle actuators.

Table 6: Nonamputee body parameters.

Participant number	Height (cm)	Weight (kg)
NA1	175	73.4
NA2	180	90.3
NA3	188	95.4
NA4	180	103

In the advancement of active transtibial prostheses, we feel a powered artificial gastrocnemius is of critical importance. It is our hope that this study will underscore the potential of this novel mechatronic approach to the biomechanical and physiological gait performance of persons with transtibial leg amputation.

Appendix

A. Neuromuscular Controller Data Collection

The parameters of the neuromuscular controller (NMC) were selected in two stages. In the first stage, the musculoskeletal model parameters were optimized for a full leg musculoskeletal model so to best match biological joint moments and metabolism, given biological kinetics and EMG data. In the second stage, the morphological model parameters for the gastrocnemius were fixed at their optimized values, and the reflex parameters were optimized for this muscle.

The gait data of four healthy, nonamputees were used to inform the parameters of the NMC. These nonamputee participants were chosen so to match the amputees as closely as possible (see Table 6). The clinical evaluation was conducted at MIT (Cambridge, MA) and was approved by MIT's Committee on the Use of Humans as Experimental Subjects (COUHES). Each participant provided written, informed consent which was obtained before data collection was initiated. These data were collected in two phases.

In the first phase, kinematic, kinetic, and electromyographic (EMG) data were collected for 90 seconds at each of six speeds (0.75 m/s, 1.00 m/s, 1.25 m/s, 1.50 m/s, 1.75 m/s, and 2.00 m/s) in random order. An infrared camera system (12 cameras, model: T40s, Vicon Motion Systems Ltd., Oxford, UK) was used to track the motion of subjects as they walked in the capture volume. Reflective markers were placed at 47 locations on each participant's body, based on the Helen Hayes marker model, and their three-dimensional trajectories were recorded at 100 Hz. The marker locations were chosen specifically to track joint motion. The ground reaction forces and contact centers of pressure were measured using an instrumented force plate treadmill (Bertec Corporation, Columbus, OH) with a sampling rate of 1 kHz. Electromyographic signals were collected at 2 kHz using a wireless surface system (Trigno, Delsys Inc., Natick MA). Twelve muscles (tibialis anterior, soleus, medial gastrocnemius, lateral gastrocnemius, rectus femoris, vastus lateralis, vastus medialis, semimembranosus, biceps femoris long head, adductor magnus, iliacus, and gluteus maximus) on the right leg of each subject were recorded, with symmetry being assumed for the other leg. Prior to the walking trials, the muscle maximum voluntary contraction (MVC) tests were performed for each of the muscles of interest, in which the participants were instructed to push as hard as possible, three times in succession for 3–5 seconds each with the given muscle group, while electromyographic data were collected.

Once the first data collection phase was completed, the markers and electrodes were removed, and the participants were equipped with an open-circuit gas exchange measurement system for estimating metabolic cost (model: K4b2, COSMED, Rome, Italy). The participants were asked to perform one standing trial to measure standing metabolism, and then walking trials were performed on the treadmill for the same six walking speeds. Each walking trial lasted six minutes.

B. Neuromuscular Controller Data Processing

Fourth-order Butterworth filters were used to filter the marker position and ground reaction force data with 6 Hz and 25 Hz cutoff frequencies, respectively. The marker and force data were postprocessed through the inverse dynamics module of SIMM (MusculoGraphics Inc., Evanston, IL), to produce joint moments and angles for ankle, knee, and hip joints, as well as muscle-tendon lengths and moment arms, all as a function of time. Only sagittal plane dynamics were considered.

Gait events were determined using vertical ground reaction force data from the embedded force plates. Approximate event timing was found by determining the times when the force increased beyond a 40 N threshold. Exact heel strike and ToeOff times where found by progressing backward and forward in time, respectively, until the force value dropped to zero. Data were then cut to gait cycles based on heel strike times and resampled to 101 points. Gait cycles were discarded for the beginning and end of each trial, during the speed transients of the treadmill. Gait cycles in which the stride times were below 0.7 seconds or above 1.3 seconds or in which a foot crossed the midline of the treadmill were also discarded. Metabolic cost for each walking speed was computed in the same manner as in the nonamputee validation trials (Section 3.4).

Several processing steps were taken to prepare the EMG signal to be processed for the estimation of muscle activation. EMG signals were first processed internally by the EMG system by applying a 4th-order bandpass filter with a pass band from 20 Hz to 450 Hz. A 60-Hz notch filter was also applied to remove mains hum. Any DC offset was removed, and the remaining signal was saturated at 5 standard deviations from zero. The signal was then normalized to the new maximum value of 5 standard deviations and rectified.

The processed EMG data were further processed with the method described in [19] to achieve estimates of muscle activation from the measured EMG signals. The activation was initially scaled by those resulting from the MVC trials, but the resulting scaled EMG signals were unreasonably scaled when compared to literature values. Therefore, the final magnitudes of the estimated activation signals were scaled so that the average values of the activation signals

Table 7: Optimized morphological parameters.

Parameter	S1	S2	S3	S4	S5	S6
F_{max}	1094	1052	1094	1936	3049	3049
l_{sl}	0.4565	0.4115	0.4565	0.4568	0.4217	0.4217
l_{opt}	0.0504	0.0454	0.0504	0.0504	0.0465	0.0465
K_{sh}	2.58	2.78	2.58	2.722	2.84	2.84
λ_{ref}	0.0593	0.0684	0.0593	0.0599	0.0846	0.0846

matched those from [34] during the range of activation for the literature data.

As was found in a previous study [19], many of the muscles spanning the hip were found to have signals too weak to be reliably measured (rectus femoris, iliacus, biceps femoris short head, hip abductors, adductor longus, and adductor magnus). For these muscles, neural excitation profiles from wire electrode experiments [34] were delayed 40 ms to simulate the delay between the EMG signals and the development of force [35] and then passed through the same activation dynamics used for the collected electromyographic data. The resulting activation signals were then used as input to the musculoskeletal model along with those derived from the electromyography.

C. Morphological Optimization Cost Functions

In the current work, two methods of evaluating the morphological model parameters were utilized. For the first cost function (used for Subjects 2 and 3), the musculoskeletal model parameters were optimized using the method described by [19]. However, using this method, it was found that the measured electromyographic data failed to produce satisfactory values for both kinetic fits and metabolic cost estimates; either kinetic fit R^2 values were low (less than a cutoff threshold of 0.7) or the metabolic cost estimates of the model were more than one standard deviation higher than the mean of the empirical metabolic cost values (from the nonamputee participants walking at their preferred speeds). As an alternative, the activation profiles derived from wire electrode experiments [34] provided both kinetic and metabolic results closer to that of biology. Therefore, for this optimization method, all muscle activation profiles were derived from the wire electrode literature [34], processed through the same activation dynamics used for the EMG [19]. Selection of the final parameter set was also performed as in [19]. For Subject 2, the HAB muscle group was used for selecting the final parameter set. For Subject 3, the VAS muscle group was used. These muscles were selected based on their dominance in the simulated fractional metabolic cost.

Some biological walking data did not produce acceptable kinetic and metabolic cost values (as described above) with the first optimization method (those for Subjects 1, 5, and 6), or the resulting model produced low average mechanical power when tested in simulation with walking kinematics and EMG as input (Subject 4). For these data sets, a different cost function was used. This metabolic cost estimation function was based on empirical measures of muscle metabolic energy consumption as a function of fiber contractile velocity and activation [36, 37]. The simulated metabolic cost was found by integrating muscle power for each muscle in the leg over the gait cycle, and summing up all muscles for the leg, assuming bilateral symmetry. The measured basal energy consumption was added to the resulting value to determine the full-body metabolic energy cost. As with the first cost function, both the simulated metabolic cost and the average kinetic fit were considered for the evaluation of parameter solutions. However, it was found that the kinetic fit was largely invariant in the range of solutions where the simulated COT was near that of the measured values. Therefore, in selecting a single solution, the parameter set with the best kinetic fit was chosen, provided that the simulated COT was within the standard error of the measured COT value. A similar parameter selection method had been used to select optimal parameter sets in previous work [38].

Table 8: Final cost values for the morphological parameter optimization. The COT values were the simulated metabolic cost of transport values, as computed by the musculoskeletal model, when given the final optimized parameter set and biological nonamputee data as input.

Cost value	S1	S2	S3	S4	S5	S6
R^2	0.71	0.76	0.80	0.85	0.80	0.80
COT	0.360	0.324	0.246	0.330	0.301	0.301

D. Morphological Parameter Optimization Results

The optimized morphological parameters for the gastrocnemius muscle are shown in Table 7. The cost values are shown in Table 8. These parameters correspond to those in the model described in previous work [19].

E. Spinal Reflex Model

The muscle model required a neural driving signal $x(t)$ to produce the activation $\alpha(t)$. Herein, the neural driving signal can be represented as [18]

$$\begin{aligned} x(t) = {} & G_F \cdot \left(F\left(t - \Delta t_F\right) - F_0\right) \cdot u\left(F - F_0\right) + G_l \\ & \cdot \left(l\left(t - \Delta t_{lv}\right) - l_0\right) \cdot u\left(l - l_0\right) + G_v \\ & \cdot \left(v\left(t - \Delta t_{lv}\right) - v_0\right) \cdot u\left(|v| - v_0\right). \end{aligned} \tag{E.1}$$

Here, G_F, G_l, and G_v are the gains; Δt_F, Δt_l, and Δt_v are the time delays for the force, muscle length, and muscle velocity

Table 9: Optimized neuromuscular model reflex parameters. Each column represents the settings for an amputee participant, with the corresponding nonamputee data set in parentheses.

	S1 (NA2)	S2 (NA1)	S3 (NA3)	S4 (NA3)	S5 (NA4)	S6 (NA4)
G_F (1/N)	$3.687e-4$	$6.238e-4$	$3.994e-4$	$6.185e-4$	$5.11e-4$	$5.11e-4$
F_0 (N)	0.1786	0.3935	0.3624	0.291	0.532	0.532
G_l (1/m)	6.88	5.22	1.3465	6.32	8.19	8.19
l_0 (m)	0.0507	0.0490	0.0528	0.0448	0.0382	0.0382
G_v (s/m)	0.9606	1.34	2.00	0.0193	2.00	2.00
v_0 (m/s)	0.1230	−0.1175	−0.1168	−0.0897	0.0340	0.0340

values, respectively. The function $u(\cdots)$ is a step function, indicating that each reflex only activates for values greater than the corresponding threshold value (F_0, l_0, and v_0 for force, length, and velocity, resp.). The time delays model the neural delay for a signal to traverse the reflex arc from muscle to spinal cord and back to the muscle. All three delays were fixed at 20 ms [39–41]. The reflex signal $x(t)$ represents the neural stimulation. The optimized parameter values for the reflex loop are shown in Table 9. The stimulation-activation dynamics described in previous work [19] were used to obtain the muscle activation, α.

Conflicts of Interest

The authors declare no conflicts of interest regarding the publication of this article.

Acknowledgments

This work was supported by NASA [NNX12AM16G] as part of the National Robotics Initiative and departmental funding from the MIT Media Lab. The authors thank Bob Emerson and Jared Markowitz for sharing their valuable expertise.

References

[1] N. H. Molen, "Energy/speed relation of below-knee amputees walking on a motor-driven treadmill," *Internationale Zeitschrift für Angewandte Physiologie Einschließlich Arbeitsphysiologie*, vol. 31, no. 3, pp. 173–185, 1973.

[2] R. L. Waters, J. Perry, D. Antonelli, and H. Hislop, "Energy cost of walking of amputees: the influence of level of amputation," *The Journal of Bone & Joint Surgery*, vol. 58, no. 1, pp. 42–46, 1976.

[3] G. Colborne, S. Naumann, P. Longmuir, and D. Berbrayer, *Am J Phys Med Rehabil*, vol. 71, no. 5, pp. 272–278, 1992.

[4] P.-F. Su, S. A. Gard, R. D. Lipschutz, and T. A. Kuiken, "Gait characteristics of persons with bilateral transtibial amputations," *Journal of Rehabilitation Research and Development* , vol. 44, no. 4, pp. 491–501, 2007.

[5] H. M. Herr and A. M. Grabowski, "Bionic ankle-foot prosthesis normalizes walking gait for persons with leg amputation," *Proceedings of the Royal Society B Biological Science*, vol. 279, no. 1728, pp. 457–464, 2012.

[6] D. Hill and H. Herr, "Effects of a powered ankle-foot prosthesis on kinetic loading of the contralateral limb: a case series," in *Proceedings of the IEEE International Conference on Rehabilitation Robotics (ICORR '13)*, pp. 1–6, Seattle, Wash, USA, June 2013.

[7] M. R. Williams, A. Grabowski, H. Herr, and S. D'Andrea, "Electromyographic effects of using a powered ankle-foot prosthesis," *American Society of Biomechanics*, 2012.

[8] E. Isakov, O. Keren, and N. Benjuya, "Trans-tibial amputee gait: Time-distance parameters and EMG activity," *Prosthetics and Orthotics International*, vol. 24, no. 3, pp. 216–220, 2000.

[9] E. Isakov, H. Burger, J. Krajnik, M. Gregoric, and C. Marincek, "Knee muscle activity during ambulation of trans-tibial amputees," *Journal of Rehabilitation Medicine*, vol. 33, no. 5, pp. 196–199, 2001.

[10] K. Endo, E. Swart, and H. Herr, "An artificial gastrocnemius for a transtibial prosthesis," in *Proceedings of the 31st Annual International Conference of the IEEE Engineering in Medicine and Biology Society: Engineering the Future of Biomedicine, EMBC 2009*, pp. 5034–5037, USA, September 2009.

[11] M. F. Eilenberg, K. Endo, and H. Herr, "Biomechanic and Energetic Effects of a Quasi-Passive Artificial Gastrocnemius on Transtibial Amputee Gait," *Journal of Robotics*, In press.

[12] R. J. Zmitrewicz, R. R. Neptune, and K. Sasaki, "Mechanical energetic contributions from individual muscles and elastic prosthetic feet during symmetric unilateral transtibial amputee walking: A theoretical study," *Journal of Biomechanics*, vol. 40, no. 8, pp. 1824–1831, 2007.

[13] R. R. Neptune, K. Sasaki, and S. A. Kautz, "The effect of walking speed on muscle function and mechanical energetics," *Gait & Posture*, vol. 28, no. 1, pp. 135–143, 2008.

[14] R. C. Browning, J. R. Modica, R. Kram, and A. Goswami, "The effects of adding mass to the legs on the energetics and biomechanics of walking," *Medicine & Science in Sports & Exercise*, vol. 39, no. 3, pp. 515–525, 2007.

[15] J. Zhang, C. C. Cheah, and S. H. Collins, "Experimental comparison of torque control methods on an ankle exoskeleton during human walking," in *Proceedings of the 2015 IEEE International Conference on Robotics and Automation, ICRA 2015*, pp. 5584–5589, USA, May 2015.

[16] J. M. Brockway, "Derivation of formulae used to calculate energy expenditure in man," *Hum Nutr Clin Nutr*, vol. 41, no. 6, pp. 463–471, 1987.

[17] M. F. Eilenberg, H. Geyer, and H. Herr, "Control of a powered ankle-foot prosthesis based on a neuromuscular model," *IEEE Transactions on Neural Systems and Rehabilitation Engineering*, vol. 18, no. 2, pp. 164–173, 2010.

[18] J. Markowitz, P. Krishnaswamy, M. F. Eilenberg, K. Endo, C. B. Chris, and H. Herr, "Speed adaptation in a powered transtibial prosthesis controlled with a neuromuscular model," *Philosophical Transactions of the Royal Society B: Biological Sciences*, vol. 366, no. 1570, pp. 1621–1631, 2011.

[19] J. Markowitz and H. Herr, "Human Leg Model Predicts Muscle Forces, States, and Energetics during Walking," *PLoS Computational Biology*, vol. 12, no. 5, Article ID e1004912, 2016.

[20] P. Krishnaswamy, E. N. Brown, and H. M. Herr, "Human leg model predicts ankle muscle-tendon morphology, state, roles and energetics in walking," *PLoS Computational Biology*, vol. 7, no. 3, Article ID e1001107, 2011.

[21] J. He, W. S. Levine, and G. E. Loeb, "Feedback Gains for Correcting Small Perturbations to Standing Posture," *IEEE Transactions on Automatic Control*, vol. 36, no. 3, pp. 322–332, 1991.

[22] C. C. Raasch, F. E. Zajac, B. Ma, and W. S. Levine, "Muscle coordination of maximum-speed pedaling," *Journal of Biomechanics*, vol. 30, no. 6, pp. 595–602, 1997.

[23] M. Palmer, *Sagittal Plane Characterization of Normal Human Ankle Function Across a Range of Walking Gait Speeds , Masters Thesis [Masters, thesis]*, MIT, 2002.

[24] R. Margaria, *Biomechanics and Energetics of Muscular Exercise*, Clarendon Press, Oxford, 1976.

[25] P.-C. Kao, C. L. Lewis, and D. P. Ferris, "Invariant ankle moment patterns when walking with and without a robotic ankle exoskeleton," *Journal of Biomechanics*, vol. 43, no. 2, pp. 203–209, 2010.

[26] C. L. Lewis and D. P. Ferris, "Erratum to "Invariant hip moment pattern while walking with a robotic hip exoskeleton" [J. Biomech. 44 (5) (2011) 789-793]," *Journal of Biomechanics*, vol. 47, no. 7, p. 1748, 2014.

[27] T. M. Griffin, T. J. Roberts, and R. Kram, "Metabolic cost of generating muscular force in human walking: insights from load-carrying and speed experiments," *Journal of Applied Physiology*, vol. 95, no. 1, pp. 172–183, 2003.

[28] R. R. Neptune, S. A. Kautz, and F. E. Zajac, "Contributions of the individual ankle plantar flexors to support, forward progression and swing initiation during walking," *Journal of Biomechanics*, vol. 34, no. 11, pp. 1387–1398, 2001.

[29] R. R. Neptune, F. E. Zajac, and S. A. Kautz, "Muscle force redistributes segmental power for body progression during walking," *Gait & Posture*, vol. 19, no. 2, pp. 194–205, 2004.

[30] J. M. Caputo and S. H. Collins, "An experimental robotic testbed for accelerated development of ankle prostheses," in *Proceedings of the IEEE International Conference on Robotics and Automation (ICRA '13)*, pp. 2645–2650, Karlsruhe, Germany, May 2013.

[31] Y. Ding, I. Galiana, A. T. Asbeck et al., "Biomechanical and physiological evaluation of multi-joint assistance with soft exosuits," *IEEE Transactions on Neural Systems and Rehabilitation Engineering*, vol. 25, no. 2, pp. 119–130, 2017.

[32] L. M. Mooney and H. M. Herr, "Biomechanical walking mechanisms underlying the metabolic reduction caused by an autonomous exoskeleton," *Journal of NeuroEngineering and Rehabilitation*, vol. 13, no. 1, article no. 111, 2016.

[33] R. W. Jackson and S. H. Collins, "An experimental comparison of the relative benefits of work and torque assistance in ankle exoskeletons," *Journal of Applied Physiology*, vol. 119, no. 5, pp. 541–557, 2015.

[34] J. Perry, *Gait Analysis: Normal and Pathological Function*, SLACK, Inc, New Jersey, NJ, USA, 1992.

[35] E. M. Arnold, S. R. Hamner, A. Seth, M. Millard, and S. L. Delp, "How muscle fiber lengths and velocities affect muscle force generation as humans walk and run at different speeds," *Journal of Experimental Biology*, vol. 216, no. 11, pp. 2150–2160, 2013.

[36] A. V. Hill, "The heat of shortening and the dynamic constants of muscle," *Proceedings of the Royal Society B*, vol. 126, no. 843, pp. 136–195, 1938.

[37] A. V. Hill, "The efficiency of mechanical power development during muscular shortening and its relation to load," *Proceedings of the Royal Society B Biological Science*, vol. 159, no. 975, pp. 319–324, 1964.

[38] K. Endo and H. Herr, "A model of muscle-tendon function in human walking," in *Proceedings of the 2009 IEEE International Conference on Robotics and Automation, ICRA '09*, pp. 1909–1915, Japan, May 2009.

[39] H. Geyer, A. Seyfarth, and R. Blickhan, "Positive force feedback in bouncing gaits?" *Proceedings of the Royal Society B Biological Science*, vol. 270, no. 1529, pp. 2173–2183, 2003.

[40] R. B. Stein and C. Capaday, "The modulation of human reflexes during functional motor tasks," *Trends in Neurosciences*, vol. 11, no. 7, pp. 328–332, 1988.

[41] M. Knikou and W. Rymer, "Erratum: effects of changes in hip joint angle on H-reflex excitability in humans," *Experimental Brain Research*, vol. 143, no. 4, pp. 149–159, 2002.

Hindawi
Journal of Robotics
Volume 2017, Article ID 9618375, 15 pages
https://doi.org/10.1155/2017/9618375

Review Article

Adaptive Foot in Lower-Limb Prostheses

Thilina H. Weerakkody, Thilina Dulantha Lalitharatne, and R. A. R. C. Gopura

Bionics Laboratory, Department of Mechanical Engineering, University of Moratuwa, Katubedda, Sri Lanka

Correspondence should be addressed to Thilina H. Weerakkody; thilinahweerakkody@gmail.com

Received 20 May 2017; Revised 1 August 2017; Accepted 3 October 2017; Published 20 November 2017

Academic Editor: Gordon R. Pennock

The human foot consists of complex sets of joints. The adaptive nature of the human foot enables it to be stable on any uneven surface. It is important to have such adaptive capabilities in the artificial prosthesis to achieve most of the essential movements for lower-limb amputees. However, many existing lower-limb prostheses lack the adaptive nature. This paper reviews lower-limb adaptive foot prostheses. In order to understand the design concepts of adaptive foot prostheses, the biomechanics of human foot have been explained. Additionally, the requirements and design challenges are investigated and presented. In this review, adaptive foot prostheses are classified according to actuation method. Furthermore, merits and demerits of present-day adaptive foot prostheses are presented based on the hardware construction. The hardware configurations of recent adaptive foot prostheses are analyzed and compared. At the end, potential future developments are highlighted.

1. Introduction

Lower-limb assistive devices can be divided into two main categories as orthosis and prosthesis. The orthosis is an orthopaedic apparatus which is used as support for adjusting deformities to improve functionalities of moving body parts whereas prosthesis is an artificial replacement for a missing body part [1, 2]. According to the literature survey on amputation in 2005, the United States (USA) recorded about 1.6 million lower-limb amputees. It was predicted that the number of lower-limb amputees would be increased to 3.6 million over the span of the next 50 years [3]. Another Tanzania-based survey reported 86.4% of total amputees as lower-limb amputees [4]. A survey conducted in Brazil reports that 25% of total amputees require foot prostheses solutions [5]. Long-term passive flat foot prostheses users tend to suffer from physical injuries such as osteoarthritis, osteopenia, and subsequent osteoporosis due to musculoskeletal imbalances or pathologies [6, 7]. Foot prosthesis with flexible adaption capabilities is a precaution for the above-mentioned injuries [6, 7]. Statistical data and possible physical injuries reflect the necessity of suitable and reliable adaptive foot prostheses which could mimic the human foot functionalities in commercial level. Foot amputees' lives can be uplifted and made comfortable and more productive to the society by developing advanced, reliable prosthetic solutions. Currently, some passive [8–16], active [17–19], and hybrid [20–30] adaptive foot prostheses have been developed with a focus on different functional requirements and design mechanisms.

The human foot has the adaptive capability which enables the foot to withstand any uneven surface. Necessary kinematic and kinetic adjustments are done to the gait pattern during ambulation by pedestrians in order to maintain stability on slopped or uneven terrains [31]. Normally, the human walking decisions are taken upon on human vision sensors and neural sensors. Amputees lack certain neural sensors due to the loss of their body part. The inability of surface adaption of the foot has significantly increased the load on the residual limb. Additionally, pressure ulcers and deep tissue injuries can occur as a result of significant pressure on a residual limb [32]. Lack of stability causes prostheses users to fall when entering an uneven surface [33]. Lack of inversion-eversion in ankle prosthesis can cause instability due to partial contraction with the surface. Suitable solutions for these physical and practical problems have to be addressed when designing an adaptive foot prostheses. However, most of the existing lower-limb ankle prostheses

have not focused on developing a proper adaptive foot prosthesis for their ankle prosthetic devices. Instead, the passive flat prosthetic foot has been commonly used as the end connector for commercial lower-limb prostheses such as Otto Bock. Since passive flat foot prostheses have limited functional capabilities and other physical side effects as mentioned above, adaptive foot prostheses are essential to be developed to regain natural foot motions in lower-limb prostheses [34–37].

In this paper, authors have reviewed designs and developments of adaptive foot prostheses that have been proposed for lower-limb prostheses since 1997. It is essential to study design features, merits, and demerits of existing designs in order to enhance the field of adaptive foot prostheses. Some of the available reviews are focused on lower-limb prostheses [38, 39], control methods of lower-limb prostheses [40, 41], and prosthetic feet devices [42]. Versluys et al. [42] classified conventional feet, energy storing feet, and bionic feet upon control, comfort, and cosmetics. They have reviewed only a limited number of existing bionic foot devices and also adaptive mechanisms have not been considered for the review article. Since 2009, a lot of active foot prostheses have been introduced with novel mechanisms. In-depth review on adaptive foot prostheses is rarely found with those novel mechanisms. A prompt review paper on adaptive foot prostheses is very useful, not only to identify the current status of research but also to provide information to anyone in the field of developing adaptive foot prostheses. This paper is prepared based on existing adaptive foot prostheses. Some passive prostheses are available with notable design functionalities and mechanisms. They can be transferred into active designs with suitable design changes which lead to adding those devices into this paper. The focus of this paper remains in existing designs, their favourable and adverse design issues, and common solutions available in adaptive foot prostheses.

The systematic review on recent developments in foot prostheses has been done based on sets of design criteria. The papers were chosen based on preselected search keywords. Out of many scientific databases, the following were selected due to the availability of a higher number of the relevant manuscripts: IEEE Xplore, Elsevier, SAGE, InTech, PLOS ONE, ASME (American Society of Mechanical Engineer's Journal), and Journal of Rehabilitation Research & Development (JRRD). The paper selection was compiled upon PRISMA criteria [43]. The selected papers were initially screened, then the duplications were removed, and the papers were further refined due to irrelevance. Later search keywords were readjusted in order to obtain a higher number of relevant results. Finally, the search keywords "adaptive foot prostheses" were selected. The detailed review methodology is explained in Section 5 below.

The paper is structured as follows. In Section 2, the anatomy of the ankle and foot has been explained briefly in order to clarify the adaptive foot prostheses functional requirements. Section 3 presents requirements and design difficulties encountered in adaptive foot prostheses development. Classification of adaptive foot prostheses is presented in Section 4. The extended details, a method of literature selection for the analysis, and comparison and review of existing prostheses are included in Section 5. Finally, discussion and future directions are included in Section 6.

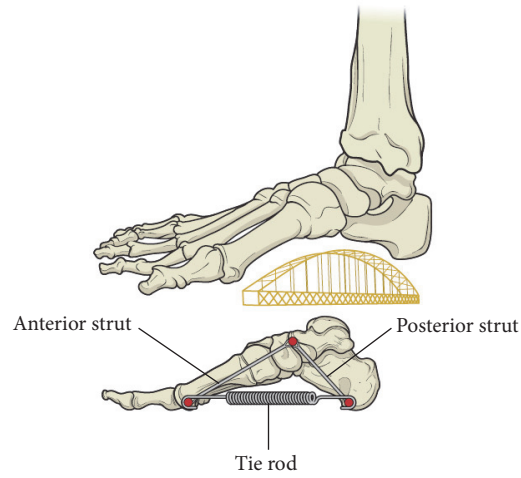

Figure 1: The arch of foot mechanism [45].

2. Anatomy of Ankle and Foot

The main function of the foot is performing gait cycle. Sufficient amount of mobility and stability is necessary for the foot to perform its tasks. Absorbing the ground reaction force is critically important for mobility. Stability is essential for well-balanced body posture [44]. The foot consists of 6 joints which can move along sagittal and transverse planes. Due to the complexity in foot joints, developing a foot prosthesis to mimic the human foot adaption capability is a challenging task. The anatomy of the human foot consists of 26 bones, 33 joints, 20 muscles, and over 100 ligaments [45, 46]. It can carry the human body weight due to its complex structure. The foot is capable of varying flexibility and elasticity of the complex structure to perform various challenging tasks such as running, climbing, balancing, jumping, hopping, and going up on the toes [45]. The foot bones are distributed along two main concurrent structures, known as the ache. There are three types which are medial longitudinal arch, lateral longitudinal arch, and transverse arch. The surface adaption (or flexibility and elasticity) of the foot occurs due to varying the arch angle of the foot (Figure 1). View along longitudinal (sagittal plane) arch is shown in Figure 2. The curvature of the bones of the foot provides a structure which is able to absorb high force repetitively similar to a bridge. Additionally, intrinsic and extrinsic muscles provide structural resilience by serving a tie rod as shown in Figures 1 and 2. As a result of contraction and relaxation of these muscles, the arch of the foot changes and increases the surface adaption capability of the foot. This geometric distribution combined with tendons and muscles creates foot windlass mechanism [47]. Windlass mechanism is used for moving heavy loads in engineering applications. Similarly, windlass mechanism provides the additional support for the foot arch to carry the load.

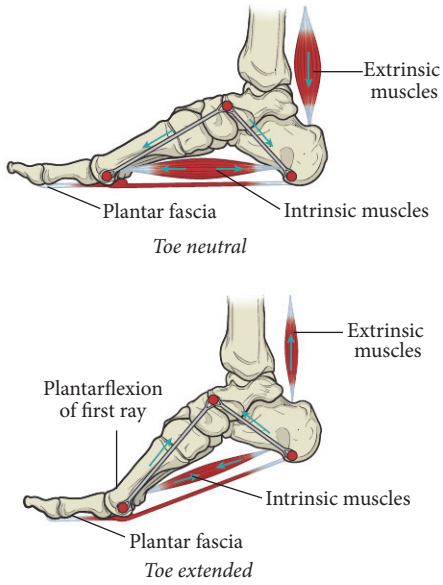

Figure 2: Windlass mechanism [45].

Table 1: Ranges of motions of human foot joints.

Motion	Human foot joint	Plane of movement	Range of motion
Dorsiflexion & plantarflexion	TC	Sagittal	N/A
	ST	Sagittal	−2.5° : 5°
Inversion & eversion	ST	Transverse	−10° : 20°
	MT - TN	Transverse	N/A
Abduction-adduction	ST	Frontal	−10° : 20°
Flexion & extension	MT-CC	Sagittal	N/A
	MTP (big toe)	Sagittal	(−) 80° : 40°
	MTP (toes 2–5)	Sagittal	(−) 60° : 40°
	Proximal IP (big toe)	Sagittal	0° : 90°
	Proximal IP (toes 2–5)	Sagittal	0° : 60°
	Distal IP	Sagittal	Hyper: 90°

The foot consists of three regions which are a hind foot (heel), midfoot, and forefoot (toe). The five major joints in the foot are ankle (or Talocrural (TC)) joint, Subtalar (ST) joint, Tarsometatarsal (TMT) joint, Metatarsophalangeal (MTP) joint, and Interphalangeal (IP) joint (Figure 3) [45, 46]. The hind foot consists of the calcaneus and talus. The midfoot consists of the navicular, cuboid, and the three cuneiforms. The forefoot consists of the metatarsals and phalanges. The ankle or TC joint is a hinge type joint which moves along the sagittal plane, providing the dorsiflexion and plantarflexion foot motions. The ST joint is a condyloid type joint which enables the movement along a transverse plane, providing inversion and eversion foot motions. The Midtarsal (MT) joint is in between ST joint and TMT joint which consists of two joints, namely, Talonavicular (TN) joint and Calcaneocuboid (CC) joint. The TN joint is a ball and socket type joint which enables the movement along transverse plane providing inversion and eversion foot motions. The CC joint is a modified saddle type joint which enables the movement along the sagittal plane, which provides flexion and extension foot motions. The TMT joint is a plane and synovial type joint which connects MTPs to the foot. The MTP joint is a condyloid type joint which moves along sagittal plane providing flexion/extension motions for proximal phalanges. This motion is essential when changing the arch of the foot on various surfaces. The IP joint is a hinge type joint which moves along sagittal plane which provides flexion/extension for middle and distal phalanges (Figure 3) [46].

There are rotation axes for each joint in the foot according to the plane of movement. The three cardinal planes of the human body are shown in Figure 4 which are a sagittal plane, transverse plane, and frontal plane. Some of the main rotation axes of the human foot are shown in Figure 5. Cardinal longitudinal axis of the foot is along the sagittal plane. Both ST joint and TC joint are joined to one another by talus bone, yet these two axes are more like perpendicular to one another due to the hinge and condyloid type joints. As a result, the toe can glide and roll. Knowledge of these movement planes and axes of rotation is important to understand the moving axes of existing foot prostheses. A better understanding of human foot anatomy is essential to identify design requirements. Table 1 summarized the ranges of motion of the above-mentioned human foot joints. (Consider supination as + direction and pronation as − direction). Distal IP has a small amount of extension which is known as hyperextension indicated in Table 1 as "hyper."

3. Requirements and Design Difficulties

The human foot consists of over 100 ligaments to control the five main joints. There are several design difficulties which can be incurred when developing an adaptive foot prosthesis. Complex nature of human foot anatomy makes it much difficult to mimic the adaptive nature of human foot through foot prostheses. The human foot maintains its stability by supinating/pronating along a longitudinal axis and plantar flexion/dorsiflexion along mediolateral axis. The surface contact area of the phalanges can be increased by flexing and extending them along mediolateral axis. A multi-DoF system with all the above-mentioned functionalities is a challenging task as actuators have to be arranged closer to each other while carrying the body load.

The human foot has arches along longitudinal and transverse axes which enable adapting to any surface by rotating along both directions. Developing a multidegrees of freedom system is a challenging task. The ankle joint is complex. Most of the existing prostheses have used high torque actuators for the ankle joint. Therefore sufficient space needs to be provided for ankle joint. Various mechanisms are available for transmitting the power to a prosthesis. Out of them, the most appropriate method has to be selected based on the power source, type of application, and expected weight of the prosthesis. The prosthesis should have the sufficient

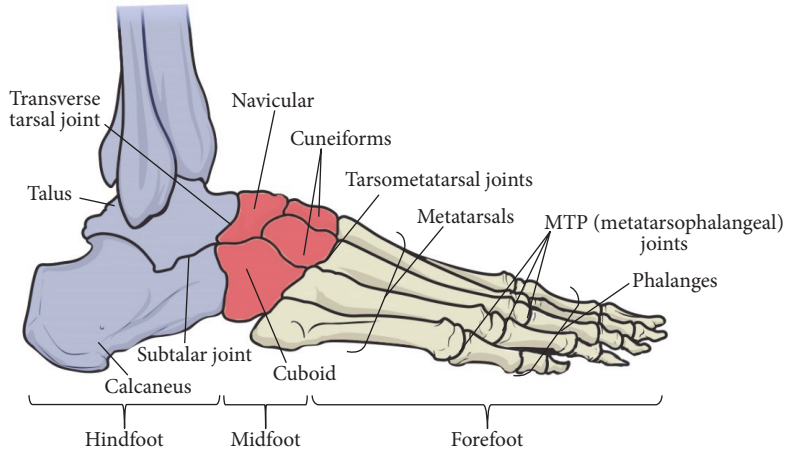

Figure 3: The human foot anatomy [45, 46].

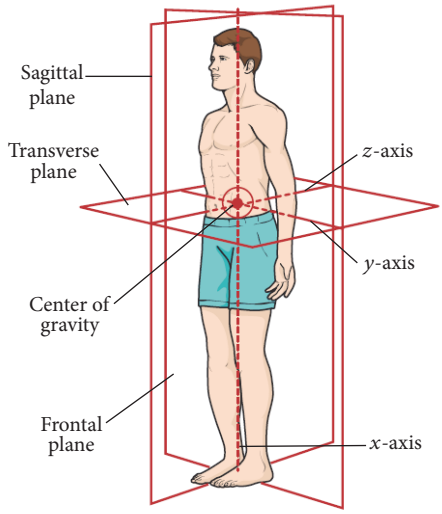

Figure 4: The three cardinal planes of the human body [45].

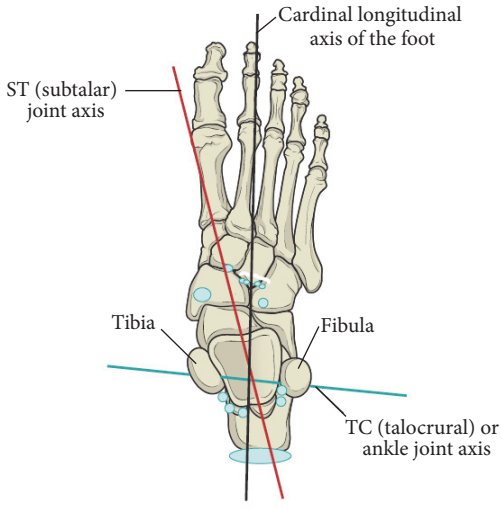

Figure 5: Human foot axes of rotation [45].

Table 2: Design requirements for a foot prosthesis development.

Requirement	Remarks
DOF	3DOF
Torque	Calculate by considering weight, type of mechanism, DOF, size, material (80–120 Nm)
Axis of rotation	Mediolateral axis, longitudinal axis, transverse axis
Type of mechanism	Coil spring, leaf spring, clutch, linkages, rolling joints, actuators, SEA, gears
Movable range	Refer to Table 1
Size	Approximately length 275 mm, width 100 mm, height 85 mm
Weight	Approximately 0.85–1.5 kg
Fabrication material	Carbon fiber or aluminum
Attachment method	Osseointegration, couplings, or pyramid adapters

moving capability along each axis as given in Table 1. The dimensions of the device have to be within the limits of average human foot size. Adaptive foot prosthesis needs to be within average human foot weight. If it exceeds this, the amputee feels uncomfortable in long-term usage. High strength materials are needed for development as the foot needs to hold the total body load and large ground reaction forces for various activities of daily living (ADL) such as running, jumping, and hopping. Some developers have used lightweight, high strength polymer type materials instead of metals. The method of attaching the foot prosthesis to the remaining lower-limb or prosthesis device is another consideration that needs to be addressed. Table 2 provides a concise design requirements list.

4. Classification of Foot Prostheses

Prostheses can be classified according to the applications: upper limb prostheses, lower-limb prostheses, and other

Table 3: Methods of classification of adaptive foot prostheses.

Classification method	Parameters
Actuation method	Passive
	Active
	Hypird
DOF	Active DOF
Type of actuators	DC brushless motors
	DC servo motors
	AC servo motors
Power transmission method	Gear drives
	Chain drives
	Linkages
	Clutch drives
Energy regeneration methods	Series elastic actuators (SEA)
	Coil springs and clutch motors
	Linkages and camshafts
	Leaf springs
Attaching method	Coupling
	Pyramid adaptor

prostheses. Orthoses can be classified in two subcategories: exoskeletons and end effector connecting devices. There are different types of lower-limb prosthetic devices available based on an application which is for hip disarticulated amputees, above knee articulated amputees (transfemoral), knee articulated amputees, below the knee (transtibial), ankle disarticulated amputees, and partial foot amputees [1, 2]. Furthermore, adaptive foot prostheses can be classified into three categories which are a passive, active, and hybrid prosthesis. Passive prostheses are functionally lacking due to the mimicking of the human leg motions compared to the active prosthesis. Therefore the development of active prosthesis is essential. Yet they are still at the research level due to lack of design and control issues. Over the years a lot of transfemoral and transtibial prosthesis have been developed. However, there is a research gap in the field of development of an adaptive foot prosthesis. The hardware construction of adaptive foot prostheses can be classified into several categories which are classified upon actuation method, DoF, and types of actuators, based on power transmission method, energy regeneration method, and attaching method to the residual limb or transtibial prosthesis and so forth. Some of the classification methods are discussed below. Table 3 summarizes the classification of the hardware construction of adaptive foot prostheses devices.

(i) Actuation Method. Lower-limb adaptive foot prostheses are classified based on power source method. Passive prostheses are body-powered or use the power of user to actuate. Active prostheses are actuated using external power sources. Most of the present-day adaptive foot prostheses are combined with both passive and active joints. This method enhances the use of available energy during ambulation through passive joints and other required motions through active joints by external power sources.

(ii) DoF. Adaptive foot prostheses can be classified according to the number of active joints or externally power actuated joints like 1 DoF, 2 DoF, 3 DoF, and so forth.

(iii) Types of Actuators. There are various types of actuators that have been used in existing prostheses. They are DC motors, brushless DC (BLDC) motors, servo motors, and AC motors. Different types of DC motors are available such as brushless motors and servo motors.

(iv) Power Transmission Method. Prostheses transmit power using various methods such as gear drives, chain drives, and linkages mechanisms which are connected to actuators, clutch drives, and so forth. Additionally, belt drives, ball screw drives, and cable drive methods are possible.

(v) Energy Regeneration Method. Existing actuators have limited torque generation capability. Therefore some researchers have developed energy regenerative mechanisms to generate the required high torque. Series elastic actuator (SEA) is one of the most popular methods in modern days. Additionally, a combination of coil springs and clutch motors, linkages, camshafts with motors, and leaf springs with motors have been used in different existing devices.

(vi) Attaching Method. Attaching method of adaptive foot prostheses to the lower-limb prostheses is essential for the amputee's use. There can be two types of attaching ends which are connecting prosthesis to residual limb and attaching adaptive foot prosthesis to transtibial prosthesis of the transfemoral prosthesis. Ankle-foot couplings and pyramid adaptors are common among other attaching available methods. Additionally, socket attaching methods are possible.

5. Review on Adaptive Foot Prostheses

Foot prosthesis is used as the terminal device for the lower-limb prosthesis. There are passive and active adaptive foot prostheses. The passive prostheses are designed to be operated with user's body power and no actuator driven joints. Fully passive devices are relatively limited with motion capabilities. Active prostheses are designed to be controlled with externally powered actuator joints. It requires a well-designed control structure to control all the joints simultaneously to mimic the actual human foot movements. Active prostheses enhance the developers to focus more on the functionalities of the foot rather than mechanisms to power the device passively. The introduction of actuators to the active prostheses makes them much heavier compared to the passive prostheses. Due to the above-mentioned favourable and adverse drawbacks of passive and active prostheses, combined passive and active joints (or hybrid) prostheses have been developed by manufacturers lately. Hybrid prostheses have advantages over other prostheses which are improved workspace, higher functional capabilities, and larger range of motions.

The prosthesis gets bulky with the introduction of external power sources. As the prosthesis mass undergoes an increase, the user feels discomfort when using it over a

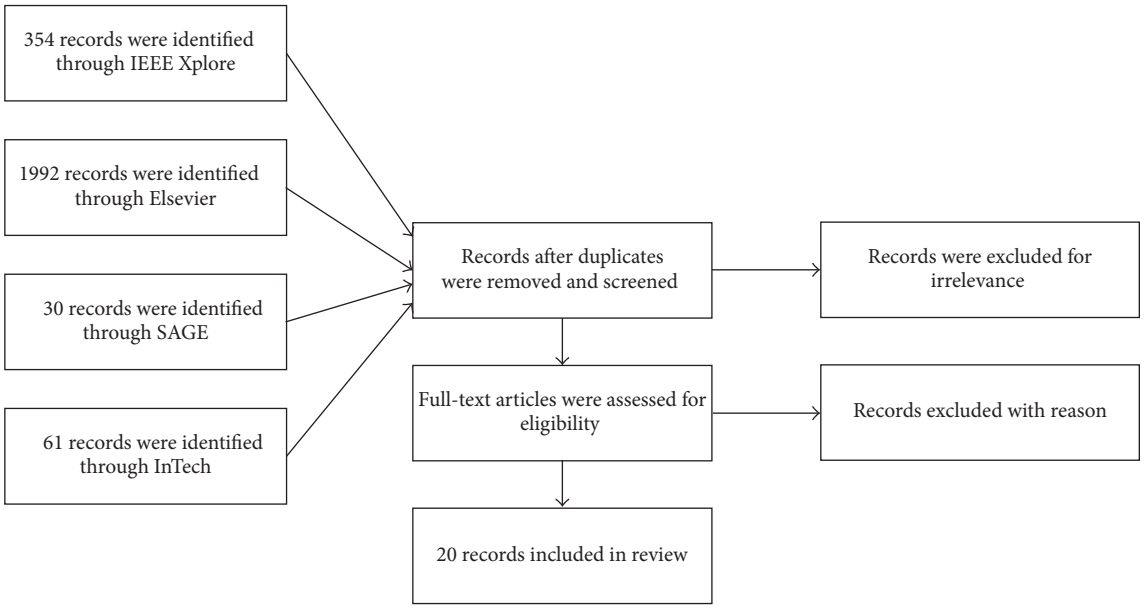

Figure 6: PRISMA flow diagram of the literature review process [43].

long period of time. Therefore energy saving mechanisms have been introduced by prosthesis developers to reduce the power requirement. The spring-based energy storing and regenerating methods like series elastic actuators (SEA) [48], parallel elastic actuators (PEA), clutchable series elastic actuators (CSEA) [49], continuously variable series elastic actuators [50], and so forth are some examples for such mechanisms. Attaching methods of adaptive foot prostheses to lower-limb prostheses are mainly coupling, pyramid type attachments. Aluminum is the commonly used material for the prototypes and expensive materials such as carbon fiber have been used in some of those developments. Tables 4, 5, and 6 provide a concise comparison of existing passive, active, and hybrid adaptive foot prostheses during 1997–2016. The weight of the adaptive foot prosthesis, actuation method and number of actuators, axis of rotation and equivalent human foot joint, working mechanism, moving range along each DoF, attaching method to remaining stump limb or transtibial prosthesis, and material used for the development are included.

In order to select databases for the paper, several generic keywords were searched such as "adaptive foot prosthesis, feet, ankle-foot prosthesis, lower-limb prosthesis, artificial limb, humanoid robots". IEEE Xplore, Elsevier, SAGE, InTech, PLUS ONE, ASME (American Society of Mechanical Engineer's Journal), and Journal of Rehabilitation Research & Development (JRRD) databases were chosen due to their high number of relevant search results. The search term of "adaptive foot prosthesis" was created in several iterations to obtain a larger number of relevant results. The search was limited to conference proceedings, journal papers, dissertations, and patents for the time period of 20 years from 1997 to 2017. Search results consisted of a significant number of control algorithms, medical researchers, and other robotic researchers. However, the basis was limited only to mechanical designs and developments. Most of those consisted of knee and ankle prostheses designs which had to be eliminated and only ankle-foot and foot were selected. With an in-depth study about available prostheses device designs and their focused area, most of them were refined and we retrieved the most appropriated few which were suitable for the topic of adaptive foot prostheses. Among the existing adaptive foot prostheses, flat foot designs were excluded. Only passive, active, and the combination of passive and active (i.e., hybrid prostheses) prostheses were adopted for the review. The number of search results obtained for each keyword in different academic databases is shown in Table 7.

The search retrieved a total of 2437 manuscripts from selected academic databases. The results were refined by manually screening for their relevance using the title and abstract. Selected remaining papers were studied further and we excluded the papers with no adaptive foot devices. A total of 20 papers were selected due to the high relevance to the topic of adaptive feet in prostheses. The PRISMA flow diagram in Figure 6 summarizes the review selection procedure. PRISMA (Preferred Reporting Items for Systematic Reviews and Meta-Analyses) is a method used in systematic reviews in contemplation of improving the reporting quality [43]. Since most of the novel designs have been developed based on available patents and some patents are beyond the scope of this review, only 4 patents have been included in the review.

5.1. The Heel Foot [8]. The Heel Foot (Figure 8(a)) was developed by the University of Twente, Enscheda, Netherlands, in 2003. This is a single DoF passive plantar flexion adaptive foot prosthesis rotating along a mediolateral axis. Plantar spring controls the arch angle of the Heel Foot for maintaining stability. The potential energy stored in compressed plantar and heel springs starting from heel-off phase is used to push forward at the toe-off point. Four-bar linkage mechanism has been used for compression springs and varying arch angle. The Heel Foot was validated for relative joint angle, joint

Table 4: Comparison of passive-adaptive foot prostheses/foot designs in lower-limb prostheses.

Country	Name/year/reference number	Weight	Axis of rotation	Type of mechanism	Movable ranges	Attaching method	Material
Netherlands	The Heel Foot (2003) [8]	0.5 kg	Mediolateral axis MTP joint axis	Spring based	(−) 20° : 20°	Knee ankle coupling	Toe-carbon fiber, forefoot, heel—aluminum
Netherlands	fully passive transfemoral prosthesis (2011) [9]	1.05 kg	Mediolateral axis at MTP joint	Spring based and linkages	0 : 30° (toe)	Prosthesis ankle joint	Carbon fiber
United States of America (USA)	Prosthetic ankle-foot system (2014) [10]	1.04 kg	Mediolateral axis	Linkages and camshafts	87° : 105°	Pyramid adapter	Nylon 6/6, polyurethane rubber, maraging steel
Japan	Bipedal walking robot with oblique midfoot joint in foot (2015) [11]	N/A	Oblique axis at MTP joint	Truss and windlass mechanism	N/A	Nut and bolt	N/A
Italy	SoftFoot (2016) [12]	N/A	Parallel to mediolateral axis	Series of rolling joints	vary with the surface	Coupling	Rapid prototyping material
United States of America (USA)	Hindfoot and forefoot stiff foot prostheses (2017) [13]	N/A	Mediolateral axis	Flexible composite forefoot keel and hindfoot of varying stiffness	sagittal declination angle 15°	Pyramid adapter	Aluminum 7075-T6
United States of America (USA)	One-piece mechanically differentiated prosthetic foot (1997) [14]	N/A	Mediolateral axis	Flex due to polymeric material	N/A	Flange type nut and bolt connector	Light weight polymeric material
United States of America (USA)	Instrumented prosthetic foot (2012) [15]	N/A	Mediolateral axis	Flex due to polymeric material	N/A	Pyramid adapter	Durometer polyurethane
United States of America (USA)	Ankle-foot prosthesis of automatic adaptation (2014) [16]	N/A	Mediolateral axis	Spring and link based mechanism	(−) 45° : 80°	Pyramid adapter	Elastomeric Materials

Table 5: Comparison of active adaptive foot prostheses/foot designs in lower-limb prostheses.

Country	Name/year/reference number	Weight	Actuator	Axis of rotation	Type of mechanism	Movable ranges	Attaching method	Material
China	PANTOE 1 (2010) [17, 18]	1.47 kg	2 DC motors	Mediolateral axis at MTP joint	SEA	(−) 16° : 27°	Socket adaptor	Aluminum alloy
USA	Universal prosthesis emulator (2014) [19]	0.96 kg	1 DC motor	Mediolateral axis at MTP joint	Spring base	(−) 12° : 12°	Universal adaptor	7075-T651 aluminum

Table 6: Comparison of hybrid adaptive foot prostheses/foot designs in lower-limb prostheses.

Country	Name/year/reference number	Weight	Passive Joint	Actuator	Axis of rotation	Type of mechanism	Movable ranges	Attaching method	Material
Japan	Parallel four-bar linkage humanoid robot (2007) [20]	0.76 kg	Toe mechanism	1 DC servo motor	Mediolateral axis at MTP joint	Actuator based	0 : 44°	Humanoid ankle	Extra super duralumin
USA	Energy recycling foot (2010) [21, 22]	1.37 kg	Springs and clutches based mechanism	2 DC motors	Mediolateral axis at MTP joint	Coil Springs, clutch motor	N/A	Pyramid adapter	7075-T6 Aluminum, Stainless steel, Carbon/fiberglass
Japan	Adaptive bipedal deformable feet (2012) [23]	1.2 kg	Torsional Springs	2 Servo motors	Mediolateral axis at MTP joint	Torsional springs and servo motor combination	N/A	Nut and Bolt	Super soft urethane resin
Germany	An adaptive sensor foot for a bipedal and quadruped robot (2012) [24]	N/A	Bowden cables and dampers	2 BLDC motors	Mediolateral axis at MTP joint	Windlass mechanism	roll −20° to 10° pitch −30° to 20° yaw −10° to 10°	Coupling	Rapid prototyping material
Belgium	The AMP-foot 1.0 (2012) [25]	3 kg	Spring-based gear mechanism	N/A	Mediolateral axis at MTP joint	Spring, planter gear mechanism	0 : 30°	Coupling	Aluminum
Belgium	The AMP-foot 2.0 (2013) [26, 27]	2.5 kg	Lever arm and spring combined mechanism	1 DC motor	Mediolateral axis at MTP joint	Springs and SEA	0 : 45°	Prosthesis ankle joint	Aluminum
United Kingdom	Virtual prototyping of a semiactive transfemoral prosthetic leg (2015) [28]	2.3 kg	Springs	1 DC motor	Mediolateral axis at MTP joint	SEA and springs	N/A	Nut and bolt	N/A
Italy	Variable compliant humanoid foot (2016) [29]	0.52 kg	Leaf springs, cam followers based method	1 DC geared motor	Longitudinal axis of the foot	Leaf spring, motor actuated	N/A	Humanoid ankle	Aluminum, rubber
China	Bioinspired tunable stiffness robotic foot (2017) [30]	N/A	Spring	Stepper motor	Mediolateral axis and longitudinal axis	Spring and ball screw	N/A	Ball joint	N/A

Table 7: Results of keyword search in respective academic databases.

Keyword	IEEE Xplore	Elsevier	SAGE	InTech	PLOS ONE	ASME
Foot/feet	7,539	120,657	101,738	1,478	2,876	149
Lower limb prosthesis	267	12,434	2184	244	10,201	35
Humanoid robots	11,404	2,276	707	772	3,693	7
Ankle-foot prosthesis	48	3,864	865	244	880	25
Adaptive foot prostheses	354	1,992	148	61	237	399
Artificial limb	1404	26,272	3,496	691	37,951	50

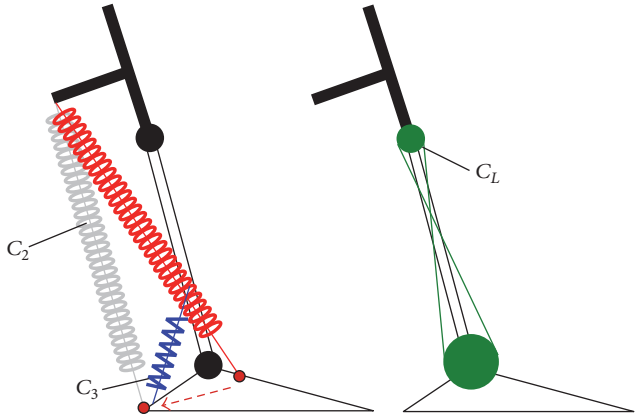

Figure 7: Spring arrangement of fully passive transfemoral prosthesis [9].

torque, joint power, and force variation for gait cycle for proving the prototype functionality.

5.2. Fully Passive Transfemoral Prosthesis Prototype [9]. Fully passive transfemoral prosthesis (Figure 8(b)) was developed by the University of Twente, Enscheda, Netherlands, in 2011. The adaptive foot prosthesis part is designed as spring-based linkage mechanism. The energy storing mechanism using springs is as in Heel Foot [8]. In this prosthesis adaptive foot manoeuvres with the aid of knee and ankle generating potential energy. During the stance phase, both knee and ankle absorb a certain amount of energy for carrying body weight. Then knee further absorbs energy for preswing and the ankle generates 80% of total energy for push-off. With the analysis of gait power requirement diagrams, this paper suggests that the knee is more like an energy absorber and ankle is more like an energy generator. This concept was the intuition for the conceptual design shown in Figure 7.

Two springs are crossed to each other and connected to ankle. During the preswing phase, knee absorbs the kinetic energy and stores it in C_L spring. Then when the swing phase arrives kinetic energy will be stored in C_2 spring. Stored energy during swing phase can be reused in stance phase while C_3 spring stored kinetic energy can be used in the next stage. Spring arrangement in the proposed mechanism is shown in Figure 7. Cable mechanism is used to govern the ankle and adaptive foot bends according to the knee flexion during the gait cycle. The conceptual design did not simulate. The prototype has been developed. However, prosthesis did not validate.

5.3. Passive Slope Adaption Prosthetic Ankle-Foot System [10]. This mediolateral direction rotating single DoF passive device was developed by a set of researchers from USA (Figure 8(c)). This prosthesis consists of link and cam on the passive ankle joint and the foot plate moves according to the slope of the surface. The moving range of the joint is only 18°. The prosthesis is validated with a set of experiments and the system has no energy regeneration method and comparatively the surface adaption mechanism is a basic method with a limited range of motions.

5.4. Bipedal Walking Robot with Oblique Midfoot Joint in Foot [11]. This foot was developed by a group of Japanese researchers in 2015. The bipedal walking robot in Figure 8(d) was developed to generate the adaptive nature of the foot with midfoot axis rotation nature. Oblique axis DoF foot prostheses are rarely used in foot prostheses due to the lack of strength. The bipedal walking robot is a humanoid robot that has been designed to replicate the human foot motions. The tendon wire mimics the arch of the foot. Yet the weight carrying capacity is limited in this design.

5.5. SoftFoot [12]. SoftFoot (Figure 9(a)) has been developed to improve the adaptive nature of the foot prosthesis. This is a complete passive foot prosthesis developed by studying the human foot arch and bone arrangement along the longitudinal direction. The prototype was developed by Research Center "Enrico Piaggio," University of Pisa, Italy, in 2016 using a rapid prototype method. SoftFoot was developed based on windlass mechanism [45]. Chain of connectors which can rotate parallel to mediolateral direction is used as foot links. The foot arch angle is fixed and no energy regeneration method is available with SoftFoot. The SoftFoot was validated with a compliant simulation for load distribution. Also the experiments were carried out to measure the performances on uneven terrains. The device was validated by comparing the surface adaption capability with a rigid flat foot.

5.6. Hindfoot and Forefoot Stiff Foot Prostheses [13]. This passive stiff foot prosthesis shown in Figure 9(b) was developed in the USA in 2017. The device consists of a rubber base which enables the prosthesis to function the push-off movement of the foot with varying arch and windlass mechanism. This

(a) (b) (c) (d)

Figure 8: Passive foot prostheses. (a) The Heel Foot [8], (b) fully passive transfemoral prosthesis prototype [9], (c) prosthetic ankle-foot system [10], and (d) bipedal walking robot with oblique midfoot joint in foot [11].

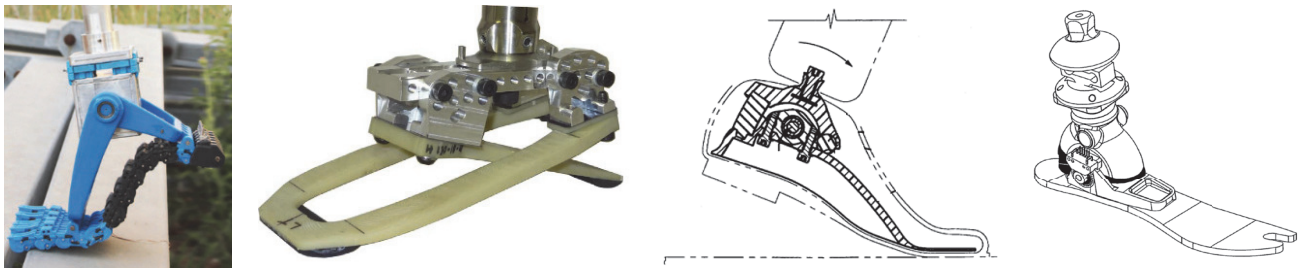

(a) (b) (c) (d)

Figure 9: Passive foot prostheses. (a) SoftFoot [12]. (b) Hindfoot and forefoot stiff foot prostheses [13]. (c) One-piece mechanically differentiated prosthetic foot [14]. (d) Instrumented prosthetic foot [15].

design has been validated and results have proved the compatibility of implementing it to an actual passive device.

5.7. One-Piece Mechanically Differentiated Prosthetic Foot [14]. This is one of the passive-adaptive foot prosthetic devices available in the patent database. These types of passive feet are very much similar to flat prosthetic feet. However, this foot prosthesis is fabricated by lightweight polymeric material which enables the foot flex on any surface. This device has been developed for ankle disarticulated amputees. Due to the material type and contact surface it has the limitation of walking along the rough uneven surface. Limitation of the bend along the longitudinal axis is another problem in this design. Load carrying capacity is limited due to the type of material used for this device. Figure 9(c) shows the design of this passive foot prosthesis which was patented in 1997.

5.8. Instrumented Prosthetic Foot [15]. The instrumented prosthetic device is a passive foot prosthesis which was developed by USA research team in 2012. This device is to be fitted to a lower-limb ankle controlled by sensors. Ankle prosthesis is connected to foot via a pyramid connector. This is made of a polymer material known as durometer polyurethane. Surface adaption of this prosthesis is obtained by the stiffness of the polymer material (refer to Figure 9(d)).

5.9. PANTOE 1 [17, 18]. PANTOE 1 is one of the advanced, energy regenerative active prostheses with mediolateral direction rotation. It has 1-DoF ankle and 1-DoF foot segment. It was developed by College of Engineering, Peking University, Beijing, China, in 2010 (refer to Figure 10(b)). PANTOE 1 consists of two series elastic actuators (SEA). SEA is one of the high torque generating actuation methods available in modern prosthesis world. Foot segment is actuated with one DC brush motor, ball screw, and SEA. PANTOE 1 was controlled by finite state control method [11] and the system was validated based on control method. The foot prosthesis segment lacks the adaption capability as PANTOE foot segment has 1 DoF. Adaption along the longitudinal axis is lacking in this design.

5.10. Universal Prosthesis Emulator [19]. This foot prosthesis was developed by Carnegie Mellon University, Pittsburgh, USA (Figure 10(c)). This prosthesis can bend through mediolateral joint the same as the human MTP joint. The significant difference compared to other prostheses is a user of chain mechanism to control foot arch angle and emulator based high-performance software environment use to control the prosthesis. This is an active foot prosthesis which has the ability to perform plantar flexion. 1.61 kW AC servo motor is used to control the arch angle of the prosthesis to maintain the stability. In this design while the prosthesis is at heel strike

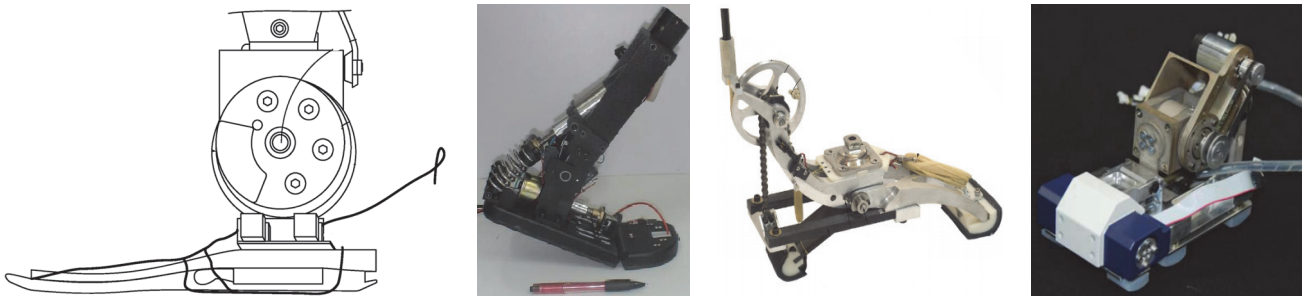

(a) (b) (c) (d)

Figure 10: Active and hybrid foot prostheses. (a) Ankle-foot prosthesis of automatic adaptation [16], (b) PANTOE 1 [17, 18], (c) universal prosthesis emulator [19], and (d) parallel four-bar linkage humanoid robot [20].

(a) (b) (c) (d)

Figure 11: Developed foot prostheses. (a) Energy recycling foot [21, 22]. (b) Adaptive bipedal deformable feet [23]. (c) An adaptive sensor foot for a bipedal and quadruped robot [24]. (d) The AMP-Foot 1.0 [25].

phase, passive heel spring bends and stores energy and pulley rotates to cause tension to the chain which is connected to passive heel to the other end.

As it is in Table 4, prostheses weighted around 1 kg range which is around average human foot weight [44, 45]. The majority of prostheses rotate along the transverse axis with no foot with a degree of freedom along both axes. Spring-based mechanisms are popular as an energy regenerative method. The motion ranges are closely following actual human joint ranges (Table 1). Lack of proper attachment methods to amputees can be seen in the majority of these designs. Aluminum and carbon fiber materials are more common due to the high strength and lightweight in the majority of these designs. Some foot prostheses have validated joint torques, forces, and angle for gait cycle [8, 9, 20] yet few simulated design performance [12].

5.11. Parallel Four-Bar Linkage Humanoid Robot [20]. Humanoid robots are too generating human foot motion. This 1-DoF humanoid (Figure 10(d)) was developed by the University of Tokyo, Japan, which attempted to mimic the toe joint motion through MTP joint of the human foot. Two parallel links have been used to connect to the toe link and foot link and developed four-bar parallel linkage mechanism. A DC servo motor (Maxon RE-max 17, 2.5 W) is used to control the toe mechanism. Toe-off can undergo maximum torque of 590 mNm. Three-axis force sensor has been attached to the base of the forefoot to detect ground reaction force and prevent the maximum torque. According to the validation results, toe-off motion can be performed with this mechanism and the toe can bend up to 44° while human MPT joint can bend about 40°.

5.12. Energy Recycling Foot [21, 22]. The University of Michigan, USA, developed this energy harvesting active prosthetic foot (Figure 11(a)) in order to introduce the control energy storage and return concept. This is a single active DoF prosthesis that stores the energy into springs and locks it during gait phase and releases it under clutch motor control based on sensory inputs. There are two DC electric motors to rotate the toe and heel. Force sensors connected to forefoot work as sensors which capture energy during heel contact phase and release it at toe-off phase. According to the validation results, this prosthesis has reduced net metabolic energy expenditure by 23% compared to normal walking.

5.13. The AMP-Foot 1.0 [25]. The AMP-Foot 1.0 was designed by the Department of Mechanical Engineering, Vrije Universiteit Brussel, Brussels, Belgium, in 2012 (Figure 11(d)). This was an initial design with a flat foot, yet with spring, locking mechanism, and planetary/epicyclical gear system to control the movement of joint. The locking mechanism was the

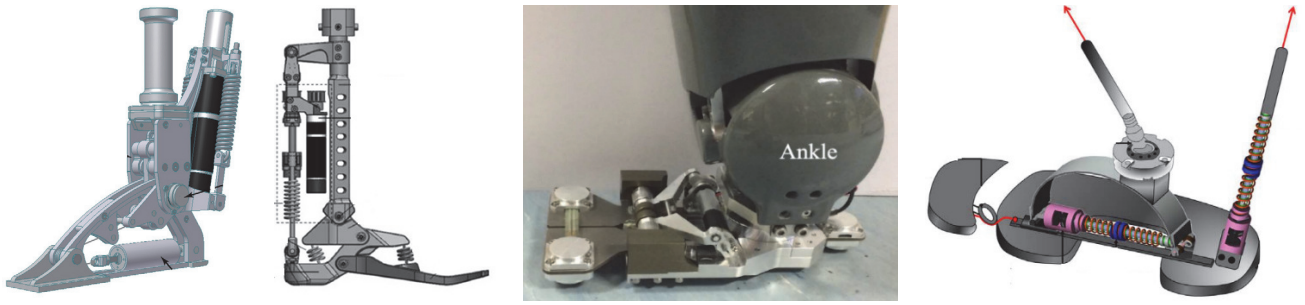

(a) (b) (c) (d)

Figure 12: Developed foot prostheses. (a) The AMP-Foot 2.0 [26, 27]. (b) Virtual prototyping of a semiactive transfemoral prosthetic leg [28]. (c) Variable compliant humanoid foot [29]. (d) Bioinspired tunable stiffness robotic foot [30].

intuition for developing the AMP-Foot 2.0 [26, 27] later with foot mechanism. This design was validated experimentally to prove the functional capability of ankle foot.

5.14. The AMP-Foot 2.0 [26, 27]. This is a further development of AMP-Foot 1.0 [25] with energy regeneration adaptive foot (Figure 12(a)). Plantarflexion spring stores energy and regenerates the same as in other active foot prostheses. Two force sensing resistors are used as input sensors to detect the surface contact. The mechanism consists of lever mechanism to control the energy storing. AMP-Foot 2.0 is at the development stage and only the design was available. Simulated results were available based on the design. Lever and locking mechanism is novel in this design compared to other existing foot prostheses.

5.15. Variable Compliant Humanoid Foot [29]. This is another human foot in humanoid robots which was developed by the Department of Advanced Robotics, Istituto Italiano di Tecnologia, Italy, in 2016 (Figure 12(c)). The significance in this development is that it can adapt along the longitudinal axis of the foot. The variable compliant humanoid foot is an active robot that consists of small geared motor (Maxon), 6-axis force/torque sensor, leaf springs, and rubber ball with pressure sensors. Cam with leaf springs connected to transverse axis store energy when the toe leaf spring bends along the longitudinal axis. The humanoid robot was validated for motion experiments as well as spring stiffness experiments to prove the design functionality. Longitudinal adaption is the significance in this design. Some existing foot prostheses [25–27] and humanoid robots [20] use electronic sensor inputs to control motions.

6. Discussion and Future Directions

The anatomical structure of the human foot has been studied from a biomechanical perspective prior to the review of design and development. Several existing adaptive foot prostheses were reviewed in this paper upon different design criteria. Subsequently, the requirements and design difficulties were identified. In this paper, adaptive foot prostheses were classified as passive, active, and hybrid based on actuation method. The key parameters of existing adaptive foot prostheses were compared in Tables 4, 5, and 6 by indicating their country of origin, references, weight, actuation method, the axis of rotation, type of mechanisms used, movable ranges, attaching method to the remaining prosthesis or residual limb, and used materials.

The human foot consists of complex sets of joints. It undergoes significant impulsive force throughout the gait cycle due to the body weight and ground reaction force. It is essential to develop a device with the strong and lightweight material. Novel mechanisms and high torque lightweight actuators are necessary for adaptive foot prostheses to reduce the weight. Total weight of the device needs to be approximately closer to average human foot weight to avoid the baring of unnecessary weight. Most of the existing adaptive foot prostheses are 1 DoF or 2 DoF and can only be rotated along MTP joint. Only a few prostheses have the rotation capability along the longitudinal axis. Thus designing and developing an adaptive foot prosthesis which can be movable along both axes are a challenging task. Yet such development will improve the stability of lower-limb prostheses on any uneven terrain.

High torque-to-weight ratio actuators are essential for high-performance adaptive foot prostheses. The joint sizes are smaller and total number of joints is larger in the toe region of the human foot. Therefore miniature actuators are needed to actuate multiple DoF in the toe region. Currently available shelf actuators do not fulfil this requirement. Few developers have overcome this issue to a certain extent by using customized actuators. Yet, it is a costly method for small scale researches.

In order to reduce the external power usage and regenerate the power, mechanisms such as SEA, coil springs clutch motors, and springs can be used as actuators. These mechanisms can store the energy and release energy repetitively throughout the gait cycle. Additionally, spring effect enables the adaptive nature up to a certain extent. Furthermore, research needs to be carried out to develop energy regeneration. Authors foretell that future adaptive prostheses will consist of energy regenerative methods and will be more convenient for users.

As for not to feel discomfort by the amputees in long-term prostheses usage, attaching method of adaptive foot

prosthesis to the lower-limb or to residual limb is crucial. Therefore, further research needs to be carried out to develop ergonomically friendly attaching sockets. Ultimately these robotic devices are to be used by humans as an artificial body part. Hence mechanical stoppers and control based safety precautions and manual maneuvering methods are necessary to be included for prostheses.

Prosthesis designs should fulfil the anatomical demands as well as the physiological demands of users. Adaptive foot prostheses are necessary to have an attractive elegant appearance with the portable facility. Some of the existing adaptive foot prostheses have managed to fulfil several of the above-mentioned design requirements, although none of them has combined all the essential functionalities to a single device. Most existing adaptive foot prostheses have limited torque, power, and ranges of motion. Unnecessary noise and vibration reduce the quality of device further. These general issues have to be addressed in future designs.

7. Conclusion

This review summarized existing design criteria of adaptive foot prostheses in order to develop an adaptive foot prosthesis. In this paper, systematic literature search approach was adopted. The scope of this paper, which is the adaptive nature of foot prostheses, has not been discussed in available review papers. This paper presented design classification parameters for each classification method of existing adaptive foot prostheses. In modern days, active and hybrid prostheses are more popular due to their high functional capabilities. Yet, in this paper some of the existing passive-adaptive foot prostheses have also been reviewed due to their significance in mechanisms and the possibility of transferring such mechanisms to hybrid devices. The adaptive foot prostheses have been classified based on actuation method and compared considering design requirements and design criteria. It enables the reader to compare and contrast the existing devices and choose the most appropriate method for their design requirements.

Conflicts of Interest

The authors declare that there are no conflicts of interest regarding the publication of this paper.

Acknowledgments

The authors gratefully acknowledge the support of the National Research Council (NRC), Sri Lanka, for the research grant (Grant no. 15-068).

References

[1] J. Martin, A. Pollock, and J. Hettinger, "Microprocessor lower limb prosthetics: review of current state of the art," *Journal of Prosthetics and Orthotics*, vol. 22, no. 3, pp. 183–193, 2010.

[2] R. A. R. C. Gopura, D. S. V. Bandara, K. Kiguchi, and G. K. I. Mann, "Developments in hardware systems of active upper-limb exoskeleton robots: A review," *Robotics and Autonomous Systems*, vol. 75, pp. 203–220, 2016.

[3] K. Ziegler-Graham, E. J. MacKenzie, P. L. Ephraim, T. G. Travison, and R. Brookmeyer, "Estimating the prevalence of limb loss in the United States: 2005 to 2050," *Archives of Physical Medicine and Rehabilitation*, vol. 89, no. 3, pp. 422–429, 2008.

[4] F. R. D. A. Senefonte, G. R. D. P. S. Rosa, M. L. Comparin et al., "Primary amputation in trauma: a profile of hospital center-west region of Brazil," *Brazilian Journal of Vascular Surgery*, vol. 11, no. 4, pp. 269–276, 2012.

[5] P. L. Chalya, J. B. Mabula, R. M. Dass et al., "Major limb amputations: A tertiary hospital experience in northwestern Tanzania," *Journal of Orthopaedic Surgery and Research*, vol. 7, no. 1, article no. 18, 2012.

[6] R. Gailey, K. Allen, J. Castles, J. Kucharik, and M. Roeder, "Review of secondary physical conditions associated with lower-limb amputation and long-term prosthesis use," *Journal of Rehabilitation Research and Development* , vol. 45, no. 1, pp. 15–30, 2008.

[7] A. H. Shultz, B. E. Lawson, and M. Goldfarb, "Walking on uneven terrain with a powered ankle prosthesis: a preliminary assessment," in *Proceedings of the 37th Annual International Conference of the IEEE Engineering in Medicine and Biology Society*, pp. 5299–5302, Milan, Italy, August 2015.

[8] F. te Riele, *The heelfoot-Design of a plantarflexing prosthetic foot [Ph.D. dissertation]*, Universiteit Twente, Enschede, The Netherlands, 2003.

[9] S. M. Behrens, R. Unal, E. E. G. Hekman, R. Carloni, S. Stramigioli, and H. F. J. M. Koopman, "Design of a fully-passive transfemoral prosthesis prototype," in *Proceedings of the 33rd Annual International Conference of the IEEE Engineering in Medicine and Biology Society*, pp. 591–594, Boston, Mass, USA, August 2011.

[10] E. Nickel, J. Sensinger, and A. Hansen, "Passive prosthetic ankle-foot mechanism for automatic adaptation to sloped surfaces," *Journal of Rehabilitation Research and Development* , vol. 51, no. 5, pp. 803–814, 2014.

[11] T. Kawakami and K. Hosoda, "Bipedal walking with oblique mid-foot joint in foot," in *Proceedings of the IEEE International Conference on Robotics and Biomimetics*, pp. 535–540, Zhuhai, China, December 2015.

[12] C. Piazza, C. Della Santina, G. M. Gasparri et al., "Toward an adaptive foot for natural walking," in *Proceedings of the 16th IEEE-RAS International Conference on Humanoid Robots*, pp. 1204–1210, Cancun, Mexico, November 2016.

[13] P. G. Adamczyk, M. Roland, and M. E. Hahn, "Sensitivity of biomechanical outcomes to independent variations of hindfoot and forefoot stiffness in foot prostheses," *Human Movement Science*, vol. 54, pp. 154–171, 2017.

[14] M. T. Wilson, "One-piece mechanically differentiated prosthetic foot and associated ankle joint with syme modification," US 5695526 A, December 1997.

[15] S. Bedard and P. O. Roy, "Instrumented prosthetic foot," US7815689 B2, December 2012.

[16] A. H. Hansen and E. A. Nickel, "Further improvements to ankle-foot prosthesis and orthosis capable of automatic adaptation to sloped walking surfaces," *US8696764 B2*, 2014.

[17] J. Zhu, Q. Wang, and L. Wang, "PANTOE 1: biomechanical design of powered ankle-foot prosthesis with compliant joints and segmented foot," in *Proceedings of the IEEE/ASME International Conference on Advanced Intelligent Mechatronics*, pp. 31–36, Montreal, Canada, July 2010.

[18] K. Yuan, J. Zhu, Q. Wang, and L. Wang, "Finite-state control of powered below-knee prosthesis with ankle and toe," in

Proceedings of the 18th IFAC World Congress, vol. 44, pp. 2865–2870, September 2011.

[19] J. M. Caputo and S. H. Collins, "A universal ankle-foot prosthesis emulator for experiments during human locomotion," *Journal of Biomechanical Engineering*, vol. 136, no. 3, Article ID 035002, 10 pages, 2013.

[20] K. Yamamoto, T. Sugihara, and Y. Nakamura, "Toe joint mechanism using parallel four-bar linkage enabling humanlike multiple support at toe pad and toe tip," in *Proceedings of the 7th IEEE-RAS International Conference on Humanoid Robots*, pp. 410–415, Pittsburgh, Pa, USA, December 2007.

[21] S. H. Collins, *Dynamic walking principles applied to a human gait [Ph.D. dissertation]*, Department of Mechanical Engineering, University of Michigan, Ann Arbor, Mich, USA, 2008.

[22] S. H. Collins and A. D. Kuo, "Recycling energy to restore impaired ankle function during human walking," *PLoS ONE*, vol. 5, no. 2, Article ID e9307, 2010.

[23] D. Owaki, H. Fukuda, and A. Ishiguro, "Adaptive bipedal walking through sensory-motor coordination yielded from soft deformable feet," in *Proceedings of the 25th IEEE/RSJ International Conference on Robotics and Intelligent Systems*, pp. 4257–4263, Vilamoura, Portugal, October 2012.

[24] K. Fondahl, D. Kuehn, F. Beinersdorf et al., "An adaptive sensor foot for a bipedal and quadrupedal robot," in *Proceedings of the 4th IEEE RAS & EMBS International Conference on Biomedical Robotics and Biomechatronics*, pp. 270–275, Rome, Italy, June 2012.

[25] B. Brackx, M. van Damme, A. Matthys, B. Vanderborght, and D. Lefeber, "Passive ankle-foot prosthesis prototype with extended push-off," *International Journal of Advanced Robotic Systems*, vol. 10, article 101, pp. 1–9, 2013.

[26] P. Cherelle, A. Matthys, V. Grosu, B. Vanderborght, and D. Lefeber, "The AMP-Foot 2.0: mimicking intact ankle behavior with a powered transtibial prosthesis," in *Proceedings of the 4th IEEE RAS and EMBS International Conference on Biomedical Robotics and Biomechatronics*, pp. 544–549, Rome, Italy, June 2012.

[27] S. Grosu, P. Cherelle, C. Verheul, B. Vanderborght, and D. Lefeber, "Case study on human walking during wearing a powered prosthetic device: effectiveness of the system 'human-Robot'," *Advances in Mechanical Engineering*, vol. 2014, Article ID 365265, 9 pages, 2014.

[28] Z. W. Lui, M. I. Awad, A. Abouhossein, A. A. Dehghani-Sanij, and N. Messenger, "Virtual prototyping of a semi-active transfemoral prosthetic leg," *Proceedings of the Institution of Mechanical Engineers, Part H: Journal of Engineering in Medicine*, vol. 229, no. 5, pp. 350–361, 2015.

[29] W. Choi, G. A. Medrano-Cerda, D. G. Caldwell, and N. G. Tsagarakis, "Design of a variable compliant humanoid foot with a new toe mechanism," in *Proceedings of the IEEE International Conference on Robotics and Automation*, pp. 642–647, Stockholm, Sweden, May 2016.

[30] Z. Qaiser, L. Kang, and S. Johnson, "Design of a bioinspired tunable stiffness robotic foot," *Mechanism and Machine Theory*, vol. 110, pp. 1–15, 2017.

[31] A. H. Hansen, D. S. Childress, and S. C. Miff, "Roll-over characteristics of human walking on inclined surfaces," *Human Movement Science*, vol. 23, no. 6, pp. 807–821, 2004.

[32] S. Portnoy, J. van Haare, R. P. J. Geers et al., "Real-time subject-specific analyses of dynamic internal tissue loads in the residual limb of transtibial amputees," *Medical Engineering & Physics*, vol. 32, no. 4, pp. 312–323, 2010.

[33] S. D. Prentice, E. N. Hasler, J. J. Groves, and J. S. Frank, "Locomotor adaptations for changes in the slope of the walking surface," *Gait & Posture*, vol. 20, no. 3, pp. 255–265, 2004.

[34] J. Friesen, J. R. Smith, and O. Pianykh, "Prosthetic foot," US20170135828 A1, May 2017.

[35] A. H. Hansen, D. S. Childress, and E. H. Knox, "Prosthetic foot roll-over shapes with implications for alignment of trans-tibial prostheses," *Prosthetics and Orthotics International*, vol. 24, no. 3, pp. 205–215, 2000.

[36] M. F. Eilenberg, H. Geyer, and H. Herr, "Control of a powered ankle-foot prosthesis based on a neuromuscular model," *IEEE Transactions on Neural Systems and Rehabilitation Engineering*, vol. 18, no. 2, pp. 164–173, 2010.

[37] J. Wernick and R. G. Volpe, "Lower extremity function and normal mechanics," in *Clinical Biomechanics of the Lower Extremities*, pp. 1–57, 1996.

[38] I. Díaz, J. J. Gil, and E. Sánchez, "Lower-limb robotic rehabilitation: literature review and challenges," *Journal of Robotics*, vol. 2011, Article ID 759764, 11 pages, 2011.

[39] S. Viteckova, P. Kutilek, and M. Jirina, "Wearable lower limb robotics: A review," *Biocybernetics and Biomedical Engineering*, vol. 33, no. 2, pp. 96–105, 2013.

[40] W. Huo, S. Mohammed, J. C. Moreno, and Y. Amirat, "Lower limb wearable robots for assistance and rehabilitation: a state of the art," *IEEE Systems Journal*, vol. 10, no. 3, pp. 1068–1081, 2016.

[41] R. Jiménez-Fabián and O. Verlinden, "Review of control algorithms for robotic ankle systems in lower-limb orthoses, prostheses, and exoskeletons," *Medical Engineering & Physics*, vol. 34, no. 4, pp. 397–408, 2012.

[42] R. Versluys, P. Beyl, M. van Damme, A. Desomer, R. Van Ham, and D. Lefeber, "Prosthetic feet: state-of-the-art review and the importance of mimicking human anklefoot biomechanics," *Disability and Rehabilitation: Assistive Technology*, vol. 4, no. 2, pp. 65–75, 2009.

[43] D. Moher, A. Liberati, J. Tetzlaff, and D. G. Altman, "Preferred reporting items for systematic reviews and meta-analyses: the PRISMA statement," *PLoS Medicine*, vol. 6, no. 7, Article ID e1000097, 2009.

[44] J. L. Johansson, D. M. Sherrill, P. O. Riley, P. Bonato, and H. Herr, "A clinical comparison of variable-damping and mechanically passive prosthetic knee devices," *American Journal of Physical Medicine & Rehabilitation*, vol. 84, no. 8, pp. 563–575, 2005.

[45] P. Houglum, D. Bertoti, and S. Brunnstrom, *Brunnstrom's Clinical Kinesiology*, F.A. Davis, Philadelphia, Pa, USA, 1st edition, 2012.

[46] J. Muscolino, *Kinesiology*, Elsevier Mosby, St. Louis, Mo, USA, 2nd edition, 2010.

[47] J. H. Hicks, "The mechanics of the foot: II. The plantar aponeurosis and the arch," *Journal of Anatomy*, vol. 88, no. 1, pp. 25–30, 1954.

[48] D. Paluska and H. Herr, "The effect of series elasticity on actuator power and work output: implications for robotic and prosthetic joint design," *Robotics and Autonomous Systems*, vol. 54, no. 8, pp. 667–673, 2006.

[49] E. J. Rouse, L. M. Mooney, and H. M. Herr, "Clutchable series-elastic actuator: implications for prosthetic knee design," *International Journal of Robotics Research*, vol. 33, no. 13, pp. 1611–1625, 2014.

[50] L. Mooney and H. Herr, "Continuously-variable series-elastic actuator," in *Proceedings of the 13th IEEE International Conference on Rehabilitation Robotics*, pp. 1–6, Seattle, Wash, USA, June 2013.

Hindawi
Journal of Robotics
Volume 2017, Article ID 7862178, 12 pages
https://doi.org/10.1155/2017/7862178

Research Article

Networked Multimodal Sensor Control of Powered 2-DOF Wrist and Hand

Masaki Shibuya,[1] Kengo Ohnishi,[2] and Isamu Kajitani[3]

[1]*Graduate School of Tokyo Denki University, Ishizaka, Hatoyama-machi, Hiki-gun, Saitama 350-0394, Japan*
[2]*Tokyo Denki University, Ishizaka, Hatoyama-machi, Hiki-gun, Saitama 350-0394, Japan*
[3]*National Institute of Advanced Industrial Science and Technology, 1-1-1 Umezono, Tsukuba, Ibaraki 305-8560, Japan*

Correspondence should be addressed to Kengo Ohnishi; ohnishi@mail.dendai.ac.jp

Received 14 April 2017; Revised 28 July 2017; Accepted 10 August 2017; Published 7 November 2017

Academic Editor: George Mann

A prosthetic limb control system to operate powered 2-DOF wrist and 1-DOF hand with environmental information, myoelectric signal, and forearm posture signal is composed and evaluated. Our concept model on fusing biosignal and environmental information for easier manipulation with upper limb prosthesis is assembled utilizing networking software and prosthetic component interlink platform. The target is to enhance the controllability of the powered wrist's orientation by processing the information to derive the joint movement in a physiologically appropriate manner. We applied a manipulative skill model of prehension which is constrained by forearm properties, grasping object properties, and task. The myoelectric and forearm posture sensor signals were combined with the work plane posture and the operation mode for grasping object properties. To verify the reduction of the operational load with the proposed method, we conducted 2 performance tests: system performance test to identify the powered 2-DOF wrist's tracking performance and user operation tests. From the system performance experiment, the fusion control was confirmed to be sufficient to control the wrist joint with respect to the work plane posture. Forearm posture angle ranges were reduced when the prosthesis was operated companying environmental information in the user operation tests.

1. Introduction

Upper limb prostheses are widely accepted by amputees to support their daily life, but their mechanical functions are limited. Hence, upper limb prosthesis users are required to manage the burdens of daily activities. For example, widely used transradial prostheses do not have wrist joint functions. The users need to compensate the orientation of the hand with shoulder and trunk movements for grasping and manipulation tasks [1–3]. One solution is to increase the number of joints of the prosthetic hand. By incorporating multiarticulated prosthetic hand with number of movable joints, various digit movements are expected to contribute to reducing the compensatory movements. However, operating multiple joints is not an easy task for the upper limb prosthesis user. The multijoint operation requires multiple independent channels of operation input signals or pattern recognition algorithm to discriminate and coordinate the joint movements. Myoelectric signal has been a choice and numbers of myoelectric control system are proposed and available for upper limb prosthesis. However, the number of available myoelectric signal source channels is limited, due to socket design and/or user's arm conditions. To overcome this problem, methods to sequentially select operation functions are widely used in upper limb prosthetic products. These methods are useful in simple and short tasks. However, as the number of functions increases, more time is needed to select the intended function [4, 5]. Cocontraction switching is commonly used for switching between functions or prehensile types in multiarticulated hand systems or powered transhumeral prostheses. There are other methods to increase the number of myoelectric signal source channels through surgical reconstruction, such as Targeted Muscle Reinnervation [6]; however, the availability of this method is still limited.

The target of our research is to contribute to this problem by engineering approaches. We proposed a multimodal sensor control method that combines information of upper

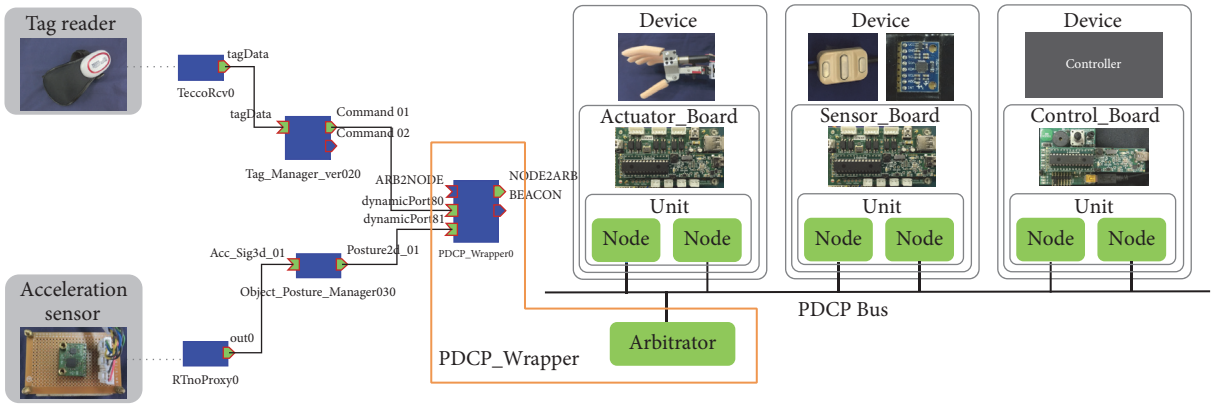

Figure 1: System structure of RTM-PDCP linkage platform.

limb posture and myoelectric sensor output to operate wrist function of a powered prosthesis [7]. Our aim is to extend this approach. Generally, selection of manipulative activities is constrained by the properties of the tasks and other surrounding conditions, such as the size and shape of the objects or target areas [8]. Therefore, our proposal is to use the information of the surrounding environment for dexterous operation of the joints and the motions of the upper limb prosthesis.

When the information of the executing task is available on beforehand, we can select the operation mode or prehensile type, as proposed by Trachtenberg et al. [9]. However, it is cumbersome to get all the required information for each task of daily life, and select the priority of the candidate tasks in advance. We believe installing identification tags and sensors to utilize environmental information is a more practical solution than extraction the information from the myoelectric signals for prosthetic operation in routine daily life activities. To implement this idea, three software technologies are required, first is for connecting environment objects, second is for communication of prosthetic components, and the third is for connecting those environment and prosthetic elements. There are several researches for connecting environment object. In this research, we applied a software platform for robot development [10] used in the development of robotic life space environment [11]. For the communication between prosthetic components, a Prosthetic Device Communication Protocol (PDCP) [12] is implemented in this work. Software component were developed to connect those two software platforms [13]. In this project, we composed and evaluated a system to operate powered 2-DOF wrist and a 1-DOF hand on these platforms. To verify the effect, the reduction of user's operational load was evaluated by conducting performance tests with nonamputated subjects.

2. Materials and Methods

2.1. System Overview. The system composed in this project consists of networking software for robotic control software components and an interlinking hardware platform for prosthetic components.

The posturing of wrist joints during prehension mainly depends on the forearm posture, the grasping object posture, and the task. In addition to the myoelectric signal and forearm posture, we use the work plane posture and the operation mode as environmental information. To compose this structure, surface electrodes are used for myoelectric signal measurement, inertial sensor for forearm posture measurement, acceleration sensor for work plane posture measurement, and RFID for selection of object information. Prosthetic hand elements with actuator, motor driver, sensor, and main controller are modularized as prosthetic device elements (right in Figure 1) to form a prosthetic limb network. Acceleration sensor and wearable RFID reader are linked to a software component as the environmental information networks (left in Figure 1). The prosthetic limb network and the environmental information network are linked for communicating between the prosthetic and environment and consist a RTM-PDCP linkage platform (center of Figure 1).

2.1.1. Networking Platform. We use RT-Middleware [10] for networking the environment. RT-Middleware was developed by a group at National Institute of Advanced Industrial Science and Technology (AIST), Japan, as a software platform for efficient development of robot system. We used Prosthetic Device Communication Protocol (PDCP) [12] for networking the sensors, motors, and microprocessors in the prosthesis. The PDCP is a communication protocol for prosthesis that was developed mainly by a group at the University of New Brunswick, Canada. The PDCP is designed to modulate the prosthetic elements [14] to satisfy the requirements of each prosthesis user. In the previous study, a RT-Middleware software component, PDCP_Wrapper [13], was developed to interpret the communication between RT-Middleware and PDCP. The PDCP_Wrapper connects the environment network composed by RT-Middleware and the prosthetic network by PDCP and interpret the information for communication.

2.1.2. Networking of Hardware. A number of multifunctional and multi-DOF upper limb prostheses with multiple active joints are developed and available [15, 16]. Montagnani et al.

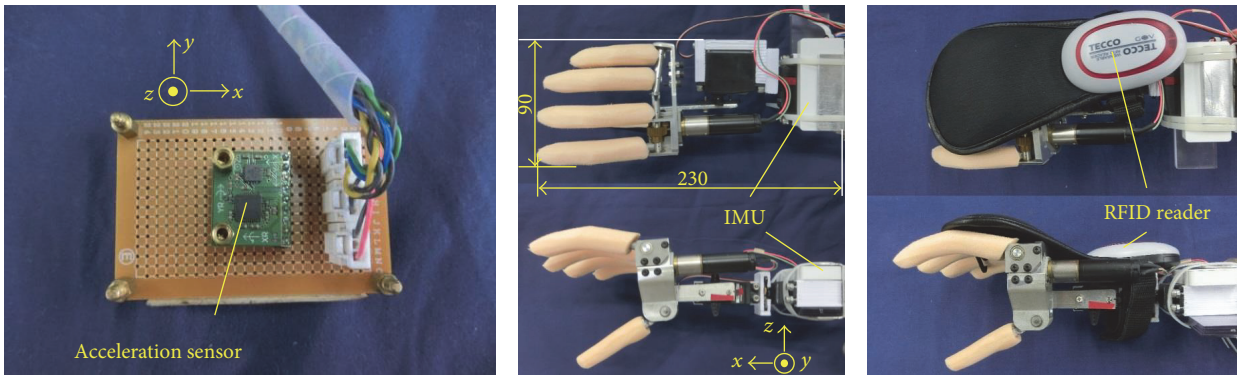

Figure 2: Hardware of system and sensor coordinate system.

[17] suggested that "a complex (and expensive) multigrasp hand cannot be fully exploited if fitted on a simple rotator; a much cheaper 1-DOF hand on a slightly more complex wrist could achieve a similar performance." Therefore, in this system, we composed a 3-DOF transradial prosthesis (center of Figure 2). The former 3-DOF transradial prosthesis consisted of a 2-finger and thumb hand driven with 1 geared DC motor, palmar/dorsal flexion with axis at the MP joint and a pronation/supination wrist each driven by a geared DC motor. The motors were driven by an H-bridge motor driver and controlled by a single chip MPU. The new mockup was composed of 2-DOF wrist and 1-DOF hand. The palmar/dorsal flexion and pronation/supination wrist consists of 2 servomotors (Standard Servo, Parallax). As a terminal device a 5-digit hand (YS-2002, Tokyo Denki University) is attached to the wrist. A geared DC motor drives the linked digits through a worm gear and universal joint. Surface electrode (13E200, Ottobock), inertial sensor (MPU6050, InvenSense), and powered 3-DOF transradial prosthesis (TDU) were networked by microcomputers (dspic33F, Microchip) and the development boards (Microstick II and MicrostickPlus ver.C of Microchip and Microstick IO Board of AIST/WIN Electronic Industries). Software programs for PDCP-base communicating are those released from UNB. Acceleration sensor (ADXL330, AnalogDevices) for work plane measurement (left in Figure 2) and wearable RFID tag reader (TECCO, GOV), right in Figure 2, were networked [18] by RT-Middleware. PDCP_Wrapper was installed on the laptop (Latitude3340, Dell, OS: Microsoft Windows 7) and connected to the PDCP-Bus using an adapter (CANUSB, LAWICEL).

2.1.3. Integration of Information. Tag_Manager sets information such as the priority and hand posture for RFID tag (left in Figure 1). The information is sent to PDCP_Wrapper whenever the configured tag is read. The work plane posture and the upper limb posture are presented by Euler angles. The Euler angles are calculated from the rotation of the acceleration vector measured by acceleration sensor. First, the instantaneous direction vector of the acceleration is computed from the acceleration vector. Since the acceleration vector is composed of gravitational acceleration and inertia, the acceleration vector measured when the acceleration sensor is set horizontally is used to calibrate as a reference vector. Then, Euler angles representing the sensor's posture are calculated from the rotation from the reference vector to the unit direction vector. The work plane posture is calculated by Object_Posture_Manager and sent to PDCP_Wrapper (left in Figure 1). Upper limb posture is calculated by Sensor_Board and transmitted to the PDCP-Bus which is a CAN-BUS standard network (right in Figure 1). Myoelectric signals are AD converted by Sensor_Board and transmitted to the PDCP-Bus. The Control_Board receives the information and use it for operation.

2.1.4. Operation of Powered 2-DOF Wrist and Hand. Two electrodes were used, and hand opening and closing are, respectively, operated with myoelectric signal from the flexor muscle and extensor muscle of the user. In this system, when the tag is read by the wearable RFID reader, and the myoelectric signal of the flexor muscle exceeds the threshold value, the wrist joint servocontrol traces the work plane posture angle, and when the myoelectric signal of the extended muscle exceeds the threshold value, the tracing of the wrist joint control is canceled. In the track mode of the wrist joint, two kinds of modes were prepared: a mode that keeps the hand horizontal relative to the work plane and a mode that keeps the hand perpendicular to the work plane (Figure 3). Flowchart of a hand open/close is shown in Figure 4 and flowchart of wrist action is shown in Figure 5. The wrist joint angles setting in each mode are shown in the following function:

(i) Horizontal Mode (Supination and flexion directions are positive.):

Pronation/supination angle = −(work plane roll angle − forearm roll angle) [deg.].
Flexion/Extension angle = 0 [deg.].

(ii) Vertical Mode:

Pronation/supination angle = −(90 + work plane roll angle − forearm roll angle) [deg.].

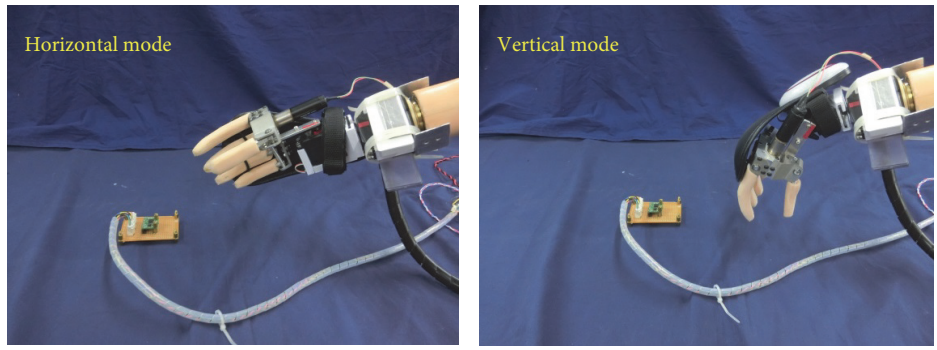

Figure 3: Horizontal mode and vertical mode of the wrist joint tracking control.

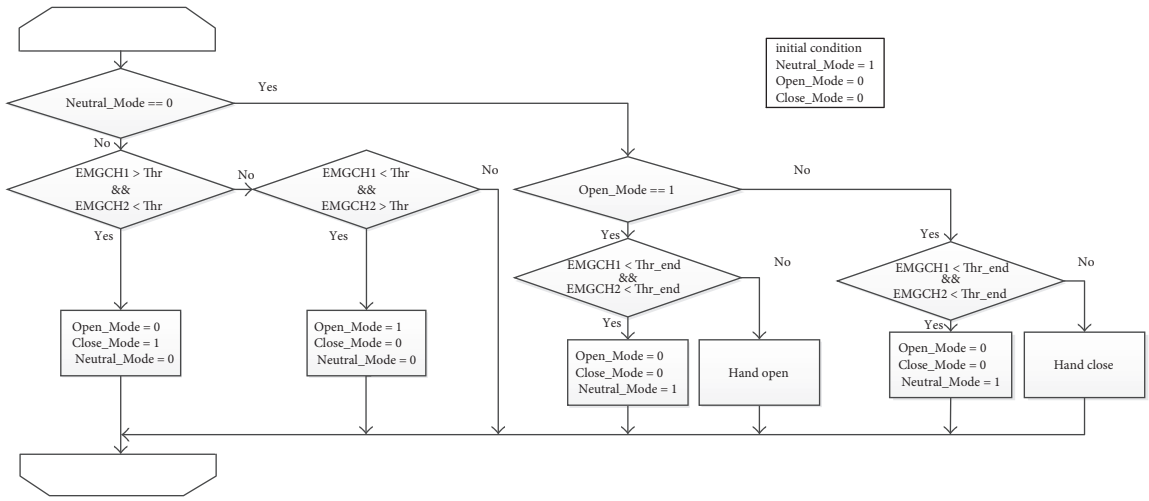

Figure 4: Flowchart of hand open/close. "Thr" and "Thr_end" are threshold value to control of the prosthetic hand opening and closing.

Flexion/extension angle = − (−90 + work plane pitch angle − forearm pitch angle) [deg.].

2.2. System Performance Tests. We conducted an experiment to investigate the performance of the system. In this experiment, the tracking performance of the wrist joint posture with respect to the work plane posture is identified. We assembled an angle representation device, which alters the work plane posture for the experiment (Figure 6). By entering the target angle to the controller component of the angle representation device, the attitude angle of the representation device is shifted with the servomotor and the acceleration sensor signal on the device is transmitted to the wrist joint angle controller through the PDCP_Wrapper for the wrist joint to follow.

In the experiment, an infrared reflective markers were attached to measure the movement of the angle representation device and the transradial prosthesis's powered 2-DOF wrist joint angles with optical motion capture and motion analysis system (VENUS 3D, Nobbytech). The attachment positions of the markers are shown in Figure 6. The sampling frequency of the optical motion capture was 100 Hz. The experiments were conducted under the two conditions as follows:

(I) Horizontal mode: angle representation device tilts in the roll angle direction of the acceleration sensor to identify the dynamic characteristics of the pronation/supination joint of the wrist.

(II) Vertical mode: angle representation device presents the angle in the pitch angle direction of the acceleration sensor to identify the dynamic characteristics of the flexion/extension joint of the wrist.

2.3. User Operation Tests. To verify the reduction of operation burden, we conducted experiments to operate the powered 3-DOF transradial prosthesis in performance tests with multiple manipulating tasks. The performance was compared between the prosthesis controls: the proposed method with the environmental information fusion wrist orientation and conventional method with a locked wrist at neutral position. In both conditions, the hand was controlled with myoelectric signals on the extensor and flexor muscle in the forearm.

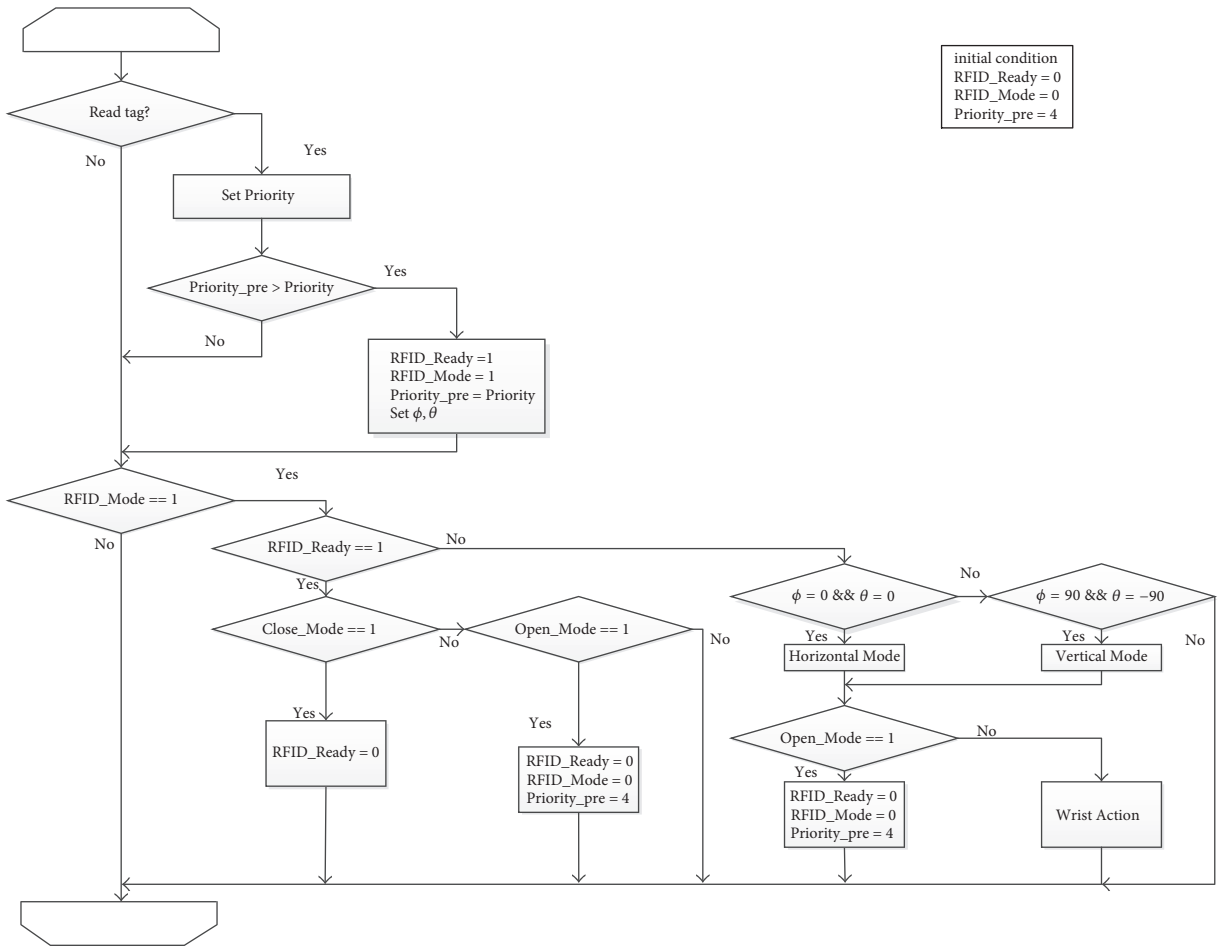

Figure 5: Flowchart of the wrist action. When RFID tag information is received and the priority of the tag information is higher than the previous value, the hand posture is set based on the tag information. The priority is set with 2 bits, and the smaller the number, the higher the priority. After the wrist joint angles (pronation/supination and flexion/extension angles) are determined based on the tag information (ϕ: roll angle of the hand; θ: pitch angle of the hand), the work plane posture, and the upper limb posture, the wrist joint starts action when Close_Mode is set and it stops the operation of the wrist joint when Open_Mode is set.

User operation test was conducted by operating the powered 2-DOF wrist with the proposed multimodal sensor control method (MM) and conventional neutral position locked wrist myoelectric hand control (NP). To evaluate the wrist orientation function, the tests were specialized to adjust the wrist joint when reaching to the selected target object. There were three user operation test experiments: (I) a task that travels the hand back and forth to pick and release single shape object in resembling position and orientation (Box and Blocks Test, BBT); (II) a task that adjusts hand positioning, orientating, and closing force to pick-carry-release the target object in two pickup wrist posture conditions (Clothespin Test, CPT); and (III) a task that adjusts the hand orientation to correspond to a thin plate target object randomly posed tilt angles (Random Angle Test, RAT).

All experiments were conducted by nonamputee subjects donning a 3-DOF transradial prosthesis in Figure 7. The operation time and forearm acceleration were measured for each trial. The operation time was measured with a stopwatch, and the acceleration was measured with an inertial sensor (MPU 6050, InvenSense) at a sampling frequency of 200 Hz by a microcomputer (NUCLEO-F767ZI, STMicroelectronics) wired to the sensor and installed on the socket.

The 3-DOF transradial prosthesis was attached to the right forearm of the subject with a offset position and angle to the user's hand as shown in Figure 7. The myoelectric sensors were attached to the body surface over the flexor and extensor muscles in the forearm, respectively. The experimental equipment for all tasks was set on the workbench with the table top height of 750 mm. The initial posture of the hand and wrist joint was set to the neutral position and the hand aperture was set to 50 mm.

2.3.1. Tasks

(I) Box and Blocks Test. The experimental equipment was produced in same dimension to the original BBT's box and blocks. The weight and friction are slightly smaller when compared to the original. With the hand placed at the initial position and confirming the start sign presented from the

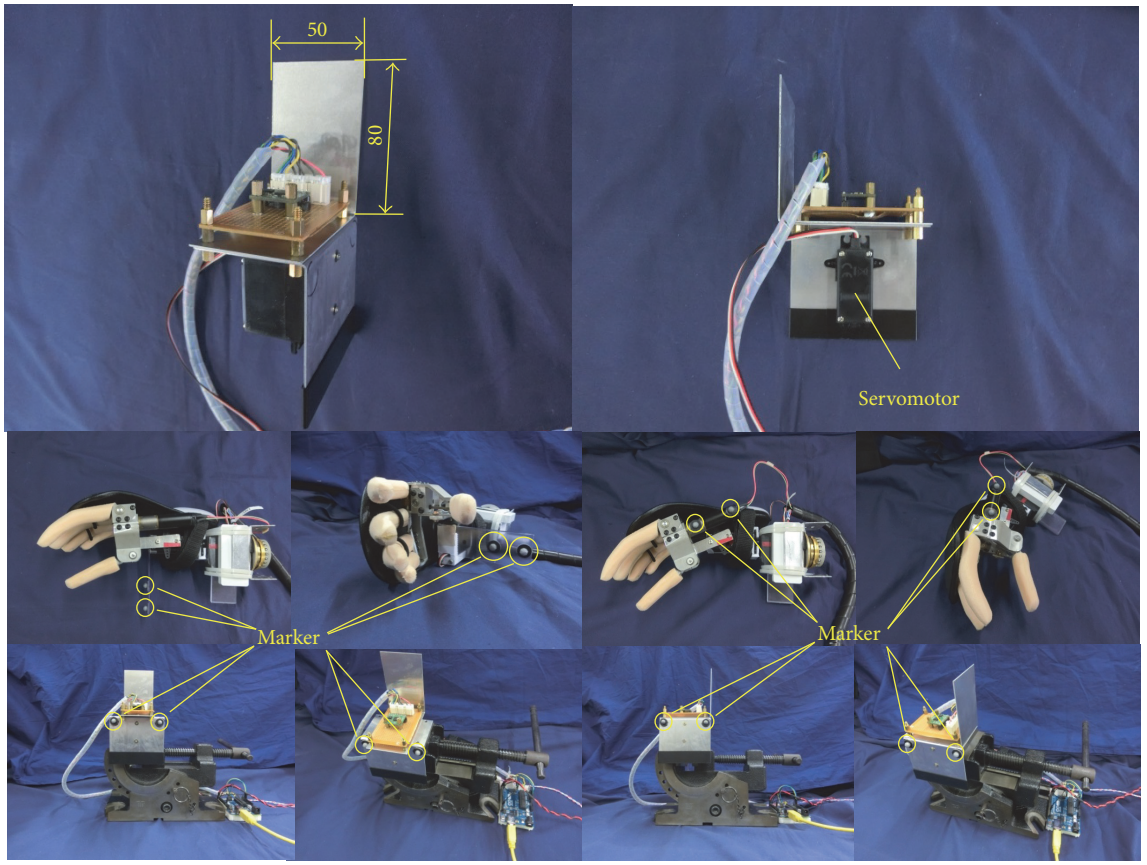

Figure 6: Angle representation device and marker positions.

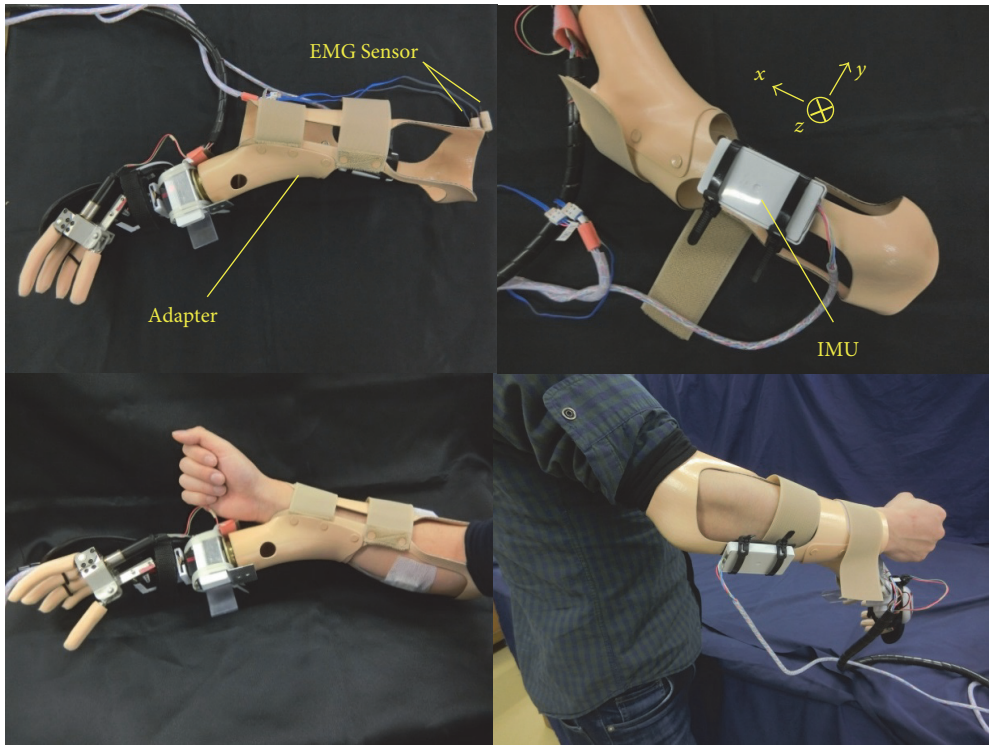

Figure 7: Powered 2-DOF wrist and hand with adapter socket for nonamputee subjects.

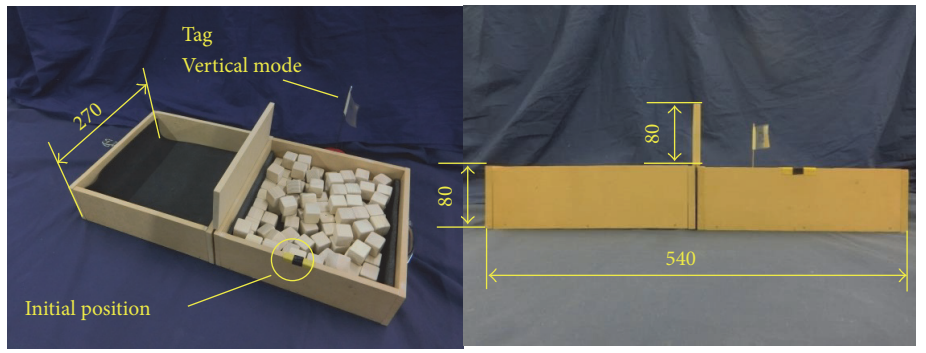

Figure 8: Experimental equipment of Box and Blocks Test.

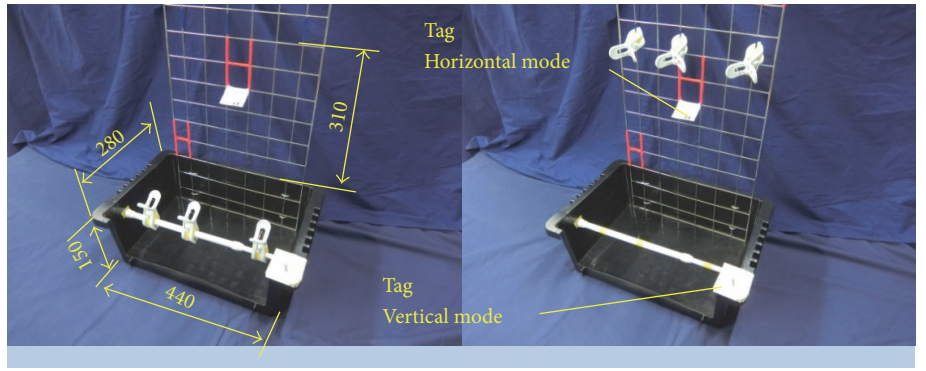

Figure 9: Experimental equipment of Clothespin Test.

experimenter, the subject moves as many blocks as possible from the right side to the left side within 30 seconds operating the prosthesis. An RFID tag was set as shown in Figure 8 to change the wrist position to vertical mode at the beginning.

(II) Clothespin Test. The test is to pick and move the clothespins from the horizontal bar in the low front to the three vertical bars, on the metal net in the back and release. With the hand placed at the initial position and confirming the start sign from the experimenter, the subject moves the three clothespins to the target vertical bars in the order from the left to right. A vertical mode tag was placed on the right front end of the case and a horizontal mode tag below the vertical bar as in the positions shown in Figure 9.

For BBT and CPT, the acceleration sensor for measuring the attitude of the work plane was installed on the work table.

(III) Random Angle Test. In daily life, the human hand orientation is operated by the wrist to adjust to the anonymous posture of the target object. To produce a similar condition for testing the hand orientation, a servomotor driven angle representation device randomly arranges five tilted angles of 10, 20, 30, 40, and 50 degrees toward the subject from the vertical upright posture. After each angle being presented, the subject grasps and picks up the clothespin attached to the angle representation device. As shown in Figure 10, the tag to invoke the vertical mode is installed to the right of the clothespin on the angle representation device. In the experiment, the motion is measured from the initial position till the prosthesis grips the clothespin and lifts it off the device.

3. Results

3.1. System Performance Tests. The presented angle and wrist angle were computed from the position data of the marker position measured and recorded through the experiment. The experimental environment, representation angles, and wrist angles relation in time series are presented in Figures 11 and 12.

Using the calculated data of 5143 sets in flexion/extension joint direction and 5024 sets in supination/pronation joint direction, the dynamics of the 2-DOF wrist unit with the transfer function of the first-order lag system, using the MATLAB 2015a System Identification Toolbox, were identified. The identified transfer function is as follows:

$$G_{\text{ExtFle}}(s) = \frac{6.052}{s + 5.384} \tag{1}$$

$$G_{\text{ProSpi}}(s) = \frac{6.087}{s + 5.134}. \tag{2}$$

3.2. User Operation Tests. User operation tests were conducted and recorded of 56 trials (4 subjects $*$ 7 tasks $*$ 2 series) in total. Range of forearm posture and operation

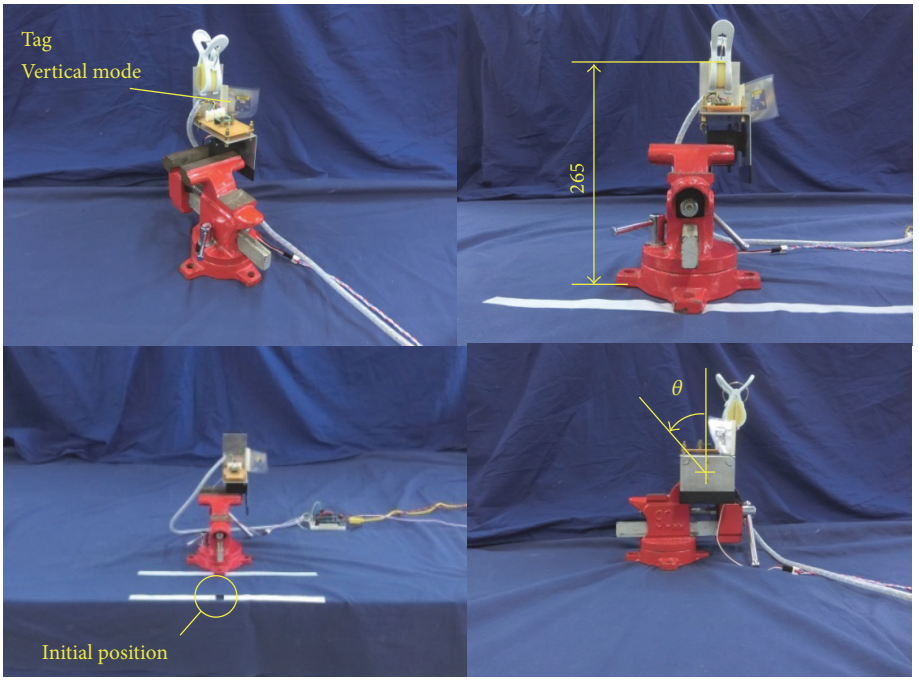

Figure 10: Experimental equipment of Random Angle Test.

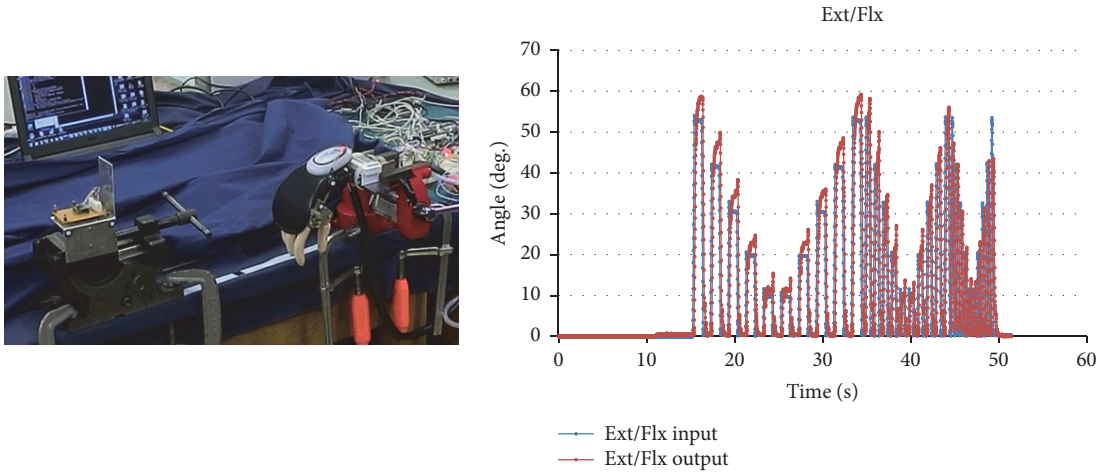

Figure 11: Results and experiment environment of flexion/extension joint.

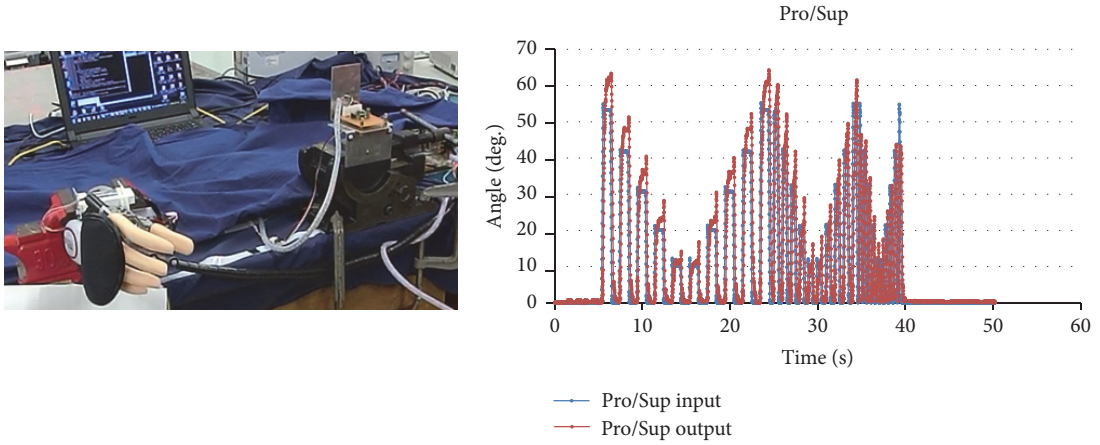

Figure 12: Results and experiment environment of supination/pronation joint.

Table 1: Means of operation times and scores ($^{*}p < 0.05$, $N = 4$).

Wrist joint operation	Neutral position	Multimodal
Box and Blocks Test score	8.25 ± SD 0.96	8.75 ± SD 0.50
Clothespin Test operation time [s]	25.59 ± SD 4.61	46.86 ± SD 18.93
Random Angle Test (10 deg.) operation time [s]*	4.29 ± SD 0.69	6.36 ± SD 1.49
Random Angle Test (20 deg.) operation time [s]	5.55 ± SD 2.30	7.34 ± SD 2.11
Random Angle Test (30 deg.) operation time [s]*	4.48 ± SD 1.16	6.28 ± SD 1.72
Random Angle Test (40 deg.) operation time [s]	7.56 ± SD 2.77	7.12 ± SD 2.83
Random Angle Test (50 deg.) operation time [s]	13.64 ± SD 8.41	6.74 ± SD 0.49

Table 2: Mean of Range of Roll ($^{*}p < 0.05$, $N = 4$).

Wrist joint operation	Neutral position [deg.]	Multimodal [deg.]
Box and Blocks Test*	53.82 ± SD 7.36	28.61 ± SD 4.59
Clothespin Test	83.73 ± SD 5.04	51.55 ± SD 19.68
Random Angle Test (10 deg.)	42.22 ± SD 3.94	24.18 ± SD 11.46
Random Angle Test (20 deg.)*	41.09 ± SD 6.28	26.64 ± SD 8.50
Random Angle Test (30 deg.)*	39.70 ± SD 7.63	22.91 ± SD 7.54
Random Angle Test (40 deg.)	36.76 ± SD 7.98	22.15 ± SD 11.36
Random Angle Test (50 deg.)*	36.90 ± SD 5.61	21.12 ± SD 5.01

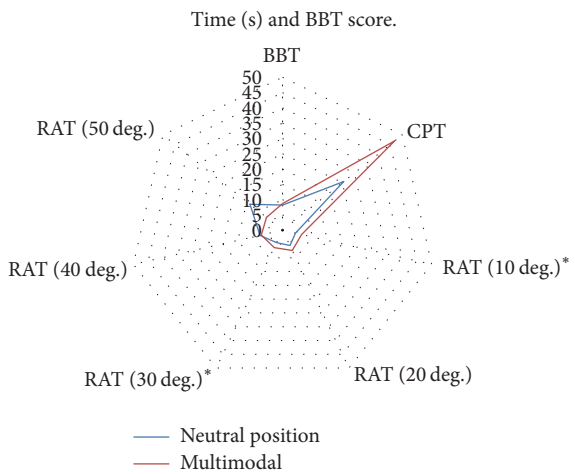

Figure 13: Radar chart of the means and significant difference ($^{*}p < 0.05$, $N = 4$).

time were compared between the fixed wrist joint at the neutral position condition and the condition with the wrist joint was operated by the proposed control method of RFID information is used to orientate the 2-DOF wrist and myoelectric control of the hand. The statistical significant difference was tested with t-test between the conditions.

3.2.1. Operation Time. The means and standard deviations of operation time are shown in Table 1; a radar chart of the means and significant differences ($^{*}p < 0.05$, $N = 4$) is shown in Figure 13.

In the results of CPT, RAT (10 deg.), RAT (20 deg.), and RAT (30 deg.), the means of operation time increased when the proposal method was used to control the wrist.

In RAT (10 deg.), the mean is 4.29 ± SD 0.69 s when operated with fixed wrist joint at neutral position and 6.36 ± SD 1.49 s by the proposed control method. The operation time was longer in the proposed control method and there was statistical difference between the two. Similar tendency was confirmed at RAT (30 deg.), where the mean was 4.48 ± SD 1.16 s for the fixed wrist joint and 6.28 ± SD 1.72 s with the proposed control method. In RAT (50 deg.), the mean of operation time was reduced when proposed control method was applied.

3.2.2. Posture Angle Range during the Operation (Roll, Pitch). The means and standard deviations of ROR (Range of Roll) are shown in Table 2; a radar chart of the means and significant difference ($^{*}p < 0.05$, $N = 4$) is shown in Figure 14.

The means of ROR were reduced in all tasks when proposed control method is applied. There were statistical differences in BBT, RAT (20 deg.), RAT (30 deg.), and RAT (50 deg.).

The means and standard deviations of ROP (Range of Pitch) are shown in Table 3; a radar chart of the means and significant difference ($^{*}p < 0.05$, $N = 4$) is shown in Figure 15. The means of ROP were reduced in CPT, RAT (10 deg.), RAT (20 deg.), RAT (40 deg.), and RAT (50 deg.) when proposed control method was applied. In RAT (50 deg.), the ROP was 61.10 ± SD 12.82 degrees when the wrist joint was fixed at neutral position and 40.34 ± SD 8.59 degrees when the proposed control method was applied. The ROP was smaller

Table 3: Mean of Range of Pitch ($^{*}p < 0.05$, $N = 4$).

Wrist joint operation	Neutral Position [deg.]	Multimodal [deg.]
Box and Blocks Test	34.00 ± SD 4.05	34.15 ± SD 8.06
Clothespin Test	56.89 ± SD 5.23	53.58 ± SD 4.32
Random Angle Test (10 deg.)	46.39 ± SD 12.40	46.23 ± SD 4.17
Random Angle Test (20 deg.)	47.81 ± SD 12.91	45.99 ± SD 7.88
Random Angle Test (30 deg.)	46.71 ± SD 10.08	46.79 ± SD 4.83
Random Angle Test (40 deg.)	52.60 ± SD 11.68	43.00 ± SD 7.32
Random Angle Test (50 deg.)*	61.10 ± SD 12.82	40.34 ± SD 8.59

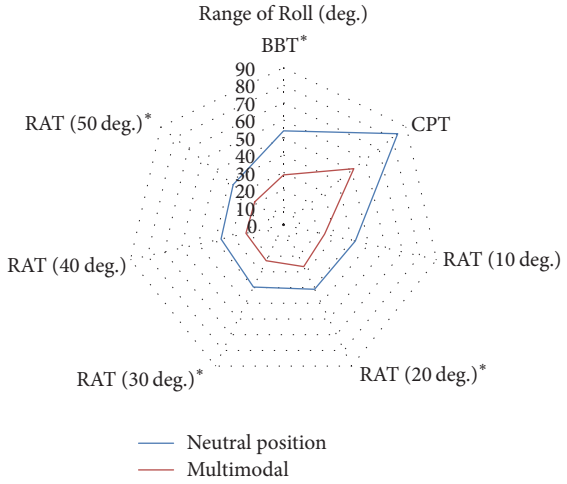

Figure 14: Radar chart of the means and significant difference ($^{*}p < 0.05$, $N = 4$).

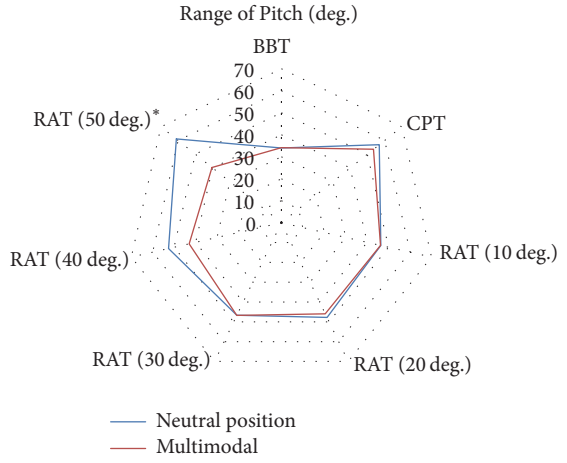

Figure 15: Radar chart of the means and significant difference ($^{*}p < 0.05$, $N = 4$).

in the proposed control method and statistical difference was confirmed in RAT (50 deg.).

4. Discussion

4.1. System Performance Tests. The cutoff frequency was calculated from the approximated transfer function, flexion/extension joint direction was 0.86 Hz, and supination/pronation joint direction was 0.82 Hz.

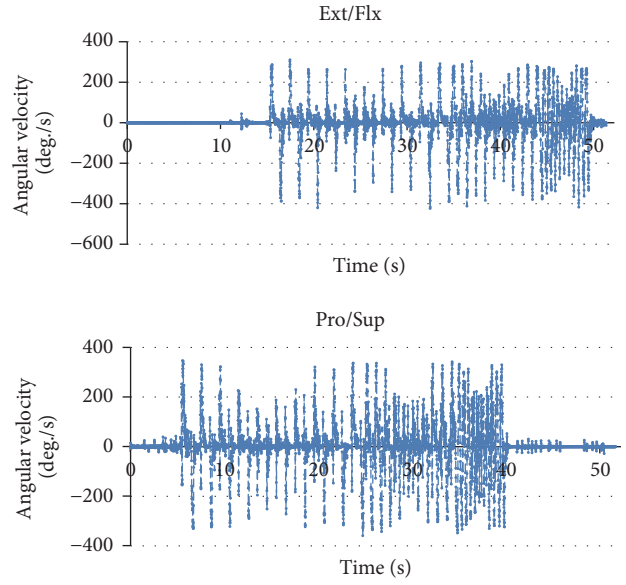

Figure 16: Angular velocity of powered 2-DOF wrist.

Table 4: Maximum value of powered 2-DOF wrist angular velocity.

	Angular velocity [deg./s]
Flexion	423.0
Extension	310.9
Pronation	346.8
Supination	358.7

The angular velocities were calculated from wrist angle during the identification experiment. The angular velocities are shown in Figure 16 and the maximum value is shown in Table 4. Commercially available wrist rotator's (Electric Wrist Rotator, Ottobock) angular velocity is 81.28 deg./s [19], and, therefore, we assume that the tracking performance of our system is, in terms of cutoff frequency and the maximum angular velocity, acceptable for use in operation experiment level. Further tests are required to discuss the daily use level.

4.2. Operation Time. By confirming the movement of the user during each test conditions when using the proposed control method, the necessity to approach the RFID tag and read the tag repeatedly is found to be the major cause of operation time to extend, such in Clothespin Test. However, when the control of the wrist joint using the environmental

Table 5: Mean and average reduction rate of Range of Roll ($^{*}p < 0.05$, $N = 4$).

Wrist joint operation	Neutral position [deg.]	Multimodal [deg.]	Reduction Rate [%]
Box and Blocks Test*	53.82 ± SD 7.36	28.61 ± SD 4.59	46.8
Clothespin Test	83.73 ± SD 5.04	51.55 ± SD 19.68	38.4
Random Angle Test (10 deg.)	42.22 ± SD 3.94	24.18 ± SD 11.46	42.7
Random Angle Test (20 deg.)*	41.09 ± SD 6.28	26.64 ± SD 8.50	35.2
Random Angle Test (30 deg.)*	39.70 ± SD 7.63	22.91 ± SD 7.54	42.3
Random Angle Test (40 deg.)	36.76 ± SD 7.98	22.15 ± SD 11.36	39.7
Random Angle Test (50 deg.)*	36.90 ± SD 5.61	21.12 ± SD 5.01	42.8

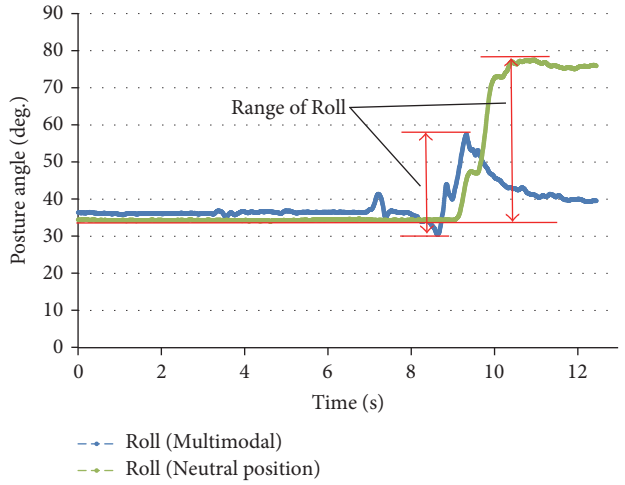

Figure 17: Example of the posture angle during operation.

information is effective in easing to grasp the object, it is inferred that the operation time is shorter compared to the grasp time with the fixed wrist, especially with deeply tilted target such as at 50 degrees of the Random Angle Test.

4.3. Posture Angle Range during the Operation (Roll, Pitch). An example of the roll angle during operation is shown in Figure 17 and average reduction rates of the Range of Roll are shown in Table 5. The average reduction rate of the Range of Roll angle is 41.1% for all tasks. In the standing posture with shoulder joint in neutral position and elbow flexion at 90 degrees, the roll angle direction of the forearm posture calculated by acceleration sensor output roughly matches the abduction direction of the shoulder joint. From this result, the proposed control method can be said to reduce compensating motion of the prosthesis user's shoulder and the operation load.

5. Conclusion

In this project, we proposed a concept model that comprehensively supports the operation of the 2-DOF wrist and 1-DOF hand by fusion of myoelectric signals and environmental information by networking the prosthesis elements with a RT-Middleware and PDCP platforms.

To verify the operation load reduction with the proposed platform and control method, we conducted performance test identification experiments of a powered 2-DOF wrist tracking performance and user operation tests. From the joint tracking performance identification experiment, it was confirmed that the ability to sufficiently control the wrist joint with respect to the multiple conditions of presented work plane posture is encouraging. To verify the load reduction, we conducted user operation test with nonamputee subject to operate the powered prosthetic wrist and hand in the proposed environmental information fusion multimodal sensor control method and compared to the neutral position locked wrist hand control. The means of Range of Roll angle on condition of proposal control method were reduced in all tasks: Box and Blocks Test, Clothespin Test, and Random Angle Tests. From these findings, the proposed multimodal sensor control with environmental information fusion and the network platform are capable of reducing compensatory motion and operation burden in routine tasks with repeated reaching and hand orientation under well-established environment such as in home and office workspace. The guarantee of the effect of the proposed method is limited to transferring postural information from the sensor in the environment when triggered by the RFID tag reading. Additional sensors (i.e., force, tactile, and distance) or RFID tags can be added to the environment and information can be transmitted through the network. The drawback will be decreasing responding speed and failing to link the prosthesis control strategy to appropriate natural human behavior (i.e., response speed tolerance and other human interface design factors) will cause complexity and low reliability which will link to rejection. Therefore, therapeutic training methodology and screening methodology of the target user should be discussed with experienced therapist and prosthetist during assessment trial phase.

Conflicts of Interest

The authors declare that there are no conflicts of interest regarding the publication of this paper.

References

[1] A. Hussaini, A. Zinck, and P. Kyberd, "Categorization of compensatory motions in transradial myoelectric prosthesis users,"

Prosthetics and Orthotics International, vol. 41, no. 3, pp. 286–293, 2016.

[2] S. L. Carey, M. J. Highsmith, M. E. Maitland, and R. V. Dubey, "Compensatory movements of transradial prosthesis users during common tasks," *Clinical Biomechanics*, vol. 23, no. 9, pp. 1128–1135, 2008.

[3] M. J. Major, R. L. Stine, C. W. Heckathorne, S. Fatone, and S. A. Gard, "Comparison of range-of-motion and variability in upper body movements between transradial prosthesis users and able-bodied controls when executing goal-oriented tasks," *Journal of NeuroEngineering and Rehabilitation*, vol. 11, no. 1, article no. 132, 2014.

[4] S. Amsuess, P. Goebel, B. Graimann, and D. Farina, "Extending mode switching to multiple degrees of freedom in hand prosthesis control is not efficient," in *Proceedings of the 2014 36th Annual International Conference of the IEEE Engineering in Medicine and Biology Society (EMBC '14)*, pp. 658–661, IEEE, Chicago, IL, USA, August 2014.

[5] M. Markovic, S. Dosen, D. Popovic, B. Graimann, and D. Farina, "Sensor fusion and computer vision for context-aware control of a multi degree-of-freedom prosthesis," *Journal of Neural Engineering*, vol. 12, no. 6, p. 066022, 2015.

[6] T. A. Kuiken, G. A. Dumanian, R. D. Lipschutz, L. A. Miller, and K. A. Stubblefield, "The use of targeted muscle reinnervation for improved myoelectric prosthesis control in a bilateral shoulder disarticulation amputee," *Prosthetics and Orthotics International*, vol. 28, no. 3, pp. 245–253, 2004.

[7] K. Ohnishi, I. Kajitani, T. Morio, and T. Takagi, "Multimodal sensor controlled three Degree of Freedom transradial prosthesis," in *Proceedings of the 2013 IEEE 13th International Conference on Rehabilitation Robotics, ICORR 2013*, Seattle, WA, USA, June 2013.

[8] R. S. Johansson, "Sensory control of dexterous manipulation in humans," in *Hand and Brain: Neurophysiology and Psychology of Hand Movement*, A. M. Wing, P. Haggard, and J. R. Flanagan, Eds., pp. 381–414, Academic Press, San Diego, Calif, USA, 1996.

[9] M. S. Trachtenberg, G. Singhal, R. Kaliki, R. J. Smith, and N. V. Thakor, "Radio frequency identification - An innovative solution to guide dexterous prosthetic hands," in *Proceedings of the 33rd Annual International Conference of the IEEE Engineering in Medicine and Biology Society, EMBS 2011*, pp. 3511–3514, Boston, MA, USA, September 2011.

[10] N. Ando, T. Suehiro, K. Kitagaki, T. Kotoku, and W. Yoon, "RT-Middleware: distributed component middleware for RT (Robot Technology)," in *Proceedings of the IEEE IRS/RSJ International Conference on Intelligent Robots and Systems (IROS '05)*, pp. 3555–3560, Edmonton, Alta., Canada, August 2005.

[11] K. Ohara, T. Tanikawa, M. Toyoda et al., "Smart home network system integration with RT middleware for embedded controller," *Journal of Robotics and Mechatronics*, vol. 24, no. 6, pp. 1014–1022, 2012.

[12] Y. Losier, A. Clawson, A. Wilson et al., "An overview of the UNB hand system," in *Proceedings of the MyoElectric Controls/Powered Prosthetics Symp.*, Institute of Biomedical Engieering, Fredericton, New Brunswick, Canada, 2011.

[13] I. Kajitani, A. Miwa, and T. Kotoku, "Combining a PDCP (Prosthetic Device Communication Protocol) and an OpenRTM," in *Proceedings of the Robotics and Mechatronics Conference 2013 (ROBOMECH '13)*, pp. 1P1-C02(1)–1P1-C02(3), Tsukuba, Japan, 2013 (Japanese).

[14] P. J. Kyberd, A. S. Poulton, L. Sandsjö, S. Jönsson, B. Jones, and D. Gow, "The ToMPAW modular prosthesis: A platform for research in upper-limb prosthetics," *Journal of Prosthetics and Orthotics*, vol. 19, no. 1, pp. 15–21, 2007.

[15] Touch Bionics Inc., and Touch Bionics Limited, i-Limb, 10 Apr. 2017, http://www.touchbionics.com/products.

[16] Otto Bock HealthCare GmbH, Michelangelo, 10 Apr. 2017, https://professionals.ottobockus.com/Prosthetics/Upper-Limb-Prosthetics/Michelangelo-Axon-Bus-System/Michelangelo-Hand/c/2001.

[17] F. Montagnani, M. Controzzi, and C. Cipriani, "Is it finger or wrist dexterity that is missing in current hand prostheses?" *IEEE Transactions on Neural Systems and Rehabilitation Engineering*, vol. 23, no. 4, pp. 600–609, 2015.

[18] Y. Suga, "Development of "RTno" for development of embedded system using Arduino and OpenRTM-aist," in *in Proceedings of the Robotics and Mechatronics Conference 2011 (ROBOMECH '11)*, pp. 2P1-K12(1)–2P1-K12(2), Okayama, Japan, 2011 (Japanese).

[19] Otto Bock HealthCare GmbH, Electric Wrist Rotator, 10 Apr. 2017, https://professionals.ottobockus.com/Prosthetics/Upper-Limb-Prosthetics/Myo-Hands-and-Components/Myo-Wrist-Units-and-Rotation/Electric-Wrist-Rotator/p/10S17.